The University Of Sheffield.

Development of telecom wavelength InAs Quantum Dot lasers by MOCVD

By:
Chufan Wang

A thesis submitted in partial fulfilment of the requirements for the degree of
Doctor of Philosophy

The University of Sheffield
Faculty of Engineering
Department of Electronic and Electrical Engineering

Submission Date: Aug 2022

Intentionally Blank

Abstract

The subject of this thesis is to develop quantum dot lasers around the telecom wavelengths of 1300nm and 1550nm for optical fibre communications. Quantum dots (QD) were grown by Metal-Organic Vapour Deposition (MOCVD) utilising both the conventional Stranski-Krastanov (S.K) method and a novel droplet epitaxy (DE) approach. The first section compares 1.1 μm InAs/GaAs QD lasers grown on the on-axis GaAs(100) substrates and substrates offcut 3° towards (110). QD lasers on the off-axis substrates had a lower threshold current density (J_{th}) and higher gain. An ~20% increase in the QD density for the 3-degree off-axis sample was found compared to the on-axis samples. The higher QD density is related to the change of morphology of the GaAs spacer layer, with more steps formed on the surface of the off-axis GaAs, providing a favourable nucleation site for QDs. These 1.1μm QDs are the first step towards the future realisation of 1.3μm QD lasers by MOCVD in comparison to MBE literature of 1310nm QDs. The longer term aim of the research is to incorporate these QD lasers on Silicon substrate for photonic integration. The second section presents the design, growth and characterisation of 1550nm InAs QD lasers grown by Droplet Epitaxy. The DE approach has several potential advantages, including removing the influence of the well-known wetting layer seen in the SK growth of QDs. The QD structure with the InP waveguide layer blue-shifts the QDs' wavelength to 1530nm, close to the target wavelength of ~1550nm. An approximately five times increase in emission intensity from QD samples was achieved when the Zn doping was reduced. The waveguide material was changed to InP, which significantly improved the carrier injection into the QDs. A high tail of diffused arsenic and a high oxygen concentration observed on the QD & QW samples may be preventing lasing. A new Quantum Well structure incorporating AlInGaAs as waveguide layer material was also introduced and formed the basis of further optimisation in future work to achieve room temperature lasing of these DE QD lasers.

Acknowledgements

First and foremost, I would like to express my gratitude to my supervisor, Professor Jon Heffernan, for introducing me to the field of semiconductor lasers and allowing me to pursue a doctoral degree in his research group. Because of his expertise, comprehension, direction, and encouragement, I could continue working for the entirety of my PhD. In addition, I want to express my gratitude to my second supervisor, Dr. Kristian Groom, for all of his support and insight with regard to each and every aspect of my work.

I would like to express my gratitude to the many people in the group who have supported me throughout the course of my PhD. Without the help of these incredible individuals, I would not have been able to complete my thesis. Sincere gratitude goes out to Brett Harrison and Dr. Elisa M. Sala, both of whom assisted me with growth of the samples that were necessary for this work. I would like to offer my sincere gratitude to also Dr Nasser Babazadeh, who assisted me in developing my fabrication skills. In addition, I would like to extend my gratitude to Dr. Tim Robert, Dr. Edmund Clarke, and Dr. Paul Fry, who assisted me with the device measurements.

Dr. Ian Farrer, Dr. Young In Na, Dr. Aristotelis Trapalis, and the rest of my colleagues deserve my sincere appreciation for their contributions to my Ph.D.

I'd like to express my gratitude to both of my parents. Thank you for being there for me through all the good times and the bad in my life, and for always being there to support me till the very end.

Finally, thanks to all my friends who supported and encouraged me during my study life.

List of Publications

Manuscript submitted and under review by Semiconductor Science and Technology

1. **C. Wang**, B.Harrison, N. Babazadeh, E. Clarke, K,Groom and J. Heffernan, "Effect of off-axis GaAs substrates on the performance of InAs/GaAs QD lasers by metal-organic vapor phase epitaxy" ***Semiconductor Science and Technology, December (2022).***

Oral Presentations:

2. **C. Wang**, B.Harrison, N. Babazadeh, E. Clarke, K,Groom and J. Heffernan, "Effect of off-axis GaAs substrate on the characteristics of 1.1μm InAs/GaAs quantum dot lasers grown by MOCVD" ***Semiconductor and Integrated OptoElectronics (SIOE) Conference 2022,*** Cardiff University, Apirl (2022)

3. **C. Wang**, B.Harrison, N. Babazadeh, E. Clarke, K,Groom and J. Heffernan, "Effect of off-axis GaAs substrate on the characteristics of 1.1μm InAs/GaAs quantum dot lasers grown by MOCVD" ***UK Semiconductors Conference,*** University of Sheffield July (2022)

Poster:

B.A. Harrison, **C. Wang**, T.S. Roberts, A. Krysa, E. Clarke, P. Fry, D. J. Mowbray, G. Duggan, J. Heffernan, Quantum Dot Lasers for Optical Communication by MOVPE, The future photonics Hub 2020, Southampton, UK

Abbreviations

Al	Aluminum
AlAs	Aluminium Arsenide
AlGaAs	Aluminium Gallium Arsenide
a.u	Arbitary Units
As	Arsenic
AsH3	Arsine
AFM	Atomic Force Microscopy
Eg	Bandgap
°C	Celcius
cm	Centimetre
CB	Conduction Band
CW	Continuous Wave
IV	Current-Voltage
DMZn	Dimethylzinc
EL	Electroluminescence
eV	Electron Volts
E	Energy
ES 1	Excited State 1
ES 2	Excited State 2
Ga	Gallium
GaAs	Gallium Arsenide
GS	Ground State
In	Indium
InAs	Indium Arsenide
InGaAs	Indium Gallium Arsenide
InP	Indium Phosphide
MOCVD	Metal-Organic Chemical Vapour Deposition
MOVPE	Metal-Organic Vapour Phase Epitaxy
nm	nanometre
µm	micrometre
µs	Microsecond
mW	Milliwatts

MBE	Molecular Beam Epitaxy
p-type	Positive type doping
QD	Quantum Dot
P	Phophorous
QW	Quantum Well
RHEED	Reflection High-Energy Electron Diffraction
SEM	Scanning Electron Microscopy
SRL	Strain reducing layer
S-K	Stranski-Krastanov
SLED	Superluminescent Light Emitting Diode
SIMS	Secondary-ion mass spectrometry
J_{th}	Threshold current density
gth	Threshold gain
TEM	Transmission Electron Microscopy
TMAl	Trimethyl-Aluminium
TMAs	Trimethylarsine
TMGa	Trimethyl-Gallium
2D	Two-Dimentional
λ	Wavelength
XRD	X-ray Diffraction

Table of Contents

Chapter 1: Introduction & Literature Review

1.1 Introduction

For increased bandwidth and Internet traffic volumes, the communications industry requires high-speed lasers that operate at lower powers without active cooling.

It has been proposed in the literature for many years that quantum dot lasers can deliver this type of laser performance. However, the performance of such devices has been limited by the quality of the quantum dots, especially those grown by MOCVD. In this thesis, these issues were investigated using various experimental and theoretical techniques. All aspects of a new laser device are developed, including epitaxial layer structures, Quantum Dots (QD) characterisation, fabrication of the laser devices, and characterisation of the laser devices.

To this end, many important experimental techniques are employed in the following chapters, including:

1. MOCVD growth and development of the droplet epitaxy technique
2. AFM, photoluminescence, electron microscopy and other characterisation techniques to analyse quantum dot active regions
3. Fabrication of laser devices
4. Test and characterisation of laser devices, including analysis of operating conditions and experimental investigation of the physics of the devices
5. Investigation of the physics of quantum dots as gain media in semiconductor lasers

This thesis focuses on developing new long-wavelength QD lasers around the telecom bands of 1.3μm and 1.55μm using both S.K and novel growth methods called droplet epitaxy by MOCVD.

1.2 Quantum dot device and laser history

Quantum dots are semiconductor structures that exhibits 3-dimensional quantum confinement, which affects the material's electronic characteristics, making them distinct from bulk or quantum well semiconductors, as illustrate in the comparison of density of states (DOS) diagram in Fig 1. 1. One important characteristic of quantum dots is the high optical material gain that can be achieved under optical or electrical pumping conditions. This is due to the carriers being confined in three dimensions, on the order of de Broglie wavelength, resulting in a discrete density of state of QD material which has much higher gain than quantum well structures (Fig 1. 1). In theory, the discrete density of state should also leads to lower threshold current density in laser application compared with bulk and 2D quantum well structures.

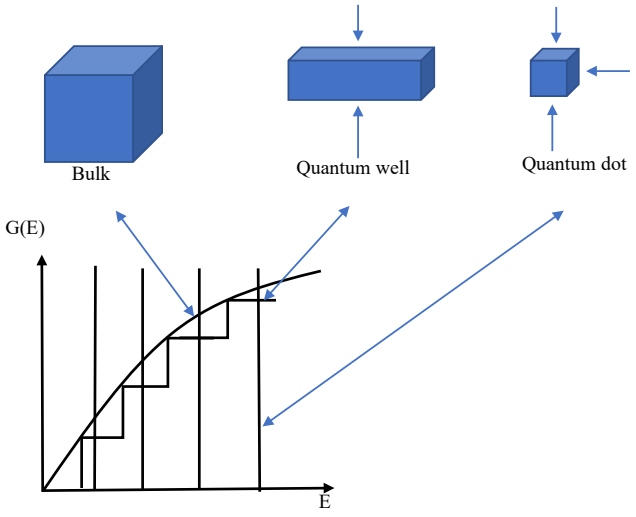

Fig 1. 1 theoretical density of state (DOS) of Bulk, quantum well and quantum dot material. (a) Bulk semiconductor has continued density of state. (b) quantum well has stepped DOS (c) QD discrete DOS

After the first 2D heterostructure semiconductor was grown by Esaki and Tsu in 1969 [1], the scale of the 2D structures has been gradually reduced and the continues improvement in growth techniques allow the transition from quantum well to quantum wire and finally nanosized quantum dots. The first quantum dot structure was inserted in glass by Rocksby in 1932 which was used as colour filter [2]. Since then, several applications for exploiting its quantum

confinement properties have been developed. In recent years, the epitaxial growth of high-density dots has become feasible with the development of the self-organised process for quantum dot formation (usually done by Stranski-Krastanov technique)[3]. This triggered interest in utilising QD in photonic devices such as solar cells[4], [5], light-emitting diodes[6], [7], semiconductor optical amplifiers[8], [9], photodetectors[10], [11], and, most importantly, laser diodes[12]–[14]. Moreover, QDs can also be implemented into photonic chips as a single photon source for Quantum Photonic Integrated Circuits (PICs) application[15]–[17]. Therefore, the QD material has been considered as best candidate for next generation of optoelectronic device.

In terms of basic laser devices, there are 3 types of transitions inside the laser cavity: spontaneous emission, stimulated emission, and absorption, as shown in Fig 1. 2. The spontaneous emission occurs when electrons and holes from the conduction band and valence band recombine and a photon is emitted. To achieve lasing operation, one critical condition called population inversion is necessary. In population inversion, the photon emitted by the spontaneous emission will excite additional photons at very high photon density. This process is referred to as stimulated emission. The absorption happens when the photon generated by the e-h pair recombination is absorbed by the electrons in the conduction band or holes in valence band, which can be seen as losses. Therefore, it is necessary to increase the carrier density in the cavity to trigger more spontaneous emission and the lasing is only occurred when the gain of the cavity equals to the loss. For the QD material, it is much easier to achieve population inversion at a specific wavelength due to its discrete density of states properties which results in higher optical gain.

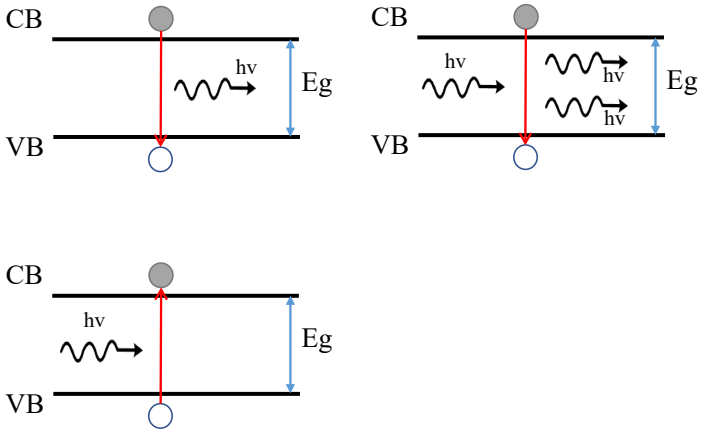

Fig 1. 2 Transition of electron and hole in laser structure (a) spontaneous emission (b) stimulated emission (c) absorption

In theory, QD material should results in higher optical confinement when compared to QW and bulk material. However due to issues such as inhomogeneous broadening of quantum dots, excited state lasing, etc. [18], the QD laser were not able to surpass the performance of the state-of-art QW laser for many years. The threshold current density of the first reported 1.26μm quantum dot lasers by Hirayama et al., in 1994, was 7.6kA/cm^2 at 77k [13]. Later, Kirstaedter *et al*., 1994 reported a reduction to 120A/cm^2 at 77K and 950A/cm^2 at 300K[12]. After a decade of intensive development, the QD laser J_{th} at 1.3μm room temperature lasing operation was achieved by Liu et al, 2004 at 39A/cm^2 for an MBE-grown device[19]. For comparison, the lowest threshold current density of quantum well laser at 1.3μm is about 212A/cm^2 at room temperature[20], higher than the state-of-art QD lasers. In addition, the work demonstrated by Arakawa and Sakaki in 1982 also shows the high temperature insensitivity of threshold current density properties of quantum dot [21] and thus it is another main advantage of quantum dot laser compared with quantum well laser in room temperature operation.

Although, in theory, quantum dots show several advantages for active region material in laser devices than quantum wells, it is still challenging to fabricate the high-quality quantum dot material to achieve better performance than QW lasers. Firstly, the fluctuation in individual QD size will cause inhomogeneous broadening of the spectra linewidth[22]. Secondly, the

distribution of the larger size and smaller size dots (Bimodal distribution) will cause the optical modes to compete with each other and reduce the gain (Fig 1. 3a).

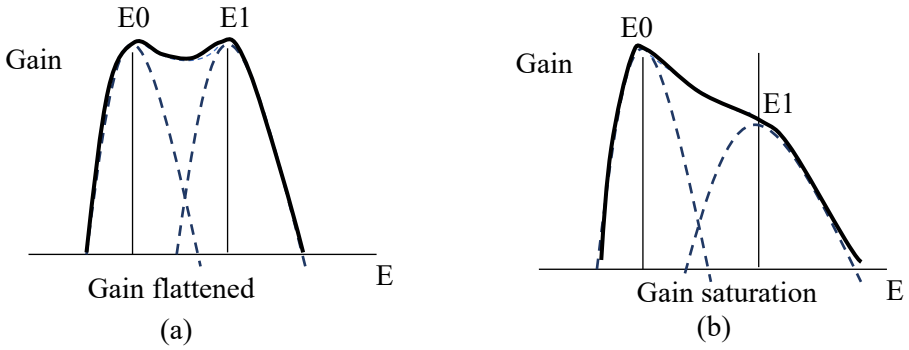

Fig 1. 3 The Gain vs Energy diagram of quantum dot (a) non-uniform dots (b) low density dots. The E0 and E1 are ground and exited state of electrons. Black line shows the optical gain profile

In addition, the optical gain will quickly saturate at ground state energy due to the low density of the quantum dot (Fig 1. 3b). This mean, as carrier injection increases, the ground state of dots is rapidly filled, resulting in excited state emission which increase the threshold current density of the laser device significantly. Moreover, as a result of degeneracy theory [22], [23], the excited state energy of the QD is usually 2 times the ground state. Thus, the excited state lasing of the QD will emit at a shorter wavelength than ground state, which is unwanted for laser application with specific wavelength requirements. Therefore, to avoid excited state lasing, uniform quantum dots with high density are necessary for using QD lasers as next generation light source in optoelectronic application.

1.3 MOCVD/MBE growth

1.3.1 MBE

Molecular beam epitaxy (MBE) is an epitaxial growth technique that deposits materials on the surface of crystalline substrates using multiple high-temperature molecular beams under ultra-high vacuum conditions. It was first introduced by J. R. Arthur and Alfred Y. Cho in 1960[24]. It can grow layers with extremely accurate interfaces and controlled doping profile at the monolayer scale. MBE enables the growth of such demanding structures as high-quality Interband Cascade laser, Quantum Cascade laser, and quantum dot laser as well as high mobility electronic devices based on 2-dimensional electron gases.

MBE is capable of both homoepitaxy and heteroepitaxy, and growth occurs within an ultrahigh vacuum (UHV) stainless steel chamber. It allows different materials, such as AlAs, GaAs, and InAs, to be grown in-situ to grow superlattice structures. A UHV environment (10^{-10} torr pressure) is needed to remove contaminants, which is facilitated by the use of liquid nitrogen. Wafers of the substrate material are heated to an optimised temperature. The molecular beam is generated by heating a nonreactive semimetal or metal to create a vapour. Atoms are released as molecular beams via each chamber cell. The molecular beams are directed at the substrate, and shutters are employed to adjust the layer thickness on the substrate. The advantage of MBE system ensures the optimum control of the deposition at atomic scale, therefore has been used as the prefer technique in growth of QD laser for research purpose.

1.3.2 MOCVD

Metal-Organic Chemical Vapour Deposition (MOCVD) or Metalorganic Vapour Phase Epitaxy (MOVPE) is a widely used crystal growth technique in which metalorganic precursors and carrier gas are deposited in gas phase and a semiconductor material layer is formed at atmospheric or low vacuum conditions. The chemical precursors used in MOCVD growth are called organometallic. The first demonstration of this technique was done by Manasevit *et al*. in 1960s[25]. At first, it was used to grow III/V single crystals of high purity. Subsequently, it has been extensively utilised for the mass manufacture of complex III/V commercial devices, such as LEDs in a broad wavelength range, 1.55μm lasers, infrared detectors, solar cells, transistors, etc.[26]–[28]

MOCVD is preferable to MBE for mass manufacturing mainly due to simpler operational procedures and greater reproducibility and scalability of the process to multi-wafer growth runs. MOCVD can produce almost every III/V device at a larger wafer scale than MBE, and as a result, MOCVD dominates the commercial manufacture of commercial semiconductor devices. However, the MOCVD process is challenging to control due to the large number of factors that affect the growth dynamics. In-situ monitoring is also less developed than MBE and emissivity corrected pyrometry (EpiTT) is less effective than MBE's RHEED, which can monitor growth at the atomic scale. To investigate the characteristics of the devices grown, ex-situ techniques such as Photoluminescence Spectroscopy (PL) and Atomic Force Microscopy (AFM) are utilised. Therefore, the growth of novel structures in MOCVD research is typically slower than in MBE. However, it has been demonstrated that the device's quality is comparable to that of other growth techniques, such as MBE and CBE.

Typically, a MOCVD system consists of three major components: a reactor system, a gas storage and transfer system, and an exhaust system. For the growth of III/V semiconductors, group III chemicals are first delivered to the chamber in the form of trimethyl or triethyl compounds, such as trimethylgallium TMG, triethylgallium TEG, and trimethylaluminum TMA, using carrier gases such as hydrogen or nitrogen. The precursors migrate to the substrate's surface and breakdown into elemental components to create epitaxial layers (Fig 1.

4). The Group V metalorganic precursors is then deposited at as well at the constant flow rate of Group III elements, the ratio between the ground V and group III elements is called V/III ratio. The valves and an electronic mass flow controller are used to control and monitor the flow rate. The substrate is supported by a graphite susceptor which is used to regulate substrate temperatures up to 1,000°C.

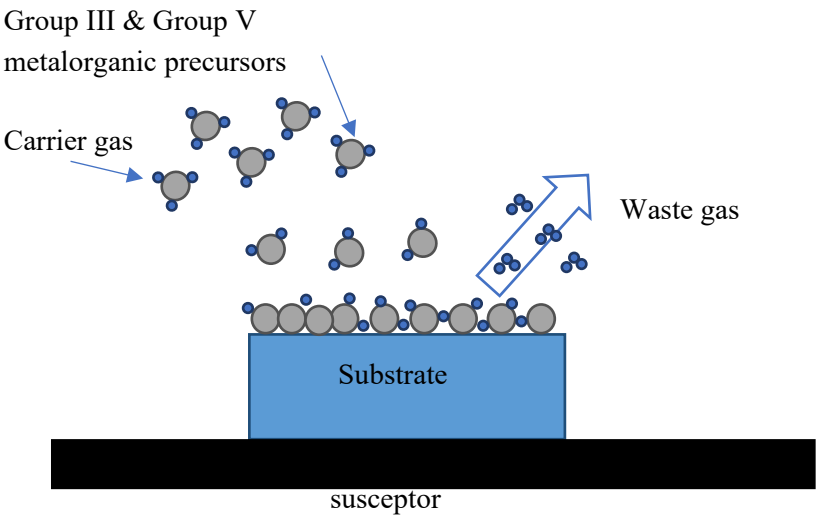

Fig 1. 4 Schematic diagram of MOCVD reaction process. The Gray circles are the precursors and bule circles are the carrier gas

After precursors decompose on the heated substrate, the reaction by-product leaves the substrate surface. This process is called pyrolysis and it is controlled by the substrate temperature and pressure as well as the chemical bond strength between substrate and film. The final remaining gases are collected by the exhaust system.

In the University of Sheffield, there are 2 MOCVD systems currently running and a third one is under calibration. The susceptor is also rotatable to provide better uniformity across the wafer. For laser applications, 1.3μm emission by MBE has already been demonstrated by several groups. But fewer works have been demonstrated by MOCVD growth at longer wavelength. Although the growth capability of 1.3μm to 1.5μm wavelength quantum dot in MOCVD has been demonstrated[19], [29]–[31], low threshold current density, high thermal stability, and high QD density are difficult to achieve in a single device.

1.4 Stranski-Krastanov and Droplet Epitaxy technique for quantum dot growth

1.4.1 SK Growth

Stranski-Krastanov (S.K) growth has been widely used for the growth of 3D islands on substrate surfaces. It was first introduced for material combinations such as InAs on GaAs, InAs on InP and Ge on Si, all of which include the deposition of lattice-mismatched materials. Because of the lattice mismatch between the substrate and the epitaxial film, a strained layer is formed. Such strain is reduced by the formation of 3D islands. The strained film has a critical thickness beyond which 3D islands will form. The critical thickness is affected by the growth rate and the kinetically driven diffusion of the adatoms[32] but primarily it is determined by the lattice mismatch between InAs/GaAs and InAs/InP[3].

Self-assembled QDs are largely grown by this type of method. The strain caused by the lattice mismatch is the main factor affecting the formation of quantum dots. This is a temperature dependent effect and if the deposition temperature is too high, it will stop the formation of islands even though the film is stressed. Normally, during QD formation, there is also a wetting layer formed on the substrate which is a thin layer of InAs left over from the spontaneous formation of 3D quantum dot islands. The presence of a wetting layer in QD lasers could competes with the QDs for carriers and reduce the gain in the QD.

The S.K growth has 3 stages (Fig 1. 5):

1. The strained film is deposited on top of the wetting layer and substrate with layer-by-layer growth. The strain is reduced by the formation of a metastable island on the surface (a-b)
2. The metastable islands will transform into quantum dots during the deposition of elements when they exceed the apparent critical thickness. (c)
3. When an excess amount of element supplied to the islands, the wetting layer is then stabilised and the strained layer disappears with QD formed on top. (d)

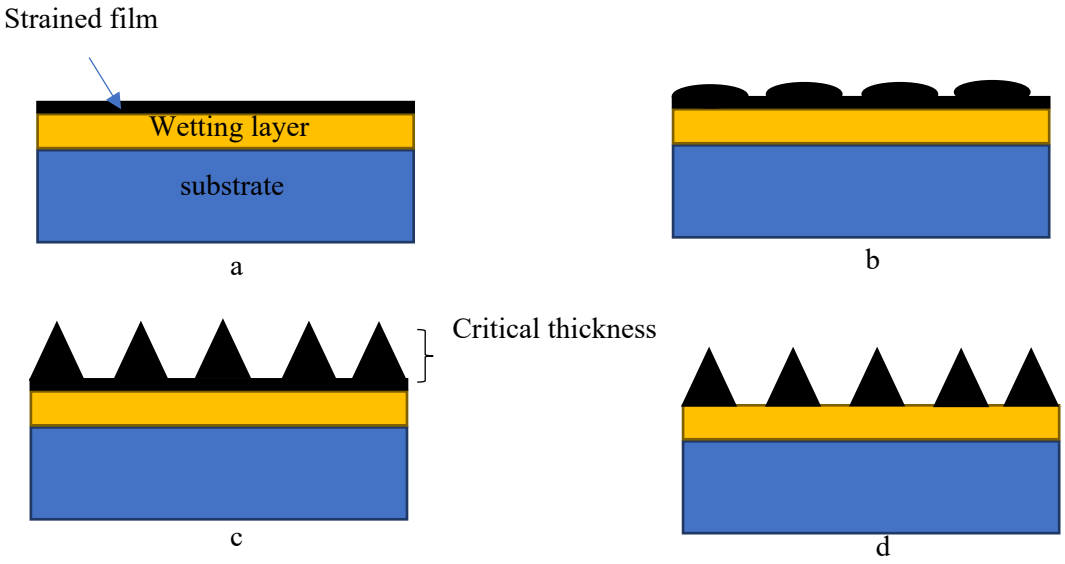

Fig 1. 5 Schematic diagram of S.K. reaction process

The surface energy has large effects in quantum dot formation process and it controls the critical thickness of the wetting layer. The critical thickness of the SK growth is increased to compensate the strained film at a higher growth temperature.

As indicated previously, the S.K. growth has been extensively studied, and a comprehensive understanding of the growth process has been developed. The published works of 1.55μm quantum dot lasers are grown mostly using S.K technique by MBE.[14], [33]–[35] However, the performance of these laser structures created by S.K using MOCVD is inferior to that of structures grown using MBE, as evidenced by a higher threshold current density and/or a lower dot density, etc.[36]–[38] Therefore, in this thesis the possibility of improving the performance of quantum dot lasers grown by MOCVD was evaluated. In addition to S.K grown lasers, lasers grown by another method, droplet epitaxy was investigated in this thesis as well.

1.4.2 Droplet epitaxy Growth

An alternative growth technique of self-assembled QDs is called droplet epitaxy. It was first introduced by Koguchi *et al*. in 1990 [39]. Droplet epitaxy has been achieved by both MBE and MOCVD and it is based on directly forming the metallic nano-sized droplets on top of the substrate which are then crystallised into QDs. It can grow QDs on lattice-matched material and potentially there is no wetting layer and thus avoids the degradation of optical properties of QD which is very promising for laser production[28].

Comparing with SK growth, which mainly relies on the lattice mismatch between the substrate and quantum dot material, droplet epitaxy does not and can therefore be applied to almost any substrate[40] and used to form QDs of materials that are lattice matched.

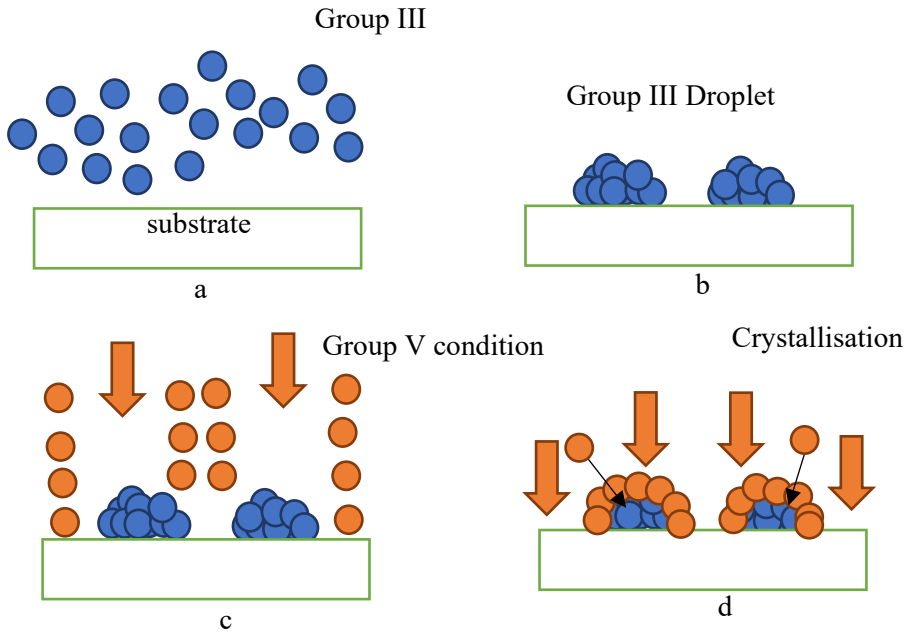

Fig 1. 6 Schematic diagram of droplet epitaxy reaction process

The droplet epitaxy process of III/V semiconductor material is generally divided into 2 steps. Firstly, a controlled amount of Group III atoms is deposited on the pre-annealed substrate and forms metal droplets on the surface under excess group III vapour conditions. The deposited atoms form bonds with the surface atoms and diffuse along the surface. The group III atoms

will coalesce together forming liquid droplet by the surface tension. The diffusion of these droplets depends on the arrangement of surface atoms and local surface energy. (Fig 1. 6a-b) Therefore, by changing the substrate misorientation and surface treatment, higher density droplets can be formed.

The next step is to supply the Group V (e.g. As) vapour to the droplet, which will react with the metal droplet and crystallised into solid. The crystallisation occurs from the outside to the core of the droplet. (Fig 1. 6d-e)

However, it has been observed that in MBE indium atoms may diffuse outwards during the crystallisation process, making quantum rings instead of quantum dots. This fluctuation in shape will cause broadening of PL[41]. Thus, it is important to control the shape of droplets in order to have an average dot-like shape rather than mixtures of dots and rings. Such diffusion is strongly depending on the substrate temperature and the Group V (As) pressure during crystallisation[42]. For high As pressure, the As diffuses into the droplet and the outermost part of the droplet is crystallised first. Whereas at low As pressure, the small droplets will migrate into larger droplets and form a ring-like structure[43]. In general, the droplets are smaller and denser when deposited on a lower substrate temperature. This is because with reduced substrate temperature, the diffusion length of atoms is reduced which makes the coalescence of large droplets reduced[28].

For MBE growth, the temperature of source and deposition are independent and hence any temperature can be used for deposition (although low temperatures come with their own problems such as incorporation of impurities). Therefore, the MBE is able to achieve very low growth temperature which favours the formation of high-density droplets. The highest QD density achieved by MBE growth is up to $7.3 \times 10^{11}/cm^2$ with deposition temperature of 30 ºC [44]. However, MOCVD is not able to achieve such low growth temperature. For example, the thermal decomposition of trimethyl gallium, the metal organic precursor for indium, is stopped when the temperature is below 250 ºC[28]. Therefore, it is very challenging to grow high-density dots by droplet epitaxy using MOCVD. It is not surprising that there are very few reports of long wavelength quantum dot lasers grown by droplet epitaxy using MOCVD compared to MBE.

Although utilising this growth technique in laser applications is challenging, the advantages of droplet epitaxy, such as growth of QDs on lattice-matched materials, the lack of a wetting layer which competes with the dots for carrier capture and gain in lasers and, in principle, a simpler epitaxy growth process due to the factoring-out of the strain component of the growth dynamics are very promising for the telecommunication industry and are the motivation for exploring this technique in this thesis. One of research topics in this project is to explore the feasibility of droplet epitaxy growth for high performance 1.55μm quantum dot lasers by MOCVD.

1.5 1.3μm & 1.55μm Quantum dot laser growth

With increasing interest in longer wavelength QD lasers, the 1.3μm & 1.55μm wavelength window both have low losses in optical fibre. Thus, it is the main wavelength for long range telecommunication[45]. Therefore, the quantum dot laser growth in this research project is focused on the 1.3 & 1.55μm wavelength range. Due to QD's 3D confinement of states and discrete energy level, QD lasers have higher differential gain, lower threshold current at room temperature and better temperature insensitivity operation compared with conventional quantum well lasers[23]. These properties make QD laser a perfect light source for the telecommunication applications.

For the development of 1.3um quantum dot lasers, there has been great interest in recent years in obtaining high gain, low threshold current quantum dot lasers at wavelength of (~1200-1300nm). The stat-of-art performance of the QD laser has been achieved especially in high temperature stability[46], room temperature operation[47] and grown on Si substrate for better integration into current Si base chips [31], [48], [49]. The lasers at 1.3um range are mostly done on the GaAs substrate and through S.K growth. This is mainly due to high lattice mismatch between the InAs QD and GaAs (~7%). However, these AlGaAs/GaAs QD lasers are usually suffering from low ground state saturation gain and often operates at excited state lasing[20], [50]. Therefore, To produce high gain, low threshold current density 1.3μm QD lasers that meet the telecommunication demand, the growth of small size, uniform and high-density quantum dots is required[51]–[53]. In general, the size of the QD is strongly dependent on the V/III ratio[54]–[57], and the QD density is strongly related to the InAs QD layer thickness and growth temperature[55], [56]. The V/III ratio has little influence on the QD density[29]. With higher V/III ratio, the shape of QD exhibits a change in shape from round to dash. This is due to the longer migration length of Indium atoms along the surface of the substrate[56]. The stacking of QD layers reduces the threshold current density and increases the optical gain due to higher optical confinement [1][22]. Vertical stacking of QD has been reported up to 8 layers[58] and the threshold current density is below 10A/cm^2 per QD layer[50]. However, it

is found to have defects accumulated as the stacked quantum layer increases. The strain field of the first QD layer would affect the layer above and the strain accumulated would alter the optical properties of the above QD layer [52], [59], [60]. This will significantly reduce the gain obtained from the higher stacking of the QD, which results in less optical gain. Another way of increasing the ground state gain of these QD lasers is to increase the quantum dot density. With InAs/AlGaAs epitaxy system, the bandgap of the structure is enough to provide the required emission wavelength with relatively high-density QD. (~$5x10^{10}/cm^2$) [53], [61], [62]. This is done through the introduction of strain reducing layer (SRL) layer into the QD active region[59], [63]–[65]. By incorporation of InGaAs (SRL) before the InAs QD growth, the highest density of the QD that can be achieved is around ~$1x10^{11}/cm^2$ with high uniformity (FWHM ~23 meV)[66]. The SRL has a strain relaxing effect between the InAs QD and the GaAs layer. This results in improved QD density and reduces the diffusion of Indium into the GaAs. The obtained laser has achieved a gain of up to ~55/cm and ground state emission above 1.3μm[62]. A double-cap procedure on InAs/InP QDs grown by MOCVD can be introduced to reduce Group III-Group V intermixing which can improve the uniformity of the quantum dots[67]. The first capping layer- FCL, which is grown at a thickness smaller than QD height, creates a lattice matched surface under Phosphorous atmosphere. The temperature of FCL is kept at the same temperature as QD growth. Then the SCL-rest of capping thickness is grown at a temperature higher than FCL after a 5min growth interruption. A 2-step growth of capping of the QDs is used to reduce the inhomogeneous of QD height which reduces the linewidth of PL. The capping layer quality can be improved by incorporation of post-annealing process[41]. The poor-quality capping layer will degrade the PL intensity and is related to the strain relaxation which will introduce dislocations to the QD layer. The critical annealing temperature that intermixing starts depends on the In composition and the density of QD[20]. Therefore, the degradation of PL can be reduced by carefully optimising the annealing temperature of the capping layer. However, all these methods have been discussed extensively. For this project, the effect of the use of substrate orientation on the growth of InAs/GaAs QD lasers has been explored. Theoretically, the misorientated substrate should have a positive influence on the

growth of the QD layer by providing a higher quality buffer layer and reducing the dislocation density[68].

Many works have been done using the S.K growth method to produce high performance of 1.55μm QD lasers by MBE growth [14], [33]–[36], [69]–[71]. The room temperature threshold current density is about 700A/cm^2 and the model gain has been reported up to ~15/cm per QD layer [72]. Although some prospects of structure design and growth technique in MBE can be applied to MOCVD growth[29], [54], [55], [73]–[75]. There is still a long way to go to achieve the MOCVD growth of similar performance 1.55μm quantum dot laser. The challenge for long wavelength QD MOCVD is the growth of capping layer which can cause a shift in emission wavelength[76]. Because MOCVD requires a relatively higher temperature for deposition than MBE, the problems of Group III-Group V intermixing in the dots during the capping layer can be severe[77]. Such effect will cause a blue shift of the wavelength and even broaden the PL linewidth, making growth of 1.55μm QD laser more difficult in MOCVD[78], [79]. One option would be to reduce the diffusion by using an alternative precursor such as tertiary-butyl-phosphine TBP instead of PH_3 to obtain lower growth temperature[29].

Although there has been a significant progress in S.K. growth of 1.55μm quantum dot laser using MOCVD in recent years[35], [36]. But the droplet growth of 1.55μm wavelength is still not researched much.[14] For droplet epitaxy at 1.55μm, the InAs QD is usually grown on the AlInAs/InP(311)A substrate[80]–[83]. In principle, the growth temperature controls the formation of the indium droplets and with lower temperatures giving higher densities[84]. In MBE, growth temperatures close to room temperature can be achieved. But in the case of MOCVD, the lowest temperature is limited to around 400 ^{o}C due to the cracking temperature of the TriMethyl Indium[28], [85]. Although a higher QD density can be obtained using MBE, droplet epitaxy of new QD optoelectronics utilising MOCVD is more commercially viable and reproducible. The reports of DE of InAs QDs directly grown on an InP substrate for MOCVD appear to have a lower density of dots ~10^9 cm^{-2} and a larger size distribution (10-30nm) than the S.K QDs and emitting at wavelengths > 2μm, making them difficult for use in telecom laser applications[85]–[88]. Thus, high quantum dot density is therefore the primary challenge for

droplet epitaxy of quantum dot lasers. However, the advantage of DE QD such as growth on lattice matched material and removal of strain effect during the formation of the dot still makes DE QDs suitable for laser application. One issue for the DE InAs QD directly grown on InP substrate is the formation of a 2D quasi-wetting layer (2D layer) [85], [88]–[90]. This quasi-wetting layer (formed by the DE process) can also compete with the QDs and reduce the available gain. In this project, an InGaAs 'interlayer' were grown between the DE dots and substrate. This way, the As-P exchange can be supressed and there is no longer a 2D quasi-wetting layer formed, and dots grown on top of this QW show a higher density and uniformity[85].

On the basis of the published figures, the growth temperature, V/III ratio, flow rate, deposition time, thickness, and material composition mentioned above cannot be applied directly. Instead, these parameters must be properly adjusted in the MOCVD systems at Sheffield University. Therefore, several growths will be required to optimise the growth parameters. Although MOCVD growth is more challenging than MBE growth, the ability to produce devices on large wafers makes MOCVD more suited for commercial production. Therefore, the realisation of MOCVD growth with minimal performance sacrifices deserves investigation. In Chapter 3, the growth of 1.1μm InAs/GaAs QD lasers on misorientated GaAs substrates is discussed. The misorientated substrate addresses the issue of the low-density dots by S.K growth and provides an important step for future realisation of 1.3μm InAs/GaAs QD laser by MOCVD. In order to extend the wavelength towards 1.55μm, the growth of a QD laser utilising MOCVD droplet epitaxy techniques are discussed in Chapter 4. The performance of such laser structures has been optimised in this thesis through simulation and experimental investigation. The ultimate objective is to develop a 1.55 μm quantum dot laser for industrial applications especially in low power high speed internet communications.

1.6 Reference

[1] G. A. Sai-Halasz, R. Tsu, and L. Esaki, 'A new semiconductor superlattice', *Appl Phys Lett*, vol. 30, no. 12, pp. 651–653, Jun. 1977, doi: 10.1063/1.89273.

[2] H. P. Rocksby, 'The Colour of Selenium Ruby Glasses', *Journal of the Society of Glass Technology*, vol. 16, 1932.

[3] A. Baskaran and P. Smereka, 'Mechanisms of Stranski-Krastanov growth', *J Appl Phys*, vol. 111, no. 4, p. 044321, Feb. 2012, doi: 10.1063/1.3679068.

[4] N. S. Beattie *et al.*, 'Design and fabrication of InAs/GaAs QD based intermediate band solar cells by quantum engineering', *2018 IEEE 7th World Conference on Photovoltaic Energy Conversion, WCPEC 2018 - A Joint Conference of 45th IEEE PVSC, 28th PVSEC and 34th EU PVSEC*, pp. 2747–2751, Nov. 2018, doi: 10.1109/PVSC.2018.8547630.

[5] N. A. Kalyuzhnyy *et al.*, 'Increasing the quantum efficiency of InAs/GaAs QD arrays for solar cells grown by MOVPE without using strain-balance technology', *Progress in Photovoltaics: Research and Applications*, vol. 24, no. 9, pp. 1261–1271, Sep. 2016, doi: 10.1002/PIP.2789.

[6] Y. Xie *et al.*, 'Highly Efficient and Thermally Stable QD-LEDs Based on Quantum Dots-SiO2-BN Nanoplate Assemblies', *ACS Appl Mater Interfaces*, vol. 12, no. 1, pp. 1539–1548, Jan. 2020, doi: 10.1021/acsami.9b18500.

[7] M. Molaei *et al.*, 'Near-white emitting QD-LED based on hydrophilic CdS nanocrystals', *J Lumin*, vol. 132, no. 2, pp. 467–473, Feb. 2012, doi: 10.1016/J.JLUMIN.2011.08.038.

[8] T. Ohtsuki and M. Matsuura, 'Wavelength Conversion of 25-Gbit/s PAM-4 Signals Using a Quantum-Dot SOA', *IEEE Photonics Technology Letters*, vol. 30, no. 5, pp. 459–462, Mar. 2018, doi: 10.1109/LPT.2018.2798645.

[9] Z. Hu, B. Xiang, and Y. Xing, 'Optical Gain Depending on Both Size Fluctuations of Quantum Dots and Temperature in InGaAs/GaAs QD-SOA', *IEEE Trans Electron Devices*, vol. 64, no. 9, pp. 3683–3689, Sep. 2017, doi: 10.1109/TED.2017.2722383.

[10] P. Kleinschmidt, S. Giblin, A. Tzalenchuk, H. Hashiba, V. Antonov, and S. Komiyama, 'Sensitive detector for a passive terahertz imager', *J Appl Phys*, vol. 99, no. 11, Jun. 2006, doi: 10.1063/1.2199107.

[11] C. M. S. Negi, D. Kumar, S. K. Gupta, and J. Kumar, 'Theoretical analysis of resonant cavity p-Type quantum dot infrared photodetector', *IEEE J Quantum Electron*, vol. 49, no. 10, pp. 839–845, 2013, doi: 10.1109/JQE.2013.2279566.

[12] M. Grundmann *et al.*, 'Low threshold, large To injection laser emission from (InGa)As quantum dots', *Electron Lett*, vol. 30, no. 17, pp. 1416–1417, Aug. 1994, doi: 10.1049/el:19940939.

[13] M. Asada, Y. Suematsu, K. Matsunaga, and H. Hirayama, 'Lasing action of Ga0.67In0.33As/GaInAsP/InP tensile-strained quantum-box laser', *Electron Lett*, vol. 30, no. 2, pp. 142–143, Jan. 1994, doi: 10.1049/el:19940082.

[14] S. Banyoudeh *et al.*, 'High-bandwidth temperature-stable 1.55-μm quantum dot lasers', Feb. 2017, vol. 10123, p. 1012306. doi: 10.1117/12.2255749.

[15] C. Bentham *et al.*, 'Single-photon electroluminescence for on-chip quantum networks', *Appl Phys Lett*, vol. 109, no. 16, Oct. 2016, doi: 10.1063/1.4965295.

[16] L. Sapienza, M. Davanço, A. Badolato, and K. Srinivasan, 'Nanoscale optical positioning of single quantum dots for bright and pure single-photon emission', *Nat Commun*, vol. 6, no. 1, pp. 7833–7833, Jul. 2015, doi: 10.1038/ncomms8833.

[17] R. Katsumi *et al.*, 'Quantum-dot single-photon source on a CMOS silicon photonic chip integrated using transfer printing', *APL Photonics*, vol. 4, no. 3, Mar. 2019, doi: 10.1063/1.5087263.

[18] O. Qasaimeh, 'Effect of inhomogeneous line broadening on gain and differential gain of quantum dot lasers', *IEEE Trans Electron Devices*, vol. 50, no. 7, pp. 1575–1581, 2003, doi: 10.1109/TED.2003.813907.

[19] H. Y. Liu *et al.*, 'Improved performance of 1.3μm multilayer InAs quantum-dot lasers using a high-growth-temperature GaAs spacer layer', *Appl Phys Lett*, vol. 85, no. 5, pp. 704–706, Aug. 2004, doi: 10.1063/1.1776631.

[20] D. Guimard *et al.*, 'Ground state lasing at 1.30 μm from InAs/GaAs quantum dot lasers grown by metal–organic chemical vapor deposition', *Nanotechnology*, vol. 21, no. 10, p. 105604, Mar. 2010, doi: 10.1088/0957-4484/21/10/105604.

[21] Y. Arakawa and H. Sakaki, 'Multidimensional quantum well laser and temperature dependence of its threshold current', *Appl Phys Lett*, vol. 40, no. 11, pp. 939–941, Jun. 1982, doi: 10.1063/1.92959.

[22] Dieter. Bimberg, Marius. Grundmann, and N. N. Ledentsov, *Quantum dot heterostructures*. John Wiley, 1999.

[23] 'Quantum Wells, Wires and Dots : Theoretical and Computational Physics of Se...: EBSCOhost'. https://web.p.ebscohost.com/ehost/detail/detail?vid=0&sid=bb8ffe96-503f-4ecf-8fd2-6762e8f848dc%40redis&bdata=JnNpdGU9ZWhvc3QtbGl2ZQ%3d%3d#AN=141706&db=nlebk (accessed Aug. 10, 2022).

[24] J. A. A.Y. Cho, 'Molecular beam epitaxy', *Progress in Solid State Chemistry*, vol. 10, pp. 157–191, 1975.

[25] H. M. Manasevit, F. M. Erdmann, and W. I. Simpson, 'The Use of Metalorganics in the Preparation of Semiconductor Materials', *J Electrochem Soc*, vol. 118, no. 11, p. 1864, Nov. 1971, doi: 10.1149/1.2407853.

[26] M. Paul *et al.*, 'Single-photon emission at 1.55 μ m from MOVPE-grown InAs quantum dots on InGaAs/GaAs metamorphic buffers', *Appl Phys Lett*, 2017, doi: 10.1063/1.4993935.

[27] M. A. Surnina, R. Kh. Akchurin, A. A. Marmalyuk, T. A. Bagaev, and A. L. Sizov, 'Growing InAs/GaAs quantum dots by droplet epitaxy under MOVPE conditions', *Technical Physics Letters*, 2016, doi: 10.1134/S1063785016070294.

[28] R. Kh. Akchurin *et al.*, 'Formation conditions for InAs/GaAs quantum dot arrays by droplet epitaxy under MOVPE conditions', *Technical Physics*, 2014, doi: 10.1134/S1063784214010034.

[29] D. Franke, P. Harde, J. Boettcher, M. Moehrle, A. Sigmund, and H. Kuenzel, 'Improved emission wavelength reproducibiliy of InP-based all movpe grown 1.55 ??m quantum dot lasers', in *Conference Proceedings - International Conference on Indium Phosphide and Related Materials*, 2007. doi: 10.1109/ICIPRM.2007.381252.

[30] D. Guimard *et al.*, 'Ground state lasing at 1.30νm from InAs/GaAs quantum dot lasers grown by metal-organic chemical vapor deposition', *Nanotechnology*, 2010, doi: 10.1088/0957-4484/21/10/105604.

[31] D. Jung *et al.*, 'High efficiency low threshold current 1.3 μm InAs quantum dot lasers on on-axis (001) GaP/Si', *Appl Phys Lett*, vol. 111, no. 12, p. 122107, Sep. 2017, doi: 10.1063/1.4993226.

[32] Y. Tu and J. Tersoff, 'Origin of Apparent Critical Thickness for Island Formation in Heteroepitaxy', *Phys Rev Lett*, vol. 93, no. 21, p. 216101, Nov. 2004, doi: 10.1103/PhysRevLett.93.216101.

[33] S. Banyoudeh *et al.*, 'Temperature-insensitive high-speed directly modulated 1.55-μm quantum dot lasers', *IEEE Photonics Technology Letters*, 2016, doi: 10.1109/LPT.2016.2600508.

[34] E. Lee *et al.*, 'Characteristics of InAs/InGaAsP quantum dot laser diodes lasing at 1.55um', Feb. 2007, vol. 6485, p. 64850K. doi: 10.1117/12.701534.

[35] D. Gready *et al.*, 'High speed 1.55 inas/ingaalas/inp quantum dot lasers', *IEEE Photonics Technology Letters*, 2014, doi: 10.1109/LPT.2013.2287502.

[36] D. Franke *et al.*, *IMPROVED OPTICAL CONFINEMENT IN 1.55 fJrn InAs/GaInAsP QUANTUM DOT LASERS GROWN BY MOVPE*.

[37] D. Franke, P. Harde, J. Boettcher, M. Moehrle, A. Sigmund, and H. Kuenzel, 'Improved Emission Wavelength Reproducibiliy of InP-Based All Movpe Grown 1.55 μm Quantum Dot Lasers', in *2007 IEEE 19th International Conference on Indium Phosphide & Related Materials*, May 2007, pp. 559–562. doi: 10.1109/ICIPRM.2007.381252.

[38] F. Wenning, H. Kuenzel, and U. W. Pohl, *EFFECT OF MOVPE GROWTH CONDITIONS ON THE FORMATION OF SELF-ORGANIZED InAs/InGaAsP/InP QUANTUM DOTS*.

[39] R. Oga, W. S. Lee, Y. Fujiwara, and Y. Takeda, '<title>Room-temperature electroluminescence at 1.55 μm from InAs quantum dots grown on (001) InP by droplet hetero-epitaxy</title&gt';, Jun. 2002, pp. 15–18. doi: 10.1117/12.510424.

[40] M. Jo, T. Mano, Y. Sakuma, and K. Sakoda, 'Extremely high-density GaAs quantum dots grown by droplet epitaxy', *Appl Phys Lett*, vol. 100, no. 21, p. 212113, May 2012, doi: 10.1063/1.4721663.

[41] T. Mano *et al.*, 'Ring-shaped GaAs quantum dot laser grown by droplet epitaxy: Effects of post-growth annealing on structural and optical properties', *J Cryst Growth*, vol. 301–302, no. SPEC. ISS., pp. 740–743, Apr. 2007, doi: 10.1016/J.JCRYSGRO.2006.11.216.

[42] E. Cohen *et al.*, 'Structure of droplet-epitaxy-grown InAs/GaAs quantum dots', *Appl Phys Lett*, 2011, doi: 10.1063/1.3599063.

[43] Á. Nemcsics *et al.*, 'Composition of the "gaAs" quantum dot, grown by droplet epitaxy', *Superlattices Microstruct*, 2010, doi: 10.1016/j.spmi.2010.07.006.

[44] M. Jo, T. Mano, Y. Sakuma, and K. Sakoda, 'Extremely high-density GaAs quantum dots grown by droplet epitaxy', *Appl Phys Lett*, 2012, doi: 10.1063/1.4721663.

[45] S. J. Sweeney, A. F. Phillips, A. R. Adams, E. P. O'Reilly, and P. J. A. Thijs, 'The effect of temperature dependent processes on the performance of 1.5-μm compressively strained InGaAs(P) MQW semiconductor diode lasers', *IEEE Photonics Technology Letters*, vol. 10, no. 8, pp. 1076–1078, Aug. 1998, doi: 10.1109/68.701507.

[46] C. sen Lee, T. Frost, W. Guo, and P. Bhattacharya, 'High temperature stable operation of 1.3-μm quantum-dot laser integrated with single-mode tapered Si

3N 4 waveguide', *IEEE Photonics Technology Letters*, vol. 24, no. 11, pp. 918–920, 2012, doi: 10.1109/LPT.2012.2190823.

[47] I. R. Sellers *et al.*, '1.3 μm InAs/GaAs multilayer quantum-dot laser with extremely low room-temperature threshold current density', *Electron Lett*, vol. 40, no. 22, pp. 1412–1413, Oct. 2004, doi: 10.1049/EL:20046692.

[48] K. Li *et al.*, 'O-band InAs/GaAs quantum dot laser monolithically integrated on exact (0 0 1) Si substrate', 2019, doi: 10.1016/j.jcrysgro.2019.01.016.

[49] N. Prtljaga *et al.*, 'Monolithic integration of a quantum emitter with a compact on-chip beam-splitter', *Appl Phys Lett*, 2014, doi: 10.1063/1.4883374.

[50] H. Shimizu, S. Saravanan, J. Yoshida, S. Ibe, and N. Yokouchi, 'InAs quantum dot lasers with extremely low threshold current density (7 A/cm2/layer)', *Japanese Journal of Applied Physics, Part 2: Letters*, vol. 44, no. 33–36, Aug. 2005, doi: 10.1143/JJAP.44.L1103.

[51] I. M. E. Butler *et al.*, 'Size anisotropy inhomogeneity effects in state-of-the-art quantum dot lasers', *Appl Phys Lett*, vol. 113, no. 1, Jul. 2018, doi: 10.1063/1.5021774.

[52] J. Tatebayashi, Y. Ota, S. Ishida, M. Nishioka, S. Iwamoto, and Y. Arakawa, 'Highly uniform, multi-stacked InGaAs/GaAs quantum dots embedded in a GaAs nanowire', *Appl Phys Lett*, vol. 105, no. 10, Sep. 2014, doi: 10.1063/1.4895597.

[53] T. Amano, T. Sugaya, S. Yamauchi, and K. Komori, 'Realization of 1.3 μm InAs quantum dots with high-density, uniformity, and quality', *J Cryst Growth*, vol. 295, no. 2, pp. 162–165, Oct. 2006, doi: 10.1016/J.JCRYSGRO.2006.08.004.

[54] K. Kawaguchi *et al.*, 'Fabrication of InAs quantum dots on InP(100) by metalorganic vapor-phase epitaxy for 1.55 μm optical device applications', in *Applied Physics Letters*, 2004. doi: 10.1063/1.1814442.

[55] N. Weir, R. Yao, C.-S. Lee, and W. Guo, 'Effects of thickness and V/III ratio of low temperature capping layer growth to the optical properties of InAs quantum dots', *Journal of Vacuum Science & Technology B, Nanotechnology and*

Microelectronics: Materials, Processing, Measurement, and Phenomena, vol. 34, no. 4, p. 041223, Jul. 2016, doi: 10.1116/1.4954000.

[56] T. Alzoubi, M. Usman, M. Benyoucef, and J. P. Reithmaier, 'Growth of InAs quantum dots and dashes on silicon substrates: Formation and characterization', *J Cryst Growth*, vol. 323, no. 1, pp. 422–425, May 2011, doi: 10.1016/J.JCRYSGRO.2010.11.170.

[57] Z. Shi, L. Huang, Y. Yu, P. Tian, and H. Wang, 'Influence of V/III ratio on QD size distribution', *Frontiers of Optoelectronics in China*, vol. 4, no. 4, pp. 364–368, Dec. 2011, doi: 10.1007/S12200-011-0180-7.

[58] S. Anantathanasarn *et al.*, 'Stacking, polarization control, and lasing of wavelength tunable (1.55μm region) InAs/InGaAsP/InP (100) quantum dots', *J Cryst Growth*, vol. 298, pp. 553–557, Jan. 2007, doi: 10.1016/j.jcrysgro.2006.10.173.

[59] S. R. Shriram *et al.*, 'The role and growth of strain – reducing layer by molecular -beam epitaxy in a multi – stack InAs/(In,Ga)As sub - monolayer quantum dot heterostructure', *Opt Mater (Amst)*, vol. 114, Apr. 2021, doi: 10.1016/J.OPTMAT.2021.110817.

[60] A. Matsumoto, 'Influence and its Optimal Design of Number of Stacked Layer in Quantum-Dot Lasers', *Physica status solidi. A, Applications and materials science*, vol. 216, no. 1, pp. 1800502-n/a, Jan. 2019.

[61] S. Banyoudeh and J. P. Reithmaier, 'High-density 1.54 μm InAs/InGaAlAs/InP(100) based quantum dots with reduced size inhomogeneity', *J Cryst Growth*, vol. 425, pp. 299–302, Sep. 2015, doi: 10.1016/J.JCRYSGRO.2015.03.027.

[62] T. Amano, '1.3-μm InAs quantum-dot laser with high dot density and high uniformity', *IEEE photonics technology letters*, vol. 18, no. 4, pp. 619–621, Feb. 2006.

[63] S. Anantathanasarn, R. Nötzel, P. J. van Veldhoven, T. J. Eijkemans, and J. H. Wolter, 'Wavelength-tunable (1.55-μm region) InAs quantum dots in

InGaAsP/InP (100) grown by metal-organic vapor-phase epitaxy', *J Appl Phys*, vol. 98, no. 1, Jul. 2005, doi: 10.1063/1.1938271.

[64] T. v. Hakkarainen, A. Schramm, J. Tommila, and M. Guina, 'The effect of InGaAs strain-reducing layer on the optical properties of InAs quantum dot chains grown on patterned GaAs(100)', *J Appl Phys*, vol. 111, no. 1, Jan. 2012, doi: 10.1063/1.3675271.

[65] Y. M. Liu, Z. Y. Yu, and X. M. Ren, 'Influence of strain-reducing layer on strain distribution of self-organized InAs/GaAs quantum dot and redshift of photoluminescence wavelength', *Chinese Physics Letters*, vol. 25, no. 5, pp. 1850–1853, May 2008, doi: 10.1088/0256-307X/25/5/089.

[66] T. Amano, S. Aoki, T. Sugaya, K. Komori, and Y. Okada, 'Laser characteristics of 1.3-μm quantum dots laser with high-density quantum dots', *IEEE Journal on Selected Topics in Quantum Electronics*, vol. 13, no. 5, pp. 1273–1278, Sep. 2007, doi: 10.1109/JSTQE.2007.903845.

[67] S. Luo, H.-M. Ji, X.-G. Yang, and T. Yang, 'Impact of double-cap procedure on the characteristics of InAs/InGaAsP/InP quantum dots grown by metal-organic chemical vapor deposition', *J Cryst Growth*, vol. 375, pp. 100–103, Jul. 2013, doi: 10.1016/j.jcrysgro.2013.04.024.

[68] J. Lee, 'Influences of crystallographic misorientation of GaAs substrateson misfit stresses and microhardness of InGaP epilayers', *Thin Solid Films*, vol. 320, no. 2, pp. 173–178, May 1998, doi: 10.1016/S0040-6090(97)00467-7.

[69] S. Bhowmick, M. Z. Baten, T. Frost, B. S. Ooi, and P. Bhattacharya, 'High performance InAs/In0.53Ga0.23Al 0.24As/InP quantum dot 1.55 μ tunnel injection laser', *IEEE J Quantum Electron*, vol. 50, no. 1, pp. 7–14, Jan. 2014, doi: 10.1109/JQE.2013.2290943.

[70] P. J. Poole, K. Kaminska, P. Barrios, Z. Lu, and J. Liu, 'Growth of InAs/InP-based quantum dots for 1.55 μm laser applications', *J Cryst Growth*, 2009, doi: 10.1016/j.jcrysgro.2009.01.129.

[71] S. A. Sayid, I. P. Marko, S. J. Sweeney, P. Barrios, and P. J. Poole, 'Efficiency limiting processes in 1.55 μm InAs/InP-based quantum dots lasers', *Appl Phys Lett*, 2010, doi: 10.1063/1.3504253.

[72] V. I. Sichkovskyi, M. Waniczek, and J. P. Reithmaier, 'High-gain wavelength-stabilized 1.55 μ m InAs/InP(100) based lasers with reduced number of quantum dot active layers', *Appl Phys Lett*, vol. 102, no. 22, p. 221117, Jun. 2013, doi: 10.1063/1.4809730.

[73] D. González *et al.*, 'Evaluation of different capping strategies in the InAs/GaAs QD system: Composition, size and QD density features', *Appl Surf Sci*, vol. 537, Jan. 2021, doi: 10.1016/J.APSUSC.2020.148062.

[74] X. Yan, X. Zhang, J. Li, J. Cui, and X. Ren, 'Controllable growth and optical properties of InP and InP/InAs nanostructures on the sidewalls of GaAs nanowires', *J Appl Phys*, 2014.

[75] C. Carmesin *et al.*, 'Interplay of morphology, composition, and optical properties of InP-based quantum dots emitting at the 1.55 μ m telecom wavelength', *Phys Rev B*, 2017, doi: 10.1103/PhysRevB.96.235309.

[76] K. Park *et al.*, 'The emission wavelength tuning of InAs/InP quantum dots with thin GaAs, InGaAs, InP capping layers by MOCVD', *Physica E Low Dimens Syst Nanostruct*, vol. 26, no. 1–4, pp. 169–173, Feb. 2005, doi: 10.1016/J.PHYSE.2004.08.046.

[77] E. C. Weiner *et al.*, 'Effect of capping procedure on quantum dot morphology: Implications on optical properties and efficiency of InAs/GaAs quantum dot solar cells', *Solar Energy Materials and Solar Cells*, vol. 178, pp. 240–248, May 2018, doi: 10.1016/J.SOLMAT.2018.01.028.

[78] T. Li *et al.*, 'The effect of growth temperature on InAs quantum dots grown by MOCVD', *2011 Asia Communications and Photonics Conference and Exhibition, ACP 2011*, 2011, doi: 10.1117/12.917614.

[79] Y. Sakuma, K. Takemoto, S. Hirose, T. Usuki, and N. Yokoyama, 'Controlling emission wavelength from InAs self-assembled quantum dots on InP (0 0 1)

during MOCVD', *Physica E Low Dimens Syst Nanostruct*, vol. 26, no. 1–4, pp. 81–85, Feb. 2005, doi: 10.1016/J.PHYSE.2004.08.028.

[80] R. Oga, W. S. Lee, Y. Fujiwara, and Y. Takeda, 'Room-temperature electroluminescence at 1.55 μm from InAs quantum dots grown on (001) InP by droplet hetero-epitaxy', Jun. 2002, vol. 5023, pp. 15–18. doi: 10.1117/12.510424.

[81] N. Ha, T. Mano, S. Dubos, T. Kuroda, Y. Sakuma, and K. Sakoda, 'Single photon emission from droplet epitaxial quantum dots in the standard telecom window around a wavelength of 1.55 μm', *Applied Physics Express*, vol. 13, no. 2, Feb. 2020, doi: 10.35848/1882-0786/AB6E0F.

[82] N. Ha *et al.*, 'Droplet epitaxy growth of telecom InAs quantum dots on metamorphic InAlAs/GaAs(111)A', *Jpn J Appl Phys*, vol. 54, no. 4, Apr. 2015, doi: 10.7567/JJAP.54.04DH07.

[83] N. Ha, '1.55 μm photon emission from droplet epitaxy InAs quantum dots on InP(111)A', *JSAP Annual Meetings Extended Abstracts*, pp. 962–962, Feb. 2020.

[84] J. H. Lee, Z. M. Wang, and G. J. Salamo, 'The control on size and density of InAs QDs by droplet epitaxy (april 2009)', *IEEE Trans Nanotechnol*, vol. 8, no. 4, pp. 431–436, Jul. 2009, doi: 10.1109/TNANO.2009.2021654.

[85] E. M. Sala, M. Godsland, Y. I. Na, A. Trapalis, and J. Heffernan, 'Droplet epitaxy of InAs/InP quantum dots via MOVPE by using an InGaAs interlayer', *Nanotechnology*, vol. 33, no. 6, pp. 65601-, Nov. 2021, doi: 10.1088/1361-6528/ac3617.

[86] R. Kh. Akchurin *et al.*, 'Formation conditions for InAs/GaAs quantum dot arrays by droplet epitaxy under MOVPE conditions', *Technical Physics*, vol. 59, no. 1, pp. 78–84, Jan. 2014, doi: 10.1134/S1063784214010034.

[87] E. M. (orcid:0000-0001-8116-8830) Sala, 'Effect of cap thickness on InAs/InP quantum dots grown by droplet epitaxy in metal–organic vapor phase epitaxy', 2021.

[88] P. Holewa *et al.*, 'Droplet epitaxy symmetric InAs/InP quantum dots for quantum emission in the third telecom window: morphology, optical and

electronic properties', *Nanophotonics*, vol. 11, no. 8, pp. 1515–1526, Mar. 2022, doi: 10.1515/NANOPH-2021-0482.

[89] D. Fuster, K. Abderrafi, B. Alén, Y. González, L. Wewior, and L. González, 'InAs nanostructures grown by droplet epitaxy directly on InP(001) substrates', *J Cryst Growth*, vol. 434, pp. 81–87, Jan. 2016, doi: 10.1016/J.JCRYSGRO.2015.11.003.

[90] R. S. R. Gajjela *et al.*, 'Study of Size, Shape, and Etch pit formation in InAs/InP Droplet Epitaxy Quantum Dots', *Nanotechnology*, vol. 33, no. 30, pp. 305705-, Jul. 2022, doi: 10.1088/1361-6528/ac659e.

Chapter 2: Quantum dot laser fabrication and gain characterisation technique

In the development of both ~1.1 μm lasers and ~1.55 μm lasers, a number of characterisation techniques were applied on fabricated lasers and mesa diode structures. This chapter introduces the fabrication methods and the techniques used for laser characterisation, gain measurements etc. Different types of devices were fabricated and characterised which allows for an assessment of fabrication skills. The characterisation of laser includes continuous IV, pulsed LI, room temperature EL spectral response and mesa diode EL spectrum. The Multisection Gain measurement is carried out and different measuring methods are compared and accessed for later use in this project.

2.1 Broad area QD laser fabrication

This section describes the fabrication process for broad area laser used in this thesis. The broad area laser device is used to determine the basic electrical & optical properties of the fabricated samples. The threshold current, internal quantum efficiency, internal loss and spectrum can be obtained from the broad area laser. The fabrication process is simpler than other processes and thus could provide fast analysis for the optimisation of growth.

1. Fabrication process

The fabrication process is carried out in the clean room including cleaning, ridges photolithography, contact metal deposition, lift-off, annealing, etch photolithography, wet etch, back contact deposition, cleave, and mount. The schematic diagram of each step is shown in Fig 2. 1 below.

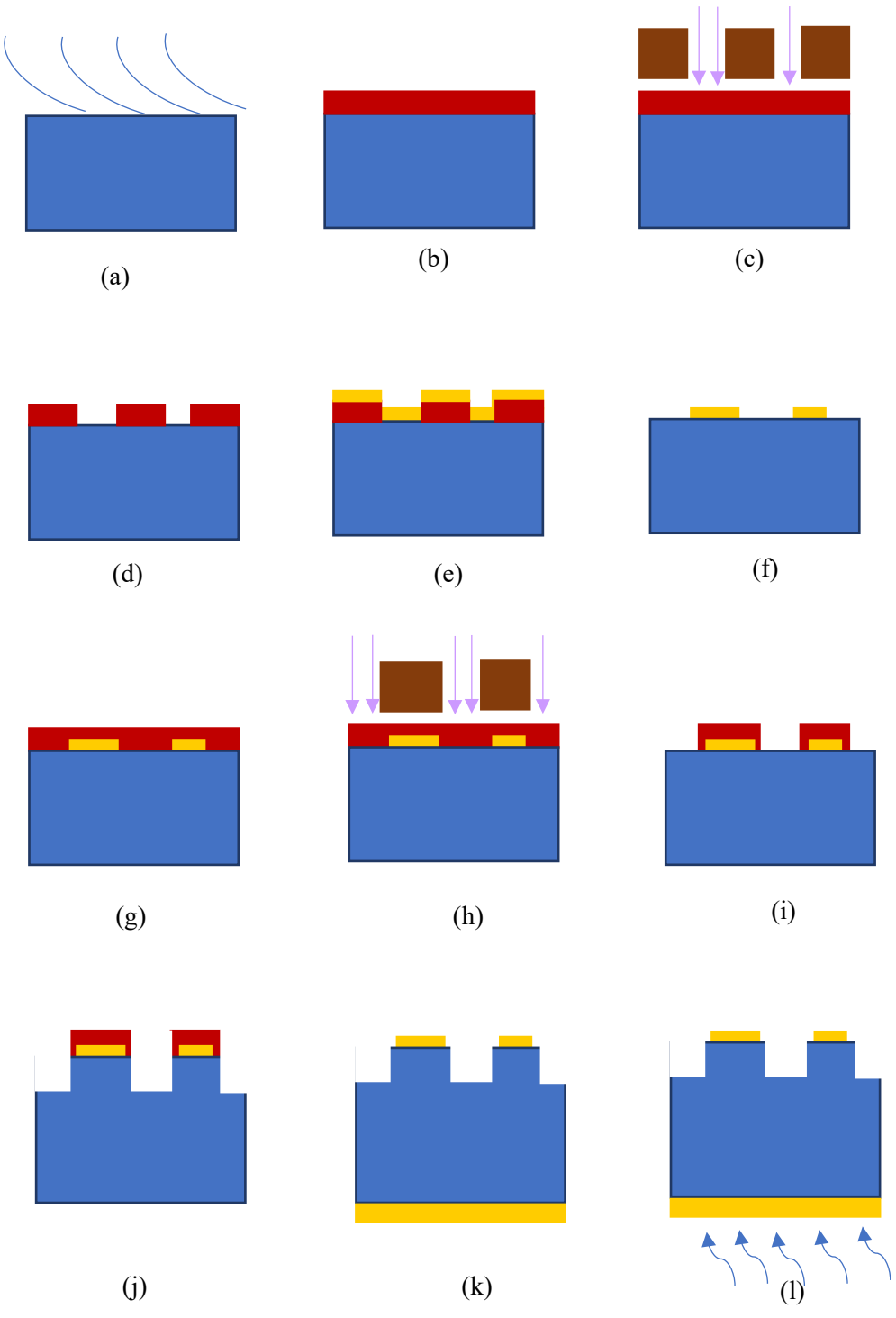
(a)
(b)
(c)
(d)
(e)
(f)
(g)
(h)
(i)
(j)
(k)
(l)
Semiconductor
Photoresist
Contact metal
Mask
UV light

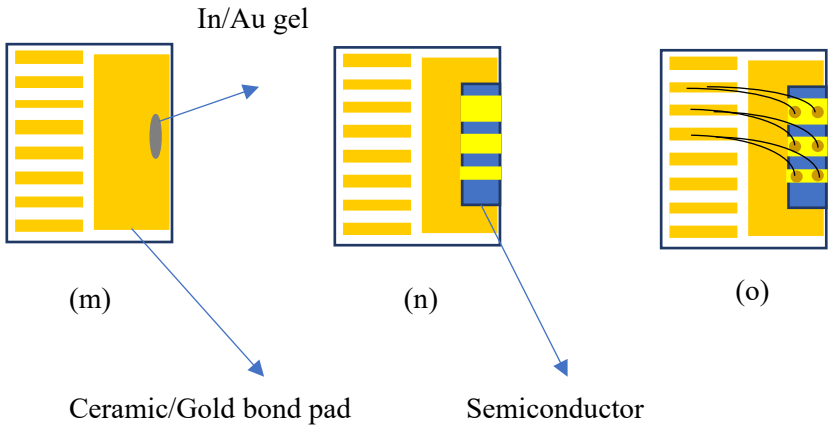

Fig 2. 1 Schematic diagram of broad area laser fabrication process

Firstly, the sample is scribed from a 2-inch wafer and cleaned using n-butyl, acetone and IPA solvent (a). After 2 min of O_2 ashing, the sample is placed under the microscope to check if the surface is clean enough for photolithography. The 3-stage clean and O_2 ash are repeated as necessary if there are any large dust or particles on the surface of the sample.

The first step of lithography is to spin the photoresist on the surface of the sample. Before the spinning, the sample is placed on the 100-degree hotplate and baked for 1min to remove any water on the surface of samples. Then HDMS and photoresist (SPR350) are spun on the surface using spinner (b). The sample is then exposed under UV 400 light for 13s, with Mask on top the sample to transform ridge pattern onto the photoresist (c). Finally, the sample is placed in the MF26A developer solution for 1min. The part of photoresist that is exposed to the UV is removed and 100/80/50 um laser bars are formed on the sample (d).

The Au/Zn/Au is deposited on the surface of the sample with a thickness of 5/20/200 nm using a thermal evaporator (e). This forms the top contact of the laser. Then, the sample is placed in acetone for a few hours. This process is called " lift-off ", because the metal and the photoresist underneath are removed. Now, only the 100/80/50 μm laser bars are covered with metal contact (f).

The second photolithography protects the contact window from the wet-etch. Thus, it needs perfect alignment with the previous pattern (g-h). The wet etch uses a H_2SO_4:H_2O_2:H_2O (1:8:80) acid to etch the ridges all the way down to the depth just above the active region of the QD

sample (i). This process creates the waveguide which creates the optically guided and amplified mode required for laser operation (j).

The back contact (InGe/Au) is then deposited on the backside of the sample using a thermal evaporator with a thickness of (20/250nm) (k). The sample is then annealed at 360^{o}C to improve the back-contact quality.

The sample is then scribed into small pieces with cavity length of 4mm using a scriber machine. A tiny bit of In/Au gel is used to hold the sample on the ceramic pad (m-n). Each laser bar is bonded to the contact tip of the ceramic pad using several gold wires. This process will spread the power along the laser bar to prevent the device breakdown from high current injection (o).

Fig 2.2 & 2.3 shows the microscope & SEM image of broad area laser fabricated. SEM image shows a nice cleaved facet and etching is uniform. From the SEM images it can thus be confirmed that the fabrication quality is good.

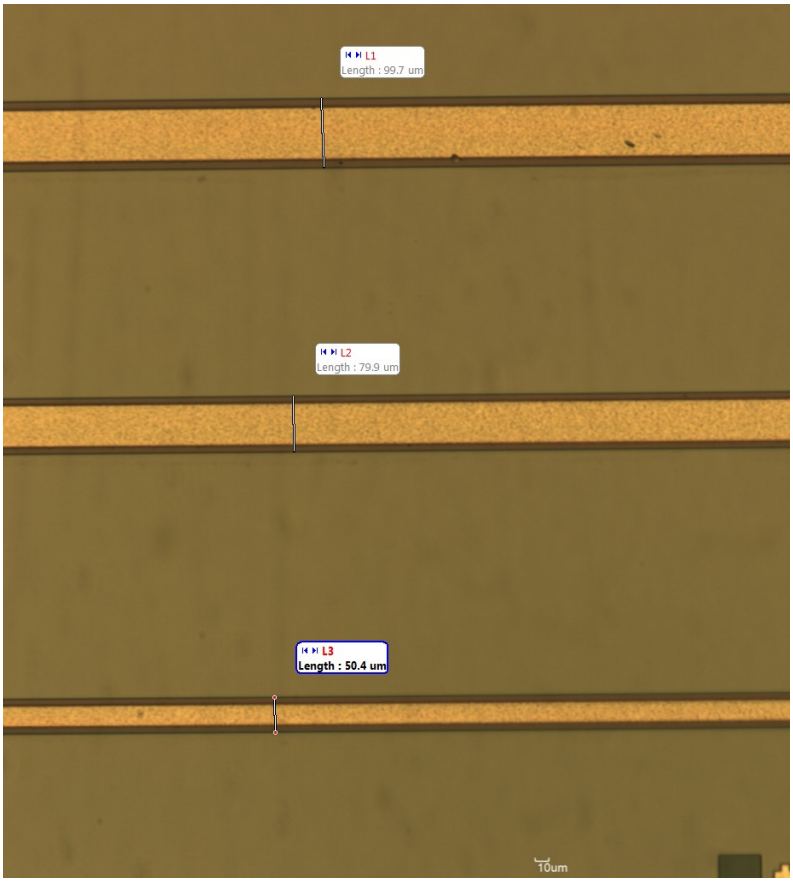

Fig 2. 2 Typical broad area laser fabricated with laser width of 100µm, 80µm, 50µm. The measured length is within the error of lithography.

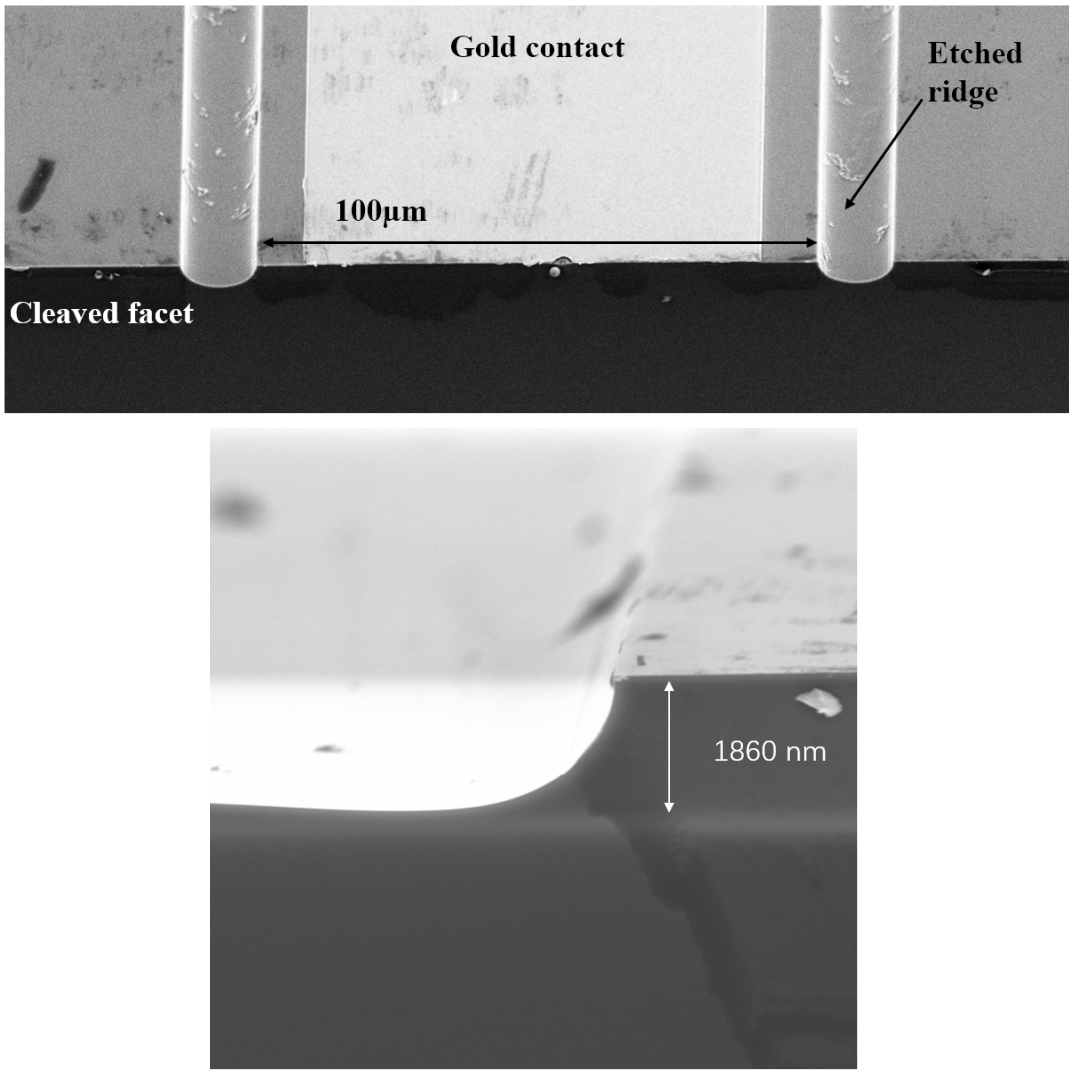

Fig 2. 3 SEM images of broad area laser fabricated. The cleaved fact is smooth without any damage. The ridge is wet etch at depth of 1860nm with require at 1900nm

2.2 Narrow ridge & multi-section QD laser fabrication

The fabrication process of the narrow ridge and muti-section QD lasers is shown below. The process is more complicated than broad area laser due to dielectric etching and photolithography processes. The fabricated devices have a ridge width of ~7μm which is narrower enough to suppress the multimode behaviour of the laser spectrum compared with broad area laser device, thus providing a single mode spectrum which is essential for precise optical measurements. The steps of multi-section devices are similar to the fabrication of the narrow ridge lasers which will be discussed in later section.

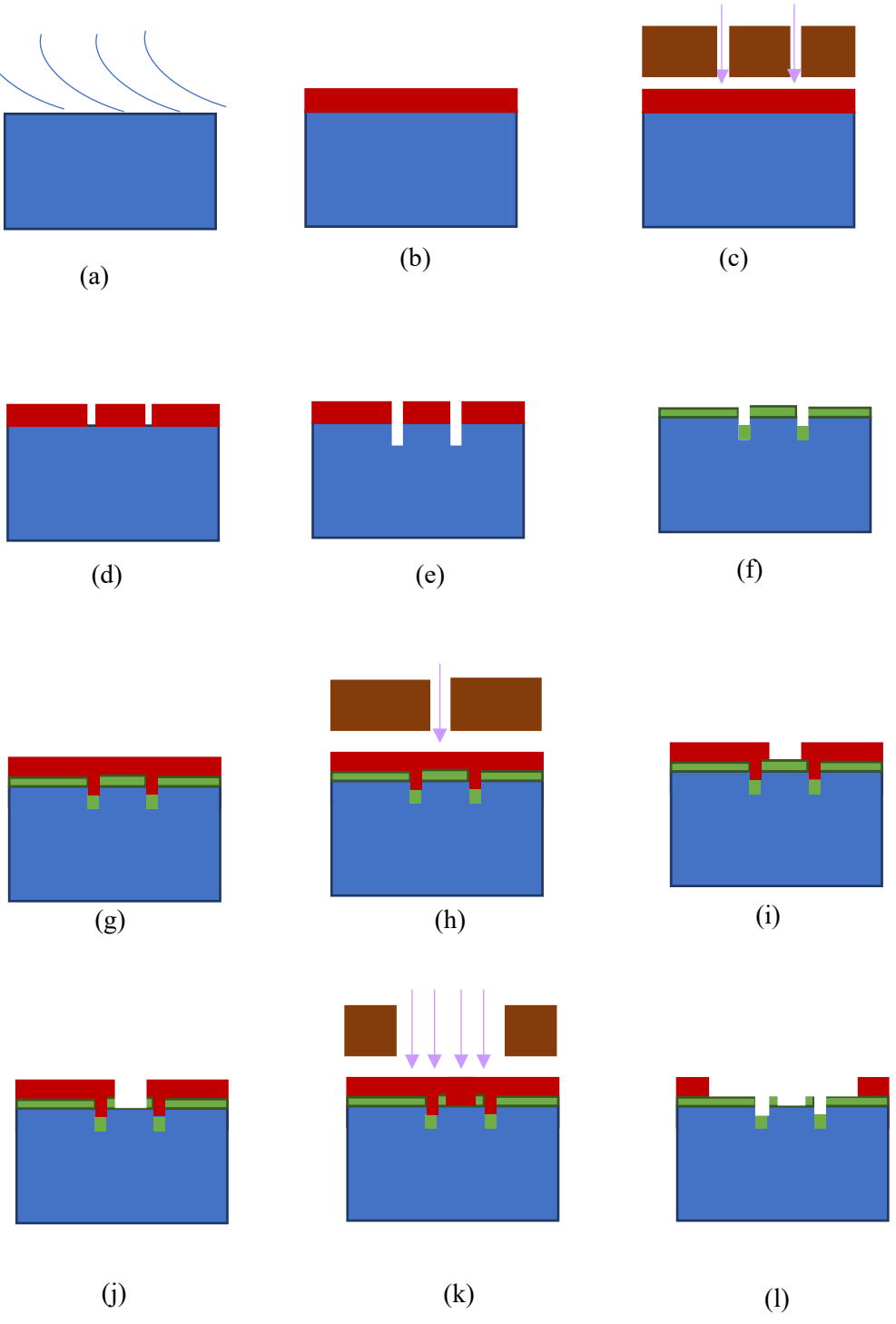
(a)
(b)
(c)
(d)
(e)
(f)
(g)
(h)
(i)
(j)
(k)
(l)
Silicon Nitride
Semiconductor
Photoresist
Contact metal
Mask
UV light

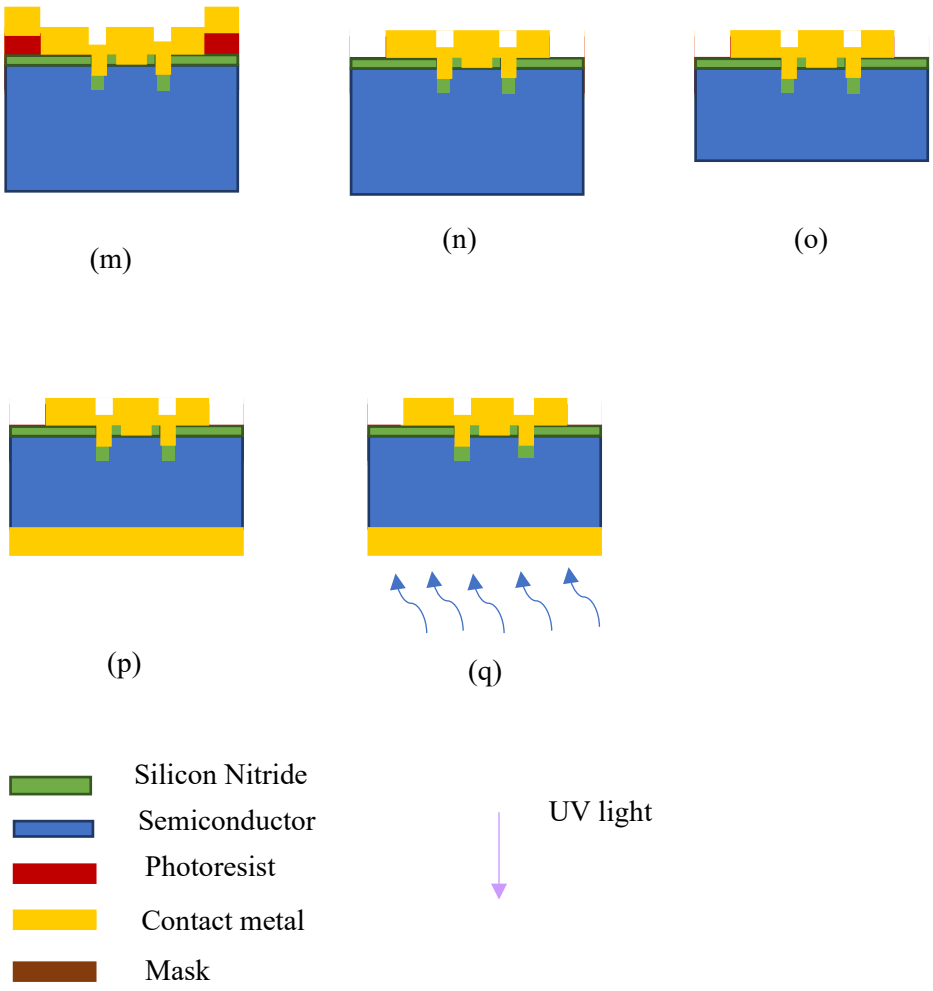

Fig 2. 4 Schematic diagram of narrow ridge laser fabrication process

1. Fabrication process

The fabrication process for narrow ridge (5um) lasers compared with broad area lasers is quite difficult. and will discuss in detail in multisection device later. Not only does it require more steps, but also it takes more time for each step. However, due to its narrow ridge nature, the QD laser will use less current and hence suffer less from thermal problems. Therefore, the threshold current is reduced. They also reduce the number of transverse laser modes which gives a better spectrum.

Firstly, the sample is cleaved and 3-stage cleaned as for broad area laser fabrication (a). After 2mins of O_2 ashing, the HDMS is spun on to the sample after being heated on the 100-degree hotplate for 1min. HDMS provides a stronger adhesion between the photoresist and sample surface (b). Then followed by the standard photolithography procedure, the 5μm narrow ridge pattern is formed on the sample (c-d). The sample is etched to a certain depth using ICP etcher (e). The etched sample is then checked under a microscope for optical inspection and the etch depth is checked using SEM for further investigation. The photoresist is removed using acetone and 5mins O_2 Asher.

The 500nm Silicon Nitride dielectric layer is deposited using PECVD (f). It is used to protect the ridges from the ICP etch. Then the contact window lithography is performed and etched using ICP (i-j). The windows should be in the middle of the ridge.

The third photolithography is used to pattern the laser bar onto the sample using PMGI and SPR350 as photoresist (k-l).

After rinsing in the diluted Ammonia solution, the top metal contact is deposited on the sample using a evaporator machine, the composition and thickness of the metal contact is same as the broad area laser process (m). Then the sample is lift-off in the acetone (n).

The sample is coated with a thick photoresist using SPR220 and sticked onto a metal plate using wax with backside pointing upwards. The thickness is recorded. The sample is polished using a MINIMET polisher and thinned for 150μm (o).

After the thinning, the sample is loaded into the evaporator for back contact metal deposition. The thickness of the InGe/Gold is 280nm (p). The sample is then annealed at 360^{o}C to lower the resistance of metal contact (q). The mounting and bonding process is carried out in the same way as broad area laser fabrication.

2.3 Characterization Technique

2.3.1 I/V and Pulse LI

The most important characterisation of quantum dot laser devices was measuring the amount of light generated by injecting a current. This measurement is called testing the Output Power-Current curve (L.I.). The IV characteristic of the device is also recorded to compare the turn-on voltage, on-state resistance and reverse leakage current. The measurement setup for pulsed LI and continuous IV includes a prob station, current source and a power meter. The broad area laser sample was fabricated from a 3-layer InAs/GaAs QD laser with 50, 80, 100 µm ridge width and a cavity length of 4mm. The sample is probed at top metal-contacts and the ground is at the bottom. The IV curves of 3-layer InAs/GaAs QD broad area laser are shown in Fig 2. 5.

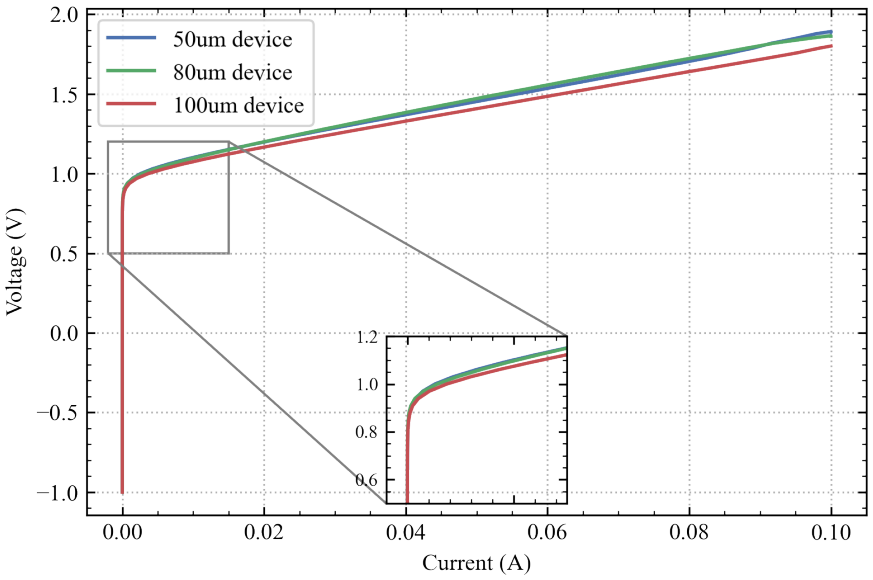

Fig 2. 5 typical IV characteristics for broad area laser of 4mm 3-layer QD laser at different ridge width. Insertion is to show the zoomed image of turn-on voltage ~0.9V

The settings for continuous IV measurement are -1 to 2V with a step size of 0.1. The 3-layer QD laser all shows the same IV curve at room temperature. The IV curve is conducted to identify whether or not a device is functional and to compare the fabrication quality of multiple laser devices on the same sample. The on-state resistance is derived from the slope of the forward bias IV, which is ~5~6 ohms for all measured devices. This is a direct comparison of the devices' ohmic contact quality. For good broad area laser fabrication, the on-state resistance should be less than 10 ohms and consistent between samples. At the same current injection, a resistance that is too high will generate more heat, reducing the laser's performance[91].

For LI measurements, output light coming out of the laser facet is aligned with the power meter using the XYZ stage. For pulsed setup, the positive end of the probe is connected in series with a 47 Ohm resistor to match the output impedance required for the pulsed current source. The measurement is set from 0 to 1000mA with step size of 10mA and pulse width of 1μS and 1% duty cycle.

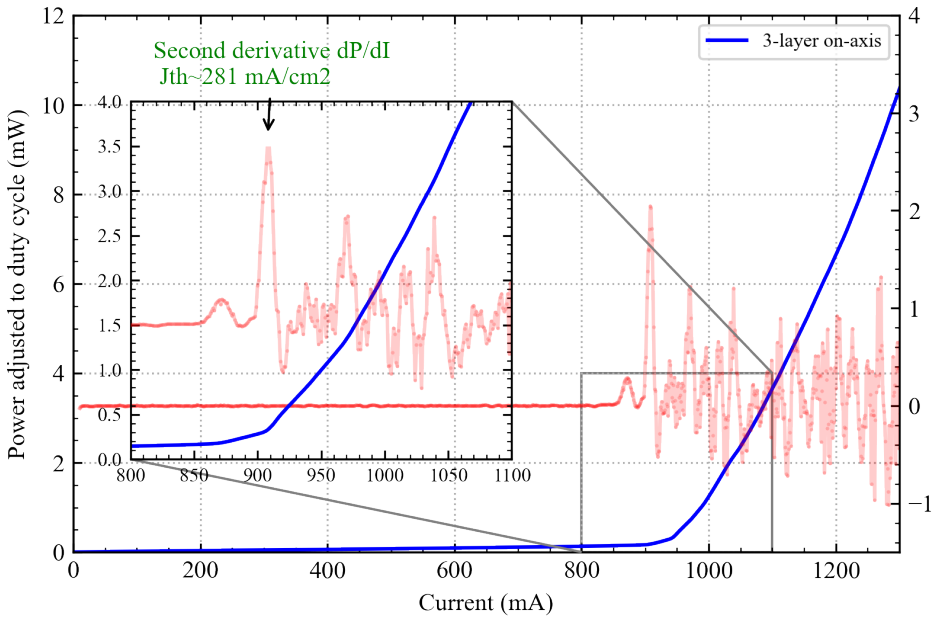

Fig 2. 6 Room temperature Pulsed LI spectral of 3-layer QD 4mm broad area laser. The threshold current density J_{th} is obtained from the maximum of second derivative of the forward curve(as shown by the arrow)

Fig 2. 6 shows the pulsed LI obtained from one of 80 μm 4mm broad area laser device. The laser device is lasing at ~900mA. Taking into account the surface area of laser, the threshold current density (J_{th}) is ~281 A/cm^2.

The threshold current density J_{th} of laser is apparent in the rapid exponential increase in output power is a signature of the lasing operation. This is the current density that triggers the population inversion inside the cavity of laser. The first ($\frac{\Delta P}{\Delta I}$) and second derivative ($\frac{\Delta^2 P}{\Delta^2 I}$) of the LI curve can be used to estimate the exact lasing threshold current, as shown in the insert of Fig 2. 6, where the highest red peak represents the threshold point. To maximise efficiency, the J_{th} should be as low as possible. The repeatability of the fabrication is measured by comparing the J_{th} of the same device manufactured at different times. At currents below the threshold, the laser's spontaneous emission area corresponds to the LED-like behaviour of the device. At currents above the threshold, population inversion develops within the laser cavity, and stimulated emission dominates the laser output light.

2.3.2 Characteristic Temperature (T_o)

The Characteristics Temperature is a measure of temperature sensitivity of the threshold current. The measurements are same as the previous L-I characteristics but the LI spectral are measured as a function of temperature, (as shown in Fig 2. 6& Fig 2. 7). The T_o, can be extracted by obtain the graph of the natural log of the threshold current density at each temperature versus the temperature using equation (2.1) [92]:

$$T_o = \frac{\Delta T}{\Delta \ln (Jth)} \quad (2.1)$$

The inverse slope of the linear fit line is the T_o. This can be used as an indirect comparison of the defect level of the laser device. Since carrier traps in the defects and the thermally activated carrier leakage out of the active region (into cladding) are causing self-heating effects, which impede the threshold current at high temperatures. The temperature range of the measurements should be as large as possible for determine the T_o. But here a smaller ΔT was used, only to compare the laser operating on the ground state. As shown in Fig 2. 7, the temperature dependent LI spectral of 4 mm broad area laser is measured.

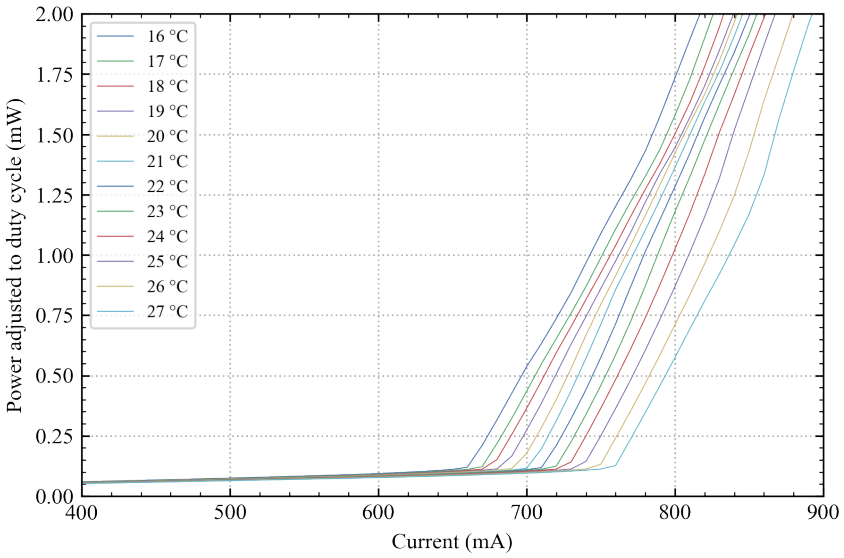

Fig 2. 7 Pulsed LI spectral of 3xQD sample with temperature varied from 16-27° C. The J_{th} of laser reduced as temperature reduced.

The calculated T_o is obtained from the inverse slop of the linear fit line as shown in Fig 2. 8 where Ln(J_{th}) is plotted against the temperature.

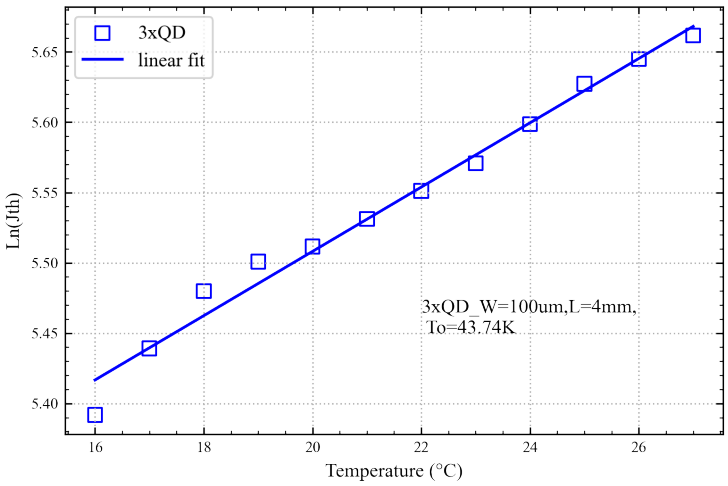

Fig 2. 8 Ln(J_{th}) plotted against the temperature of 3xQD sample, the linear fit is done and the slope is the $1/T_o$

2.3.3 EL Spectra

The room temperature Electroluminescence (EL) Spectra of 80µm 4mm broad area laser is measured using a pulsed current source and a HP3008A optical spectrum analyser (OSA). This requires a multimode fibre to align the output facet of the broad area laser as closely as possible to obtain the maximum S/N ratio. The measurements are done at controlled room temperature to allow measurements of spectrum at different current density. Fig 2. 9 is the 3-layer QD laser spectra taken at current density of $0.8J_{th}$ and $1.2J_{th}$ at room temperature. The spectra show lasing at ~1050nm as the emission spectrum narrows drastically at short wavelength and possible ground state emission at peak wavelength of ~1150um from $0.8J_{th}$ spectrum. The lasing peak wavelength is between 1045-1050nm.

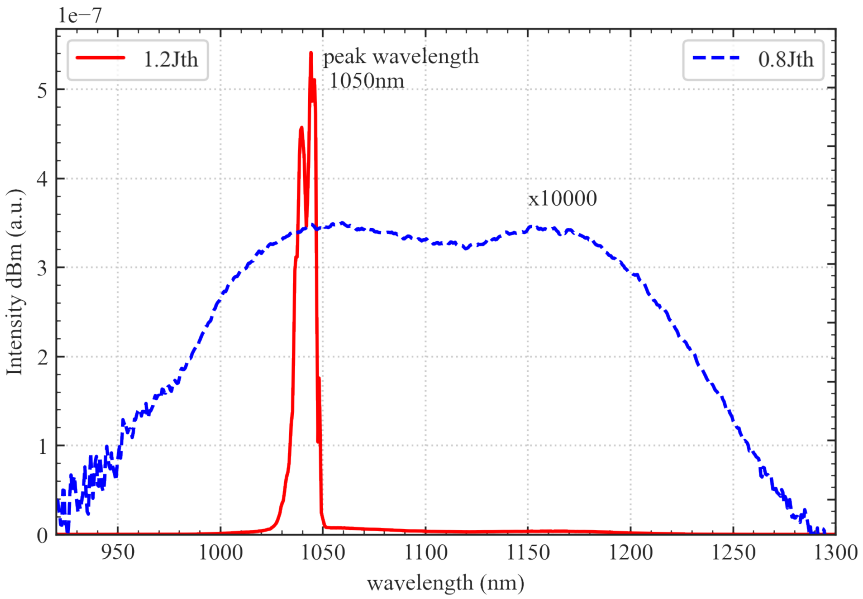

Fig 2. 9 Room temperature pulsed EL spectrum of 4mm broad area laser. The spectrum is taken above ($1.2J_{th}$) and below ($0.8J_{th}$) the threshold current density to determine the lasing spectrum.

There are 2 major peaks at the $1.2J_{th}$. Multiple modes are observed due to the nature of broad area laser and multimode fibre being used. These optical modes will compete with each other which changes the peak output wavelength at different injection currents. Fabricating the sample into narrow ridges laser will reduce this effect. The presence of several modes is worth investigation at current density below and above the threshold. It is desirable to have a clearer

single narrow linewidth spectrum at threshold current for laser application. Fabrication of narrow ridge laser could suppress the multimode behaviour of the laser.

2.3.4 Mesa diode EL Spectra

Another laser characteristic of interest is the low current EL spectra of the mesa diode devices. The measurement setup is identical to the normal spectral measurement, except the diode is emitting from the top surface. An extra optical lens is used in front of the multimode fibre to improve the output light collection efficiency, Fig 2. 10 shows the experiment setup. The continuous current is applied from 0mA until ground state of mesa diode saturates. Small diameter of mesa diode of 100μm is selected to fully fill the ground state of QDs at lower current. The temperature is controlled at same temperature for comparison between the devices. Fig 2. 11 shows the fabricated mesa diode of 100μm, 50μm & 25μm diameter. The lithography circle diameter is same as desired.

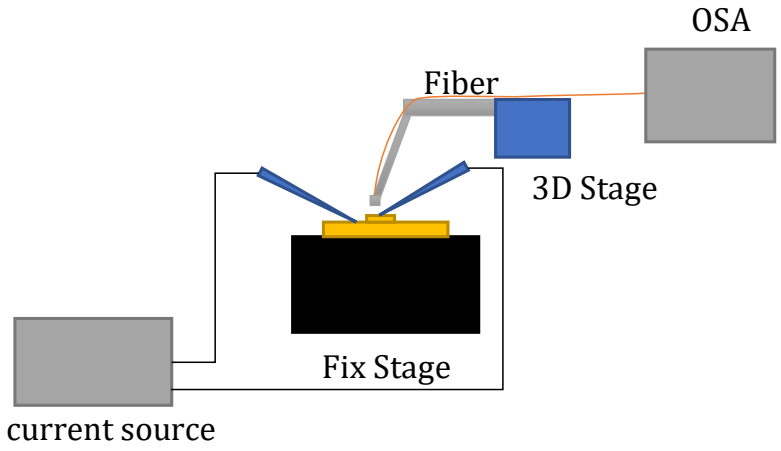

Fig 2. 10 Schematic diagram of room temperature mesa diode EL measurements, the sample is on the stage with fibre pointing down vertically.

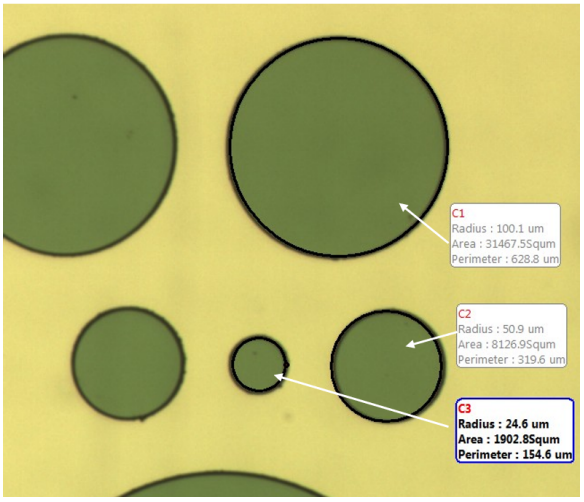

Fig 2. 11 Fabricated mesa diode etch lithography, the circles diameter is measured within the error of lithography

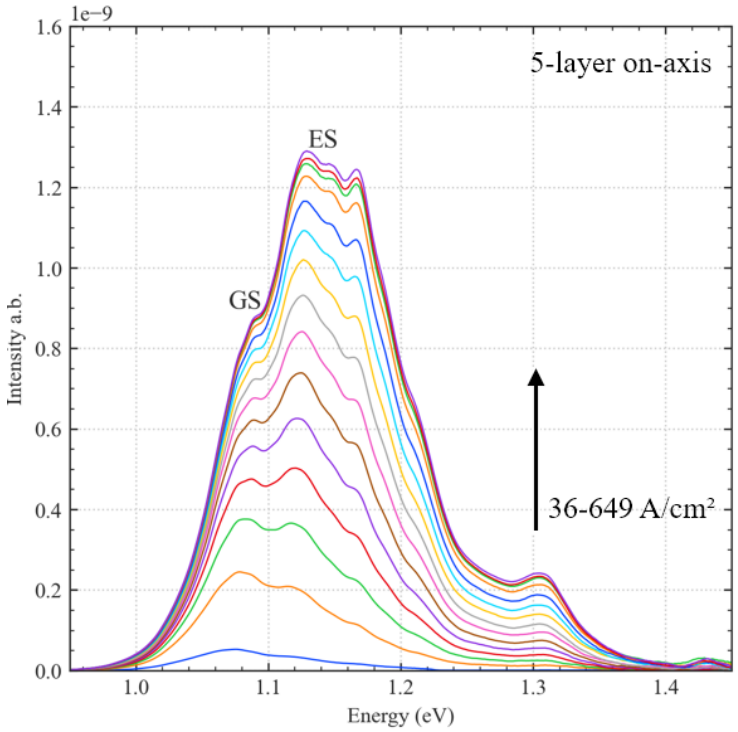

Fig 2. 12 Room temperature mesa diode EL spectrum of 5-layer QD laser at current density from 36-649 A/cm^2. The obtained the intensity is plotted against the emission energy for better identification of different state of QD

Fig 2. 12 shows the room temperature EL measurements of 5-layer QD mesa diode taken from current density of 36 to 649A/cm^2. Notice here the x-axis is photon energy (eV). The ground state and first excited state of 5-layer QD laser is observed at 1.09eV and 1.14eV. The low

current mesa diode EL measurements can be fitted with gaussian functions to obtain different quantum dot states using equation (2.2),

$$I = I_o e^{\frac{(x-x_0)^2}{\left(\frac{\Delta x}{2\sqrt{2ln2}}\right)^2}} \quad (2.2)$$

where I_0 is the maximum intensity, x_0 is the centre photon energy and Δx is the full width at half maximum of the spectrum. Multiple peaks can be fitted to obtain the cumulative fit of curve which is close to the original spectrum as shown in Fig 2. 13 where GS, ES1 & ES2 are fitted by the gaussian function and the final cumulated curve is obtained from the gaussian components.

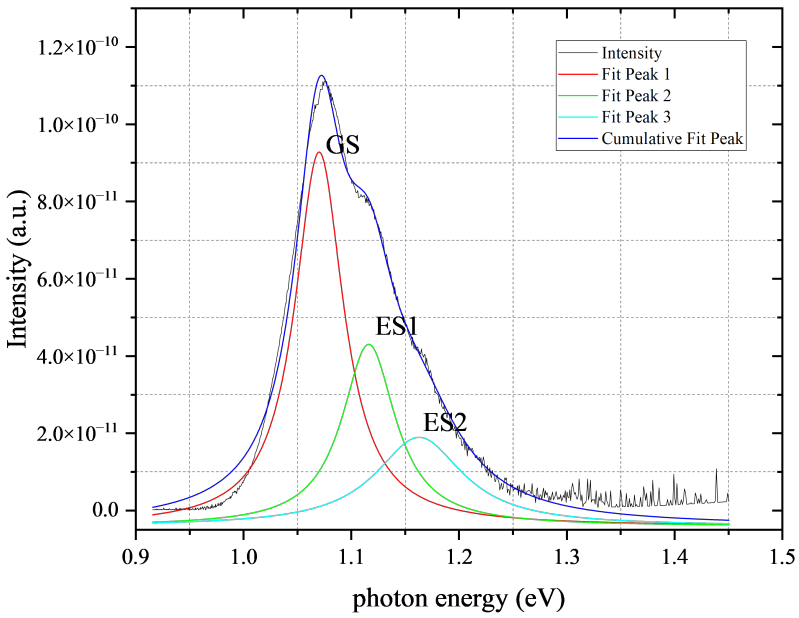

Fig 2. 13 Room temperature low intensity mesa diode EL spectrum of 5-layer QD laser at current density of 50A/cm^2. The obtained the intensity is fitted with gaussian functions

The EL measurements allow detail comparison of the number of QD states across different samples. As current injection increases, the ground state of the QD (low energy peak) starts to fill and eventually reach saturation when all the dots are filled. Then electrons move to the second state (first excited states) and increase of intensity is observed at higher energy peak.

Similar to the limited area PL experiment, the ground state saturation intensity I_{sat} is proportional to the number of quantum dots N [93]. Therefore, it can be used to compare dot density between different samples, which is a good proximation when TEM measurement of dot density is unavailable. The ground state saturation current density Jsat can be used as a measurement of quantum efficiency of active region as well, where any absorption effect from the wetting layer is excluded. Lower saturation current density means higher quantum efficiency of the active region.

2.3.5 Internal quantum efficiency

Apart from the basic IV and LI characterisation of laser diodes introduced above. The efficiency of the laser output power vs input current is another important parameter to compare. In order to calculate the internal quantum efficiency, we need to obtain the external quantum efficiency (η_d) using variable strip method. Different cavity length diodes from 4mm to 0.1mm is cleaved and LI curve of each cavity length is measured using the LI setup described in section 2.3.1.

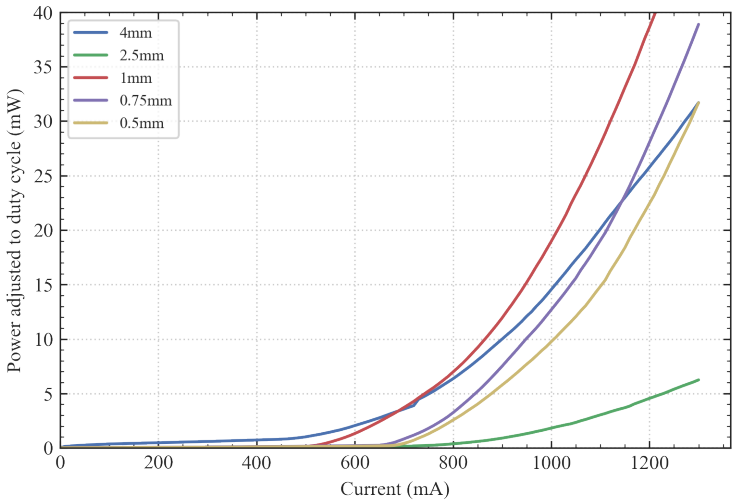

Fig 2. 14 Room temperature Pulsed LI spectral measured from the different cavity length of broad area laser.

The above threshold slope of the obtained LI curves (Fig 2. 14) can be deduced with dP/dI. This measures the ability of the laser to convert electric power to light output. For an ideal laser, the output power is $hc/q\lambda$. Therefore, the $(dP/dI)/(hc/q\lambda)$ is the external differential quantum efficiency ηd at current density above the I_{th}.

The internal quantum efficiency η_i measures the ability of laser to convert the injected electron and hole pairs into photons. This parameter is only related to the material quality and is independent of the cavity length of the laser. The internal quantum efficiency can be used to compare the material quality between wafers as it directly measures the photons generated inside the laser structure. This value is always bigger than η_d because the defects in the material reduce the photons emitted inside the cavity. The η_i is derived from the $1/\eta d$ versus the cavity

length using equation below. The interception of fitted lines with y-axis is the $1/\eta i$ in percentage (2.3)

$$\eta_d = \eta_i \frac{\alpha_i}{\alpha_i + \alpha_m} \quad (2.3)$$

The internal loss α_i can be derived from the experimental fitting as well, as shown in Fig 2. 15 using equation below (2.4)

$$\alpha_i = slope\ of\ line \cdot \eta_i \ln\left(\frac{1}{R}\right) \quad (2.4)$$

Where R is the reflectivity of mirror and for GaAs/AlGaAs lasers, it is equal to ~0.32.

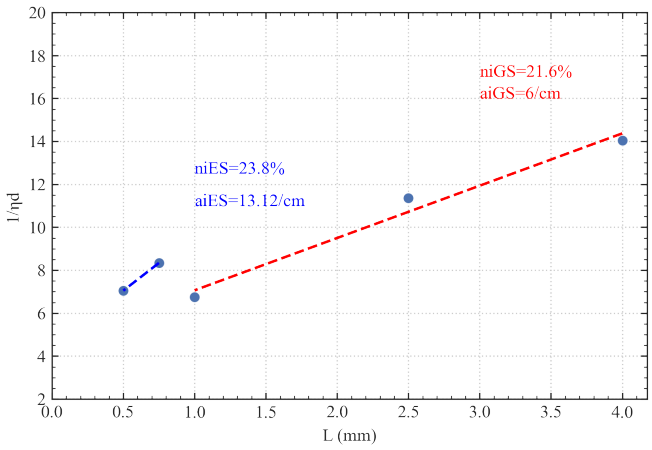

Fig 2. 15 $\frac{1}{\eta d}$ plotted against the L cavity length obtained from the striped LI spectral , the fitted line has 2 slopes, which separate the ground state and excited state of QD laser

From Fig 2. 15, the 5-layer QD sample shows that possible switching between ground state and excited state lasing below cavity length of 1mm. The obtained internal quantum efficiency and internal loss will be used in later chapters for detailed analysis.

2.3.6 Gain measurement

The gain of a semiconductor laser occurs when the population inversion is achieved during the transition process between conduction and valence band. At low carrier concentration, this band-to-band radioactive transition is mainly stimulated absorption. Therefore, there is no lasing occurred. By further increasing the current density, the electron concentration in the conduction band will exceed the electron concentration in the valence band. The stimulated emission dominates the transition process and the population inversion is achieved. At this condition, the gain is observed, and it equals to the total losses in the cavity of the laser. In a typical Fabry-Pérot laser, the laser is cleaved into 2 mirror facets 90 degrees parallel to each other along the waveguide. The photon bounces between the mirrors thus providing the necessary optical feedback for the lasing. The threshold gain, g_{th}, can be expressed as (2.5)

$$\mathrm{gth} = \alpha\mathrm{i} + \alpha\mathrm{m} \quad (2.5)$$

αi is the internal loss and αm is the mirror loss. The internal loss includes non-radioactive absorption (defects, auger, etc.) and mirror loss is caused by the 2 cleaved facets. These losses must be compensated in order to achieve the threshold condition, so that the electric field is exactly equal between each round trip (one round trip is 2L, where L is the length of cavity). The mirror loss can be expressed as (2.6)

$$\alpha\mathrm{m} = \frac{1}{L}\ln\left(\frac{1}{R1 + R2}\right) \quad (2.6)$$

and the net modal gain (2.7):

$$\mathrm{g} = \alpha\mathrm{i} + \frac{1}{L}\ln\left(\frac{1}{R}\right) \quad (2.7)$$

R is the reflectivity of cleaved facet.

A reliable and precise measurement of gain characteristics below and above the threshold is needed for understanding the physics of a laser diode. From the optical gain parameters, the high speed, temperature dependence of threshold performance of a laser diode can be obtained. These results can be used to investigate the quality of wafer and improve the design of laser structure or the growth process.

To have sufficient gain for lasing, the optical gain must overcome the internal αi and mirror loss αm. The internal loss α_i is the loss that is related to the scattering in the material which is related to the material quality. There are many ways to measure the gain of a laser. One of the well-known methods is Hakki-Paoli method [94]. The advantage of this method is that the device can be measured directly without being fabricated into stripes of different cavity lengths. Therefore, the same device can be used for lasers after the measurement.

In Hakki-Paoli method, the net model gain, g, is measured by the ratio between peak and the bottom of Fabry-Perot resonance spectrum of amplified spontaneous emission (ASE).
The actual ratio x is calculated from the average of 2 consecutive peak power divided by the valley power between the 2 peaks at each wavelength. Then by inserting the ratio into the equation (2.8) below

$$g = \frac{1}{L} ln\left(\frac{x^{1/2}+1}{x^{1/2}-1}\right) \quad (2.8)$$

R is reflectivity, g is the net model gain and L is the cavity length. The Γ is the optical confinement factor, Once the Γ is calculated, the real material gain gm can be calculated from the $g+\alpha_i=\Gamma gm$.
For a laser device, the gain measurement of the Hakki-Paoli method is only related to the facet reflectivity R, optical confinement and the Fabry-Perot resonance quality. The R can be improved by depositing a reflective coating on both facets of the device. The optical confinement of a laser consists of 2 polarisations, the transverse electric mode TE and transverse magnetic mode TM. In Hakki-Paoli method, it is assumed that the spectra of ASE at TE polarity are measured. The ASE is measured through the front facet of laser and coupled through an optical isolator and a single mode fibre to act as a spatial filter. This filter removes other transverse modes that we do not want. Therefore, the only factor affecting the accuracy of gain measurement is the device itself. This can be improved easily by chosen the device that has cleaner spectrum.

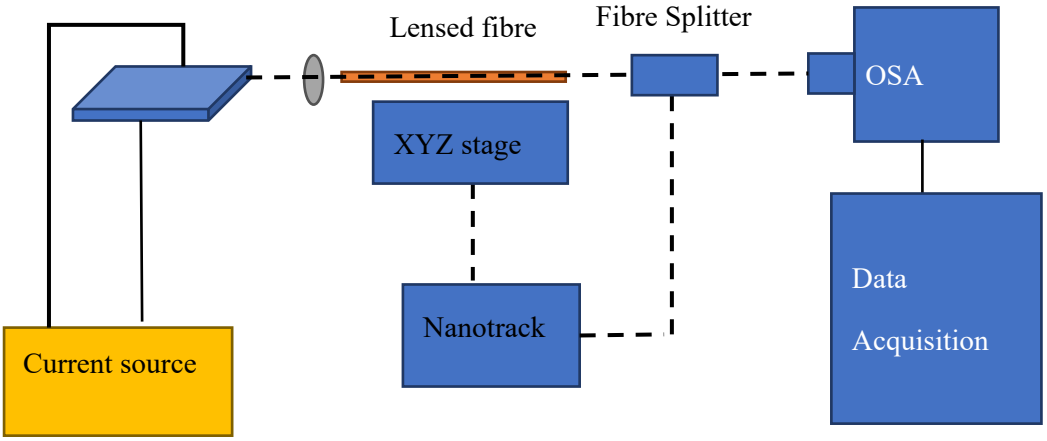

Fig 2. 16 The schematic diagram of H.P gain measurement setup

The schematic diagram of the set-up for Haki Paoli gain measurement is shown in Fig 2. 16. However, there are some disadvantages and limitations of Hakki-Paoli measurements. Firstly, the measurement setup needs a very high resolution OSA with bandwidth resolution smaller than 0.5nm. This means low output power laser devices cannot be measured if it is close to the noise level of the instrument, where the 'valley' measurement is close to the noise limit. Another disadvantage of H.P method is the long measurement time, which usually takes about 20 mins for one single spectrum. Any change of alignment during the measurement process will affect the results, thus a complex auto-alignment piezo-stage is required. Fig 2. 17 shows the obtained H.P gain spectra from a commercial 1.55μm laser with cavity length of 350μm and ridge width of 3μm, the spectrum is obtained from a high resolution (capable of 0.05nm resolution) OSA.

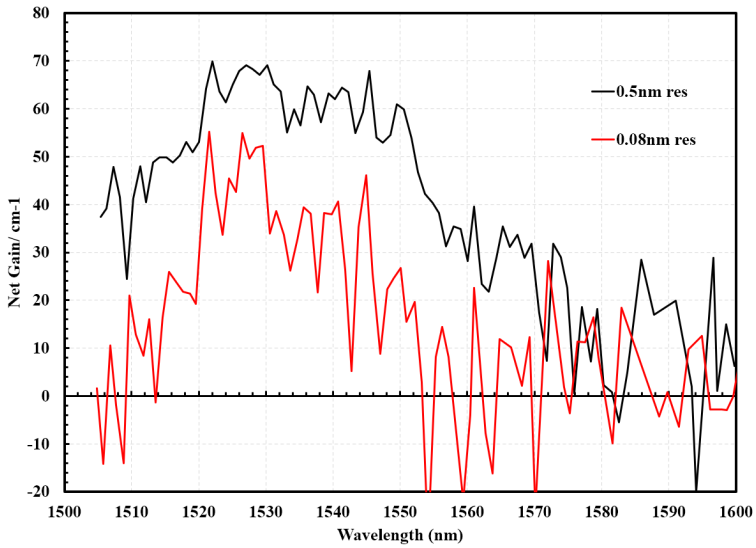

Fig 2. 17 Calculated Hakki-Pauli gain spectrum from the commercial QD laser at 1.55μm with 1.55μm laser with cavity length of 350um and ridge width of 3μm

The gain spectrum quality degrades as resolution of OSA increases. The S/N ratio of the spectrum at gain below the zero is approaching the noise floor at longer wavelength. This commercial laser is capable of ~1mW of output intensity at J_{th}. Unfortunately, in this project, the fabricated laser usually output power at around 0.01mW which is not suitable for H.P measurement. The maximum resolution for the HP 3008A OSA is ~0.8nm which is not enough to obtain the individual F.P mode at cavity length of 0.5mm, which is close to the shortest cavity length that we can cleave. Therefore, another technique called Segmented Contact (multisection) Gain Measurement is used in this project for gain measurement.

2.3.7 Segmented Contact Gain measurement

The segmented contact gain measurement is another well-known gain measurement technique [95]. The gain is obtained from the single pass ASE from the front 2-section of multisection device. It has the advantage of low requirements on measurement setup and fast measurement time [96]. However, it requires a specific device to be fabricated with multiple sections on one single device. The Fig 2. 20 below shows the structure of multisection device. The laser width is 7um, and each section is 1mm long with isolation etched between. The fabrication of multisection laser is similar to the narrow ridge laser fabrication except it has an absorber etched at the end of device to suppress the round-trip gain to achieve single pass gain. Fig 2. 18 shows the important fabrication process called isolation which is used to stop the electrical contact between the sections. The 300nm of GaAs p-contact layer is etched by wet etching to provide ~1-2 MΩ resistance between the contacts. This process is thus ensuring good isolation between the sections which poor isolation will turn-on neighbouring sections and result in unusable data. Fig 2. 19 shows the SEM image of etched isolation which is important as it will affect the individual section electrical characteristics. Thus, it is necessary to obtain a high quality uniform etch across the whole device.

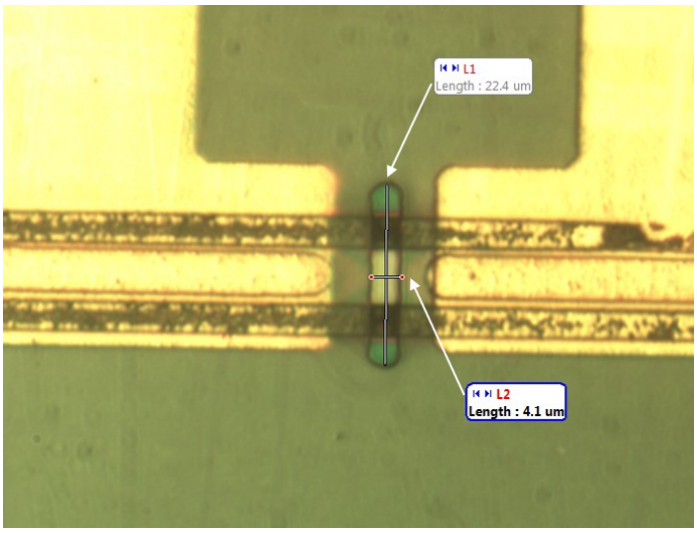

Fig 2. 18 Isolation between the sections of multisection device fabrication, the measured separation is 4.1µm and length is 22.4µm. The isolation must covers the whole area of the ridge

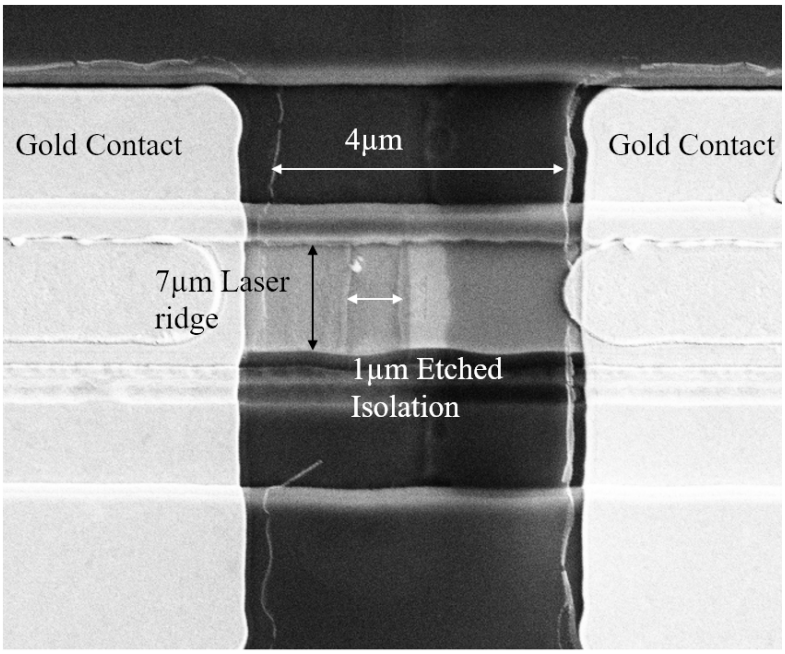

Fig 2. 19 SEM image of Etched Isolation between the sections of multisection device fabrication. The SEM image clearly shows the etched isolation covers the whole ridge

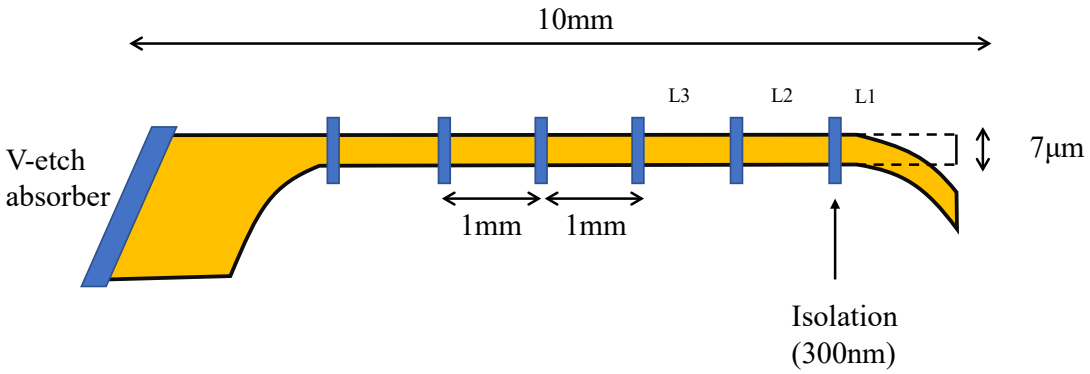

Fig 2. 20 Schematic diagram of multisection device fabricated, the section is L1, L2, L3 with same length of 1mm

Usually, the front 2 sections of the device are used for the gain measurement. By pumping the first section, the multimode fibre collects the amplified spontaneous emission and using OSA to measure the spectral as I_{1L}. Then pumping both front 2 sections together at same current density, the measured spectral is I_{2L}. The net modal gain can be obtained by using equation (2.9):

$$net\ modal\ gain = \frac{1}{L} ln\left(\frac{I_{2L}}{I_L} - 1\right) \quad (2.9)$$

where L is the length of one section, the signal to noise ratio can be improved by using longer sections together as one unit L and pumping 2 times the section length accordingly. Fig 2. 21 shows the calculated multisection gain spectral for the 5-layer QD laser sample.

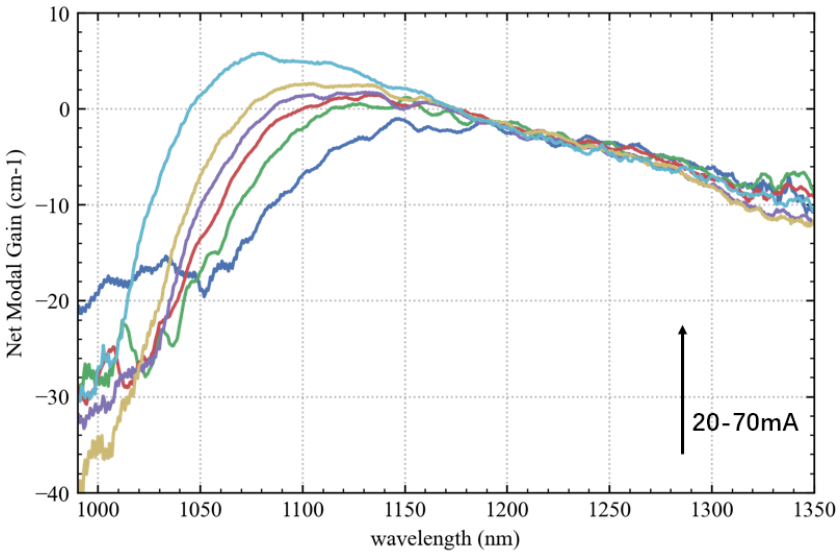

Fig 2. 21 Calculated multisection gain from the 5-layer QD sample at injection current between (20-70mA)

To be noticed, it is important to make sure all sections that measured have similar IV characteristics and temperature is controlled to avoid any difference caused by the heating effects. Fig 2. 22 shows the measured continuous LI and amplified spontaneous emission from the front 3 sections.

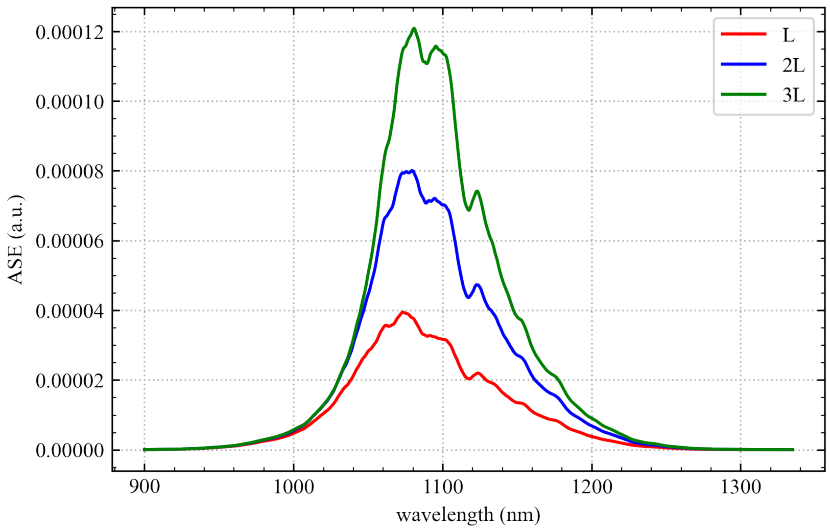

Fig 2. 22 Amplified spontaneous emission obtained from one section L, 2section 2L and 3section 3L pumped at same current for each section

A multimode fibre is used to couple the signal from device to the OSA which improves the coupling efficiency compared to the H.P lensed single mode fibre. The resolution of the OSA is usually kept at 5nm, with low requirements on the sensitivity. These 2 factors improve the S/N ratio and reduce the measurement time. Therefore, segmented contact gain measurement is very suitable for low power device gain measurement.

However, sometimes the laser output spectrum contains not only the fundamental modes, higher order modes that can also contribute to the output spectra. To eliminate such effect, the front section can be used as integrated mode filter. This method introduced by P. Blood *et al.*[97] suggests higher order modes can be filtered by leaving the front section L1 unpumped (0V) or at an optimum current density where gain is sufficient. Fig 2. 23, compares different measurement methods for multisection laser devices.

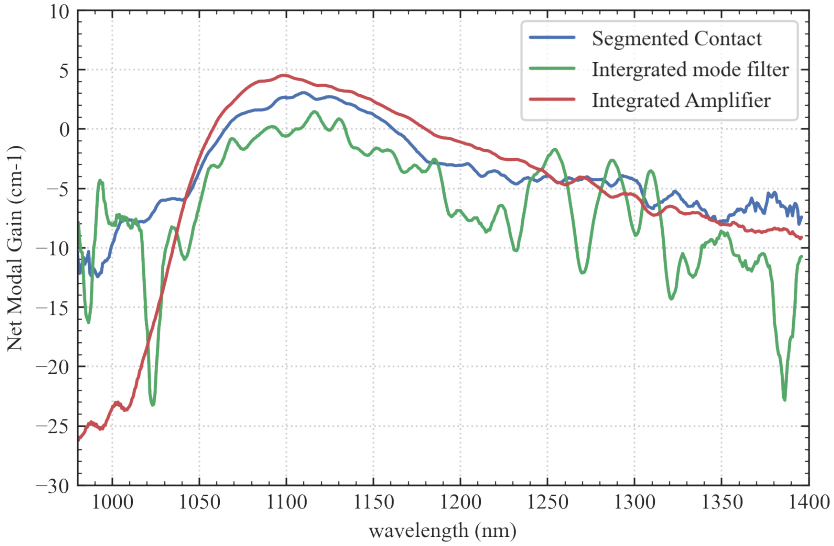

Fig 2. 23 comparison of gain spectrum obtained from different measurement methods of same multisection device

Because the mode filter is integrated with the device, the experiment setup is the same as the previously mentioned normal spectral measurement setup. From the Fig 2. 23, the main difference between different gain measurement methods is at short wavelength region and at the long wavelength end where signal is approaching the noise level of the OSA. For integrated mode methods, the net modal gain can be extracted using equation (2.10):

$$net\ modal\ gain = \frac{1}{L}\ln\left(\frac{I_{L3+L2+L1} - I_{L1}}{I_{L2+L1} - I_{L1}} - 1\right) \quad (2.10)$$

When the front section is unpumped, the signal is largely attenuated due to total absorption of front section as seen in the fig. To overcome this issue, one can also pump the front section with a current to amplified the signal. An integrated amplifier and mode filter is combined where front section provides the gain to the signal and later deduced from the gain calculation, providing a good S/N ratio in the low signal regime. The resulted gain spectral has better resolution on both ends thus, the integrated amplifier is the best methods for the gain measurement.

2.3.8 SEM

To further investigate the reproducibility of QD samples, several SEM images have been taken between several steps at fabrication and characterisation. The SEM stands for Scanning Electron Microscopy. It is used to investigate the surface and cross-section of the device through a high energy electron beam scanned through the surface of the sample. It is capable of resolution down to sub-micron. The contrast of the SEM is provided by the interaction of electron beam with the surface of the sample which produce the secondary and backscattered electrons. These electrons caused a difference in the surface voltage of the material and provides the contrast in the SEM image. The SEM are often used to measure the etched depth and determine the cleaved fact and also surface morphology. Fig 2. 24 shows the SEM cross section image of a broad area laser fabricated with a required etch depth of 1.5µm and actual etched of 1.364µm.

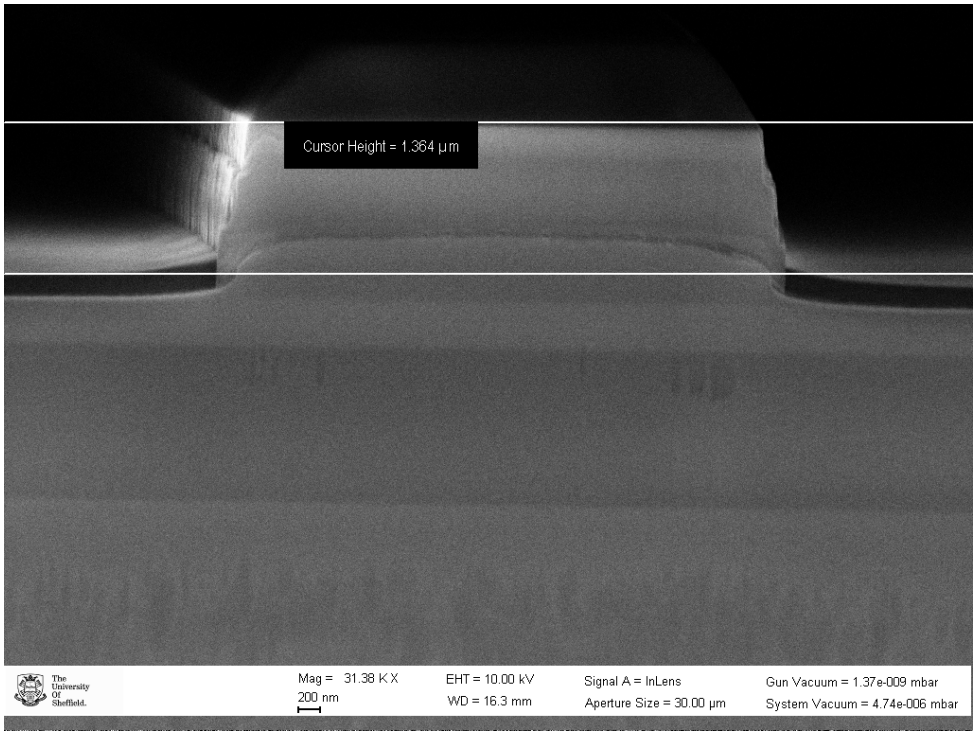

Fig 2. 24 SEM cross section image obtained from broad area laser with ridge etched to 1.364µm

2.3.9 TEM

Transmission Electron Microscopy (TEM) is used to determine the epitaxial layer thicknesses and QD densities on a nano-scale. It uses the transmission of electrons which are diffracted by the material to produce an image when the electron beam is scanned across the sample. In this thesis, all the TEM images were obtained by the University of Warwick. TEM has several imaging modes and thus can be used to extract different information from the sample. The most common one is the bright field image and all TEM images used in this thesis use this mode unless otherwise stated in the caption. The bright field image is produced by collecting the transmitted electrons when a focussed electron beam hits the surface of the sample. The bright field image shows the sample in light and the background in dark. By contrast, the dark field image collects the scattered electrons and the sample's surface is dark and the background is light. This mode is useful for studying the crystal lattice down to 0.2nm scale, which is the highest resolution mode. The third imaging mode is phase contrast mode. This can be used for imaging the dislocations and defects in the sample where the diffracted Bragg scattering of the electron beam is collected. The contrast of the image also reveals the strain field of the specimen. However, the resolution of the image is limited to ~1nm.

The Fig 2. 25 shows the bright field TEM image of stacked QD sample which has InAs QD layer separated by 50nm of GaAs spacer. From the image, we can resolve individual quantum dots in the active region and thus can be used to estimate the QD density by counting the number of QDs at certain area.

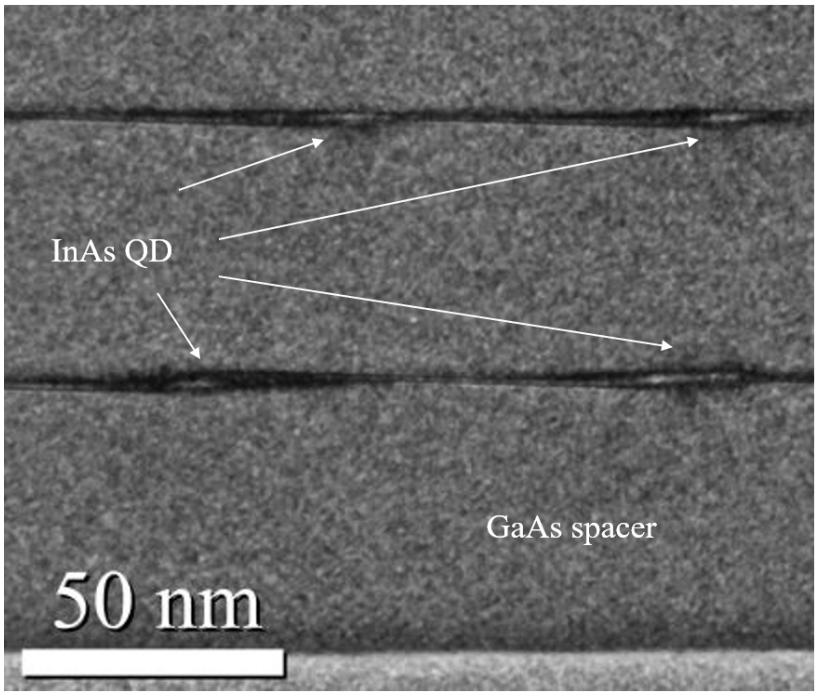

Fig 2. 25 TEM cross section bright field image obtained from QD lasers with InAs QD layer separated by 50nm of GaAs spacer

2.3.10 SIMS

The SIMS stands for Secondary Ion Mass Spectrometry. In this thesis, we used the depth profiling SIMS to measure the layer composition, doping concentration and oxygen impurities of the sample grown. The SIMS is done by company called Aystorm Scientific. It is capable of measuring the materials such as [98]:

1. Si , SiGe , SiC
2. PSG , BPSG , Oxides , Nitrides
3. GaAs, AlGaAS, InP, AlInP
4. GaN , InGaN, AlGaN , AlN, Diamond

The samples' surfaces are sputtered by specimen with a focused primary ion beam and the released secondary ions is collected for analysis. Thus, the SIMS requires accurate calibration of each layer of material to obtain the concentration of atoms correctly. Fig 2. 26 shows the typical measurements of SIMS which contain the Zn, Si concentrations as well as the As counts.

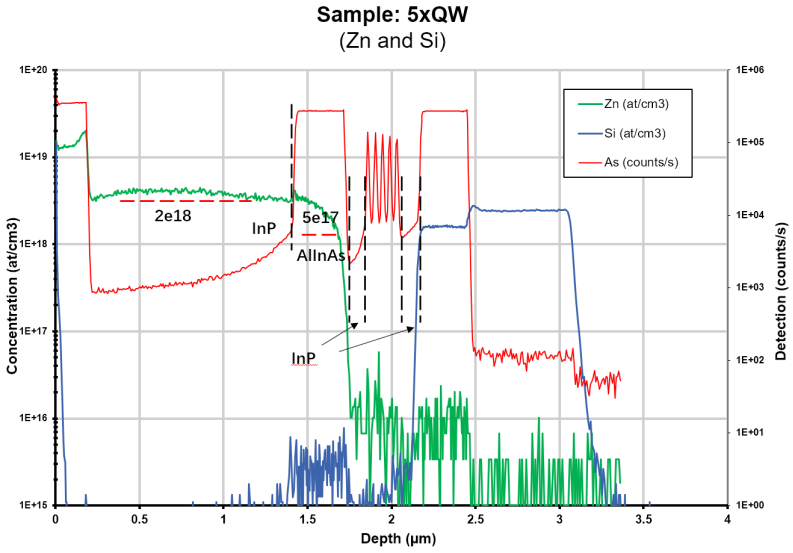

Fig 2. 26 SIMS analysis of Zn, Si concentration and As counts of 5xQW. The black dotted lines are drawn to separate different layer. The red dotted line are drawn to show the expected Zn concentration at the growth of sample.

From the SIMS analysis, several growth-related issues can be identified from the concentration of the doping and the elements counts in different layers (such as diffusion of Zn).

2.4 Reference

[91] R. Wang, S. F. Yoon, H. X. Zhao, and C. Y. Liu, 'Self-Heating Effect on Modal Gain of 1.3-InAs/GaAs QD Lasers With Different Doping Levels', *IEEE Photonics J*, vol. 3, no. 4, pp. 713–717, Jan. 2011, doi: 10.1109/JPHOT.2011.2161865.

[92] K. S Mobrahan, *Test and Characterization of Laser Diodes: Determination of Principal Parameters*. Newport: Application Note, 1999.

[93] E. C. le Ru, A. J. Bennett, C. Roberts, and R. Murray, 'Strain and electronic interactions in InAs/GaAs quantum dot multilayers for 1300 nm emission', *J Appl Phys*, vol. 91, no. 3, pp. 1365–1370, Feb. 2002, doi: 10.1063/1.1429797.

[94] B. W. Hakki and T. L. Paoli, 'Gain spectra in GaAs double-heterostructure injection lasers', *J Appl Phys*, 1975, doi: 10.1063/1.321696.

[95] K. L. Shaklee and R. F. Leheny, 'DIRECT DETERMINATION OF OPTICAL GAIN IN SEMICONDUCTOR CRYSTALS', *Appl Phys Lett*, vol. 18, no. 11, p. 475, Oct. 2003, doi: 10.1063/1.1653501.

[96] A. Oster, G. Erbert, and H. Wenzel, 'Gain spectra measurements by a variable stripe length method with current injection', *Electron Lett*, vol. 33, no. 10, pp. 864–866, May 1997, doi: 10.1049/EL:19970605.

[97] J. D. Thomson, H. D. Summers, P. J. Hulyer, P. M. Smowton, and P. Blood, 'Determination of single-pass optical gain and internal loss using a multisection device', *Appl Phys Lett*, 1999, doi: 10.1063/1.125066.

[98] 'SIMS Analysis Service | Aystorm Scientific |'. https://www.aystorm.com/secondary-ion-mass-spectrometry (accessed Aug. 15, 2022).

Chapter 3: Comparison of on-axis & off-axis 1.1µm Quantum dot laser

3.1 Introduction

QD lasers are attractive for a variety of optoelectronic applications, and their performance is predicted to surpass that of bulk or quantum well semiconductors[99]. Nonetheless, the growth of quantum dot lasers with a high-density quantum dot as required for high optical material gain remains difficult[100]. Quantum dot optical gain from the ground state (low injection energy) is affected by fluctuations in individual QD size (often a bimodal distribution) and quantum dot density. Various techniques for obtaining high-quality dots, such as changing the growth temperature[101]–[104], incorporating post-annealing procedures[105]–[108], *etc.*, have already been thoroughly reviewed. However, little attention has been paid to the effect of the GaAs substrate orientation growth on the performance of InAs/GaAs QD lasers. In this chapter, we investigate 1.1µm InAs/GaAs QD lasers grown via metal-organic vapour phase epitaxy. Identical laser structures are grown upon on-axis GaAs (100) substrates and on substrates misorientated with an offcut of 3° towards the (110) plane. The optical gain and lasing thresholds of broad area lasers containing 3x and 5x layers of InAs/GaAs QDs has been measured. The length-dependent LI measurements are carried out to determine the internal loss coefficient and internal quantum efficiency between 5x layers on-axis and 3-degree off-axis samples. The impact of on-axis and off-axis growth on the gain of 3 & 5-layer QD lasers has been demonstrated by multisection gain measurements. The results demonstrated that the QD laser grown on the 3-degree off-axis substrate has lower threshold current density and higher gain than on the on-axis substrate. In addition, 100µm mesa diodes are fabricated for vertical EL measurements, which can be used to compare QD densities. The obtained EL measurement result shows a ~20% increase in the QD density for the 3-degree off-axis sample compared to

the on-axis sample, which is correlated with the transmission electron microscopy (TEM) images. The higher QD density of the off-axis sample, as determined by transmission electron microscopy, can be related to the sample's GaAs spacer layer morphology changing, with more steps formed on the surface of GaAs, which provides a favourable growth site for QDs. This work is a solid milestone towards realisation of 1.3μm QD laser grown by MOCVD as comparison with the current state-of-art MBE QD work. The successful developed high density QD lasers would be useful in the future heterogenous integration on the silicon platform.

3.2 offcut growth of GaAs substrate

Lattice mismatch between the epilayer and substrate is one of the most significant factors affecting the quality of heterostructures [109]. The substrate's orientation angle will impact the quality of the epilayers grown upon it. Misorientated substrates are known to a have positive influence on supressing the dislocation of the epilayer [110]. The effects of substrate misorientation angle on the buffer layer dislocation level, substrate misfit stress, and p-doping concentration for quantum well lasers have also been documented [68], [111], [112].

For typical epilayer growth on top of a GaAs substrate, the lattice misfit ($\Delta a/a$) can be calculated using the equation (3.1), where $a_{s.f}$ is the strain-free lattice constant of the epilayer and a_b is the substrate lattice constant. For GaAs substrates, the lattice constant is 0.56532nm.

$$\frac{\Delta a}{a} = \frac{a_{s.f} - a_b}{a_b} \quad (3.1)$$

This parameter is critical for high quality epilayer growth. The lattice mismatch of the epilayer should be kept as small as possible in order to reduce the formation of dislocations and other defects, which would otherwise present a major impediment to semiconductor laser diode performance. The lattice mismatch also plays an important role in the Stranski–Krastanov (S.K) growth of QD, where the formation of self-assembled InAs QD in fact depends on the presence of strain & lattice mismatch in the epilayer. Thus, in theory, the change in off-cut angle will have an effect on the QD size and density through its effect on the SK growth mechanism. According to research studies of InGaP on a misoriented GaAs substrate[68], as illustrated in Fig 3. 1 from XRD measurements on different substrate misorientation angles. With an increase in the off-cut angle, the lattice misfit of the epilayer decreases, which also promotes the reduction of strain and inhibits dislocation formation.

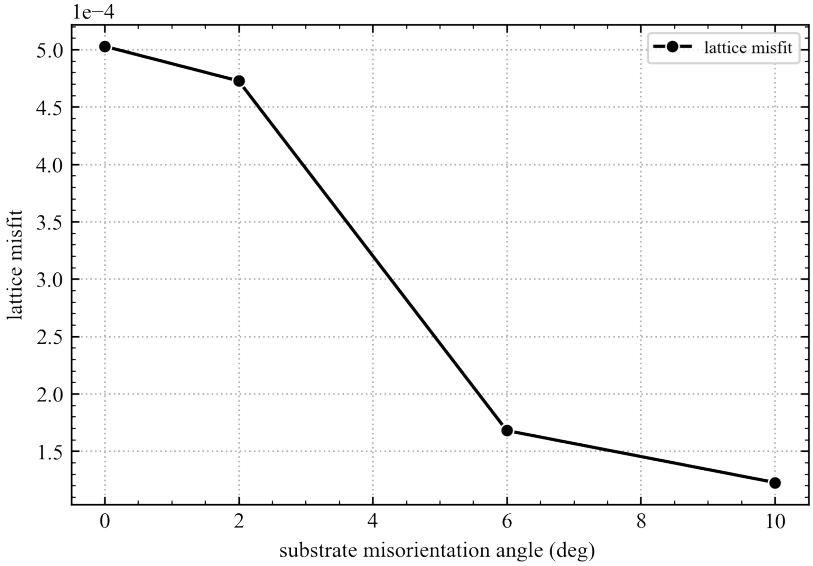

Fig 3. 1 Lattice misfit for InGaP/GaAs epilayer versus GaAs substrate off-cut angle[68]

In addition, through TEM images of misorientated substrates discussed in various works[112]–[114], arrays of steps are present on the surface of the off-cut substrate. The elastic properties of the epilayer are enhanced as the misorientation angle increases, resulting in a smooth surface for the epilayer above the substrate[68]. Since off-cut effects spread through the growth, these benefits can be applied to the QW laser growth directly.

In the case of self-assembled QDs, the conventional growth mechanism is S.K. growth, where surface strain plays a significant role in their formation[115]–[118]. Due to the large amount of strain between the QD layer and the buffer layer, dislocations may also be generated during the growth of QD[119], [120]. Therefore, it is essential to implement strategies that release this strain without compromising the quantum dot's gain or emission wavelength for high performance QD lasers (particularly problematic for lasing at longer wavelength). This issue is of particular importance in multiple QD layer stacking, as it is difficult to stack QD layers close together in order to achieve higher dot density due to the significant strain accumulated during growth [58], [121]. Theoretically, the use of a misorientated substrate should have a positive influence on the growth of the QD layer by providing a higher quality buffer layer and reducing the dislocation density[112], [113]. However, very few research has been conducted on the influence of substrate orientation on the size and density of S.K growth of QDs. The research

done on the gain spectrum of the InP/GaInP QD laser suggests the mis-orientated substrate has altered on the size distribution of quantum dot[122]. However, the results are only compared based on gain characteristics, and the origin of mis-orientated substrate on the performance of QD laser is not thoroughly discussed. Since this could provide a new optimisation technique for future InAs/GaAs QD laser growth. The off-axis substrate growth on the performance of InAs/GaAs QD lasers is worth investigation.

3.3 Experiment

The National Epitaxy Facility currently has 3 MOCVD reactors and we are using the 7x2" Thomas Swan showerhead reactor for this project. In these experiments, QD laser samples were grown on 2-inch Si doped GaAs (001) or 3-degree towards the (110) plane substrates. MOCVD growth of the laser structures was carried out by NEF staff member, Brett Harrison, in Sheffield.

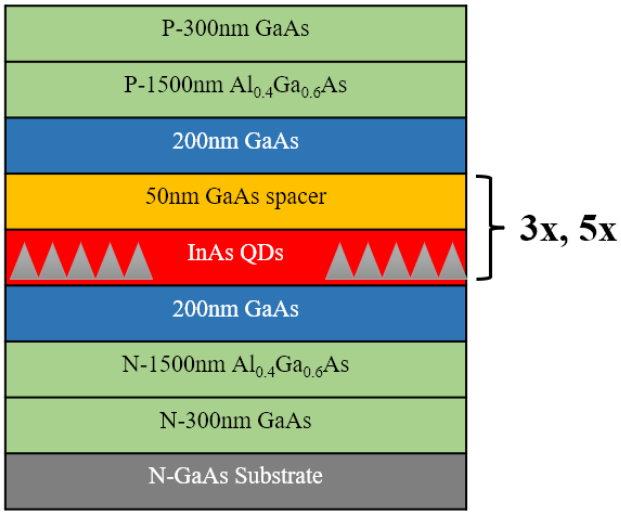

Fig 3. 2 Structure of S.K. growth of InAs/GaAs QD laser. It has 3 & 5 stacks of QD layer with separation of 50nm.

The multi-wafer chamber of the TS reactor allows for the simultaneous growth of identical laser structures under the same growth conditions on both on-axis and 3-degree substrates. The only possible difference apart from substrate misorientation is the position of the substrates in the substrate susceptor, but separate investigations show that this is not significant in this reactor. Fig 3. 2 shows the QD laser structure grown. Firstly, a 300nm buffer layer is grown on the Si-doped GaAs substrate. This is followed by a 1500nm AlGaAs lower cladding layer and the separate confinement heterostructure (SCH) layer consisting of 200nm of GaAs is grown on either side of the QD active region. Inside the active region, the QDs are formed by S.K. growth. 2ML of InAs QDs were deposited at 485°C at a growth rate of 0.95ML/s. The V/III ratio is kept at 4.7 for the QD layer and 2.1 for the capping cladding layer. After 20s of growth interruption, the QD is then capped with a 2-step capping process of 10nm of low-temperature GaAs capping

(485 ºC) and 40nm of high-temperature GaAs spacer (560 ºC). Finally, the 1500nm upper cladding layer of $Al_{0.42}GaAs$ was grown at 575 ºC. The doping density for the upper & lower cladding layer is p-1x10^{18}/cm^3 and n-1x10^{18}/cm^3. The growth temperature is adopted from [123], [124] and the 2-step capping process is used for improving the linewidth of the QD[125], [126]. Room temperature photoluminescence (PL) spectra were obtained using a 1 W 532nm He:Nc laser to excite the sample surface, with the PL emission detected by an InGaAs detector. The PL spectrum obtained from single layer QD grown with same laser structure for reference is plotted in Fig 3. 3.

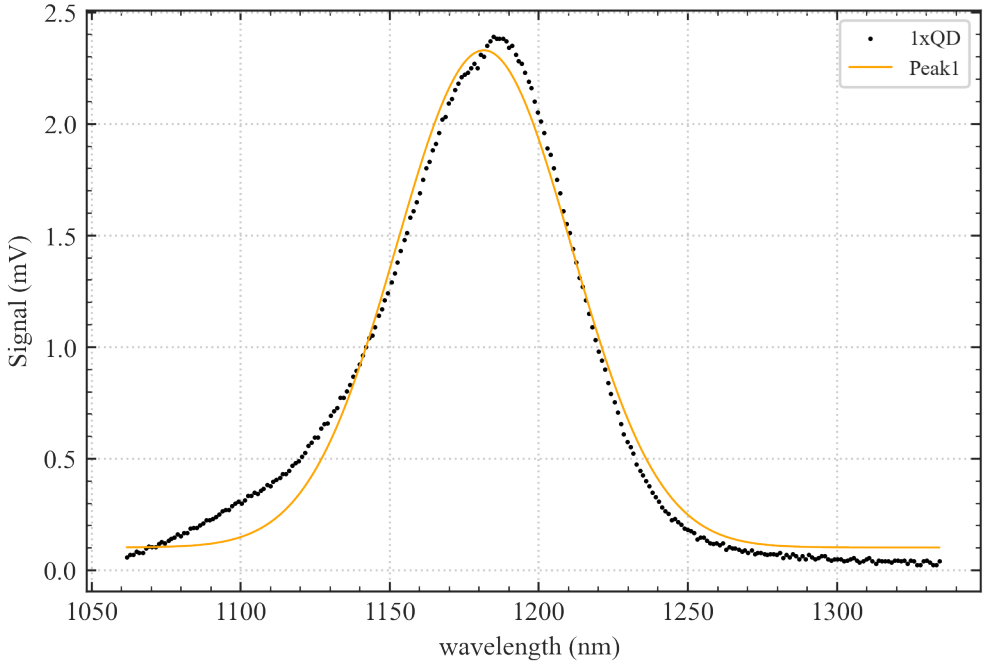

Fig 3. 3 Room temperature PL of single layer QD reference structure, the single peak gaussian fit is performed

For growth of 1.8ML of InAs QDs and a 0.95nm/s deposition rate with a V/III ratio of 6, the PL spectrum (Fig. 3.3) of a single layer of QD with an actual laser structure on the on-axis substrate shows a peak wavelength of ~1185nm. From the gaussian fit, the RT-PL shows a single peak at ~1180nm, with FWHM at ~69nm. For each layer number (3 or 5), room temperature PL measurements were carried out for the QD laser structure. From the PL measurements (Fig 3. 4) of 3- & 5-layer QD lasers on different substrates, we observe a central emission wavelength of around 1.15µm for all QD laser samples, with a small shift to a longer

wavelength for the 5-layer sample. Table 3.1 summarises the peak wavelength and FWHM for each sample's PL spectrum.

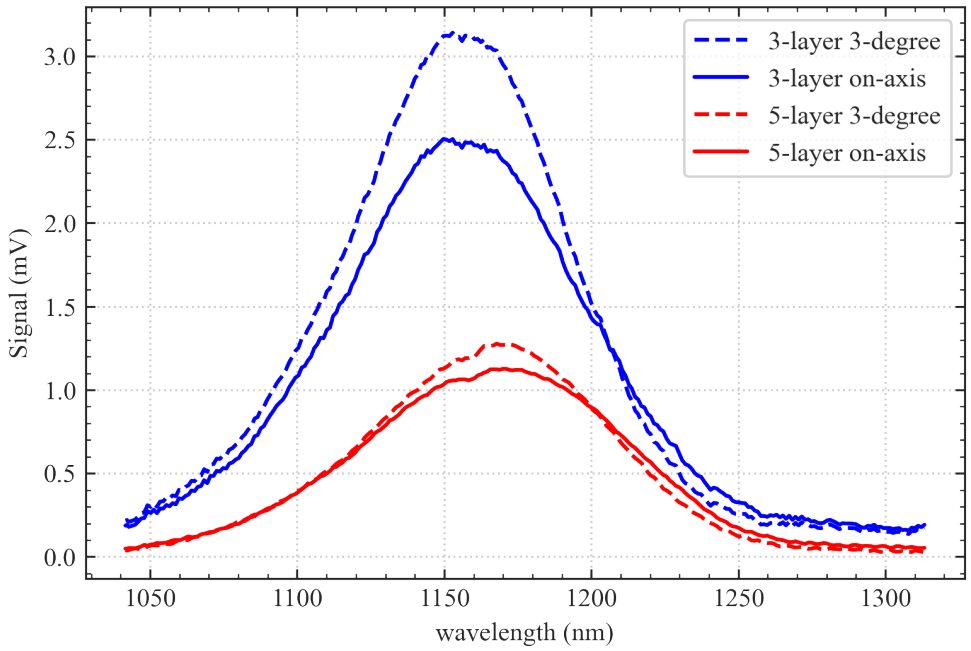

Fig 3. 4 Room Temperature PL spectral of 3 & 5-layer QD laser structure on different substrate off-cut angle

Sample	PL Intensity (V)	PL Centre (nm)	FWHM (nm)
Single Layer Reference	2.42	1190	69.5
x3 Stack 3 Deg-off	3.207	1154	85
x3 Stack on-axis	2.567	1154	91.8
x5 Stack 3 Deg-off	1.279	1166	93.7
x5 Stack on-axis	1.143	1166	103.2

Table 3.1 Summary of room Temperature PL spectral of 3 & 5-layer QD laser on different substrate off-cut angle, reference with single layer PL spectral

In Fig 3. 4, The PL peak wavelength for the 5-layer QD samples has a small red-shift of ~12nm compared to the 3 stacked samples on both substrates. This indicates that such red-shift is likely a result of a slight change in the quantum dot distribution to larger size dots on the 5-layer sample. The red-shift is not due to mis-cut substrate as we have observed same PL emission between different substrates of the same stacked QD layer. This implies that the off-axis substrate does not change the average QD size distribution compared with their on-axis counterparts. Compared to the single layer reference, we observed a blue-shift in PL of ~25nm for the 3 & 5-layer QDs on both substrates. This is due to the compressive strain accumulated during the stacking where the thin GaAs spacer does not fully relax the strain, which affects the QD layer grown above. This interaction of the strain field in the first QD layer will modify the transition energy of the second QD layer[127]. Such blue-shift in wavelength is also reported by Somintac *et al*.[128]

For the on-axis substrate, the FWHM of the 3-layer sample is 91.8nm and 103.2nm for the 5-layer sample. In comparison with the PL of reference single-layer QD sample, the linewidth of all the stacked QD samples has increased. This is a typical issue seen in the stacking of QD layers[58]. Linewidth broadening is seen in QD ensembles as a result of the accumulation of strain as multiple layers are stacked[60], [129]. The effect of inhomogeneous broadening worsens as the number of stacked layers increases, hence the broad FWHM for the 5-layer sample. There is a 34% increase in FWHM from single layer to 3-layer on-axis QD sample. The increase in FWHM per layer is ~11.3% and if such an increase is linear, we will expect ~56.5% increase in FWHM for the 5-layer QD sample. However, we only obtain ~48.2% increase in FWHM of 5-layer sample compared with single-layer sample. This suggests the effect of inhomogeneous broadening is probably going to saturates at higher stacking, which is not surprising since the effect of strain on the SK process is non-linear. For both the 3-layer and 5-layer QD samples, a ~10% reduction in linewidth is seen when comparing the 3-degree samples to their on-axis counterparts. This implies that a more uniform distribution of QDs is achieved on a substrate with a 3-degree mis-orientation. There is also an increasing peak PL intensity for both 3-degree substrate samples compared with their on-axis counterparts in Fig 3. 4. The possible explanation for such increase in intensity could be that a higher density of

quantum dots is formed on the mis-cut substrate and/or fewer non-radiative defects are incorporated in sample grown upon the 3-degree surface.

After the room temperature PL measurements, the wafers were then fabricated into broad area lasers with ridge width of 100μm, 80μm and 50μm for device characterisation. The laser characterization includes IV, output intensity vs current (LI) and spectral measurements. The laser cavities were cleaved in length of 4mm to 0.5mm to determine the internal quantum efficiency through length-dependent measurements. To reduce self-heating effects, the temperature is maintained at room temperature for all measurements using a Thorlabs TEC temperature controller. For optical gain measurements, a multisection laser with a 7μm ridge width was fabricated using methods described in Chapter 2. In addition, 100μm diameter mesa diode devices on the different substrate samples can be used to compare the electroluminance (EL) spectrum at room temperature for more detailed optical analysis.

3.4 Results and Discussion

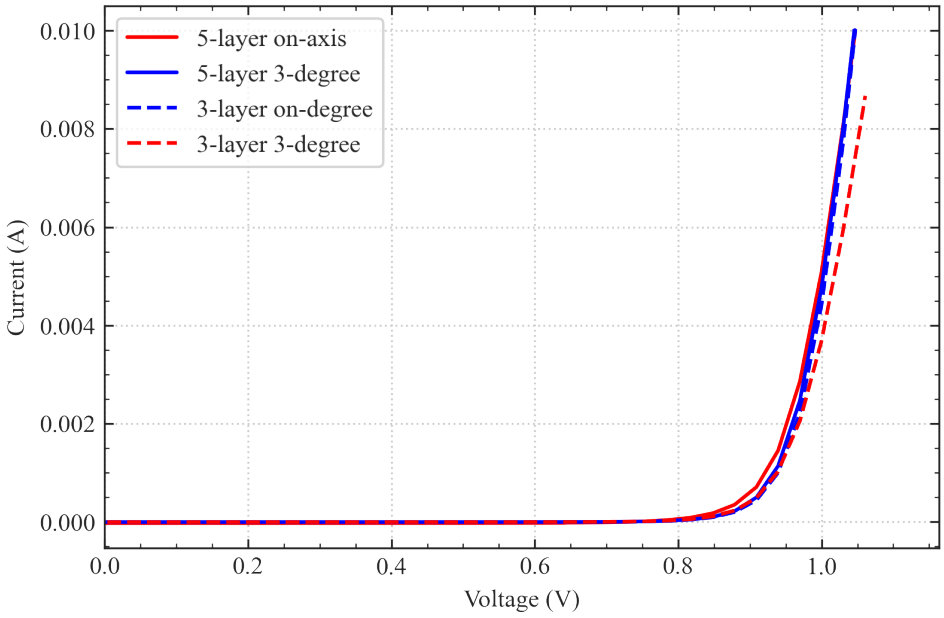

Fig 3. 5 IV measurements of 4mm broad area laser fabricated from 3- & 5-layer QD lasers at different substrate misorientation angle

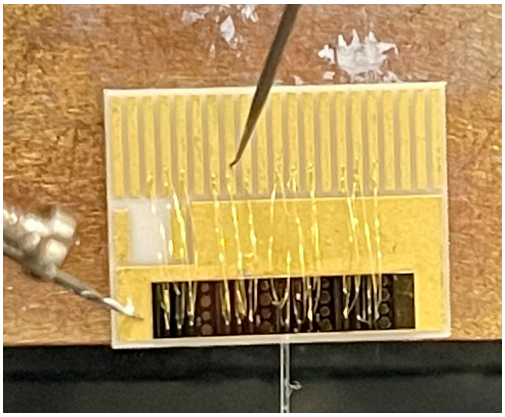

Fig 3. 6 Image of a typical mounted broad area laser on ceramic tile

Fig 3. 5 shows the IV characteristics of 4mm long broad area lasers fabricated from 3- and 5-layer QD laser samples on different substrates. The typical turn-on voltage for these laser diodes is 0.8V, which is the case for all of the fabricated devices. The slope of the forward bias curve IV, which reflects the resistance in the forward bias on- state, is 8.5 Ohms. The forward slope

for different devices is almost identical. This implies that the quality of the samples' fabrication is identical, which is essential for further analysis.

Broad area lasers with 4mm cavity lengths were fabricated for all 4 samples and measured using the LI setup described in chapter 2. As shown in Fig 3. 6, the devices are then mounted on AlO_2 ceramic tiles and wire-bonded to facilitate electrical injection. The LI characteristics of on-axis & 3-degree substrate 3-& 5-layer lasers are presented in Fig 3. 7. The threshold current density is obtained by taking the second derivative from the P/I and the maximum point is the J_{th}, as shown in Fig 3. 8. To avoid self-heating effects, the measurement is performed with a pulse width of 1μs and a duty cycle of 1%. The collected power is adjusted to the duty cycle, which represents the average power. The threshold current density obtained from each of these curves is summarised in Table 3.8.

The threshold current density (J_{th}) of 5-layer sample is ~180A/cm^2 for on-axis and ~110A/cm^2 for 3-degree substrate sample, as shown in Table 3.2. On both substrates, the threshold current density of 5-layer samples is ~61% less than that of 3-layer samples. Such improvements can be expected to result from the stacking of more QD layers, which should effectively increase quantum dot density and therefore the optical gain. In ideal conditions, the ratio of reduction in J_{th} should be roughly proportional to the increase in QD layer stacking[60]. However, we observed a 1.61-fold decrease in J_{th} from 3- to 5-layer QD on the on-axis substrate, which is slightly less than the 1.67-fold increase in the number of QD layers. This is likely due to the accumulation of strain and defects during the stacking process, which could reduce the optical gain obtained from the stacking of the QD layer, resulting in a non-linear reduction in J_{th}[130], [131]. Furthermore, the effect of wider active region of 5-layer QD lasers on the optical confinement factor can't be ignored. Either way, the J_{th} and optical gain aren't expected to scale properly with the layer number. In addition, 3- and 5-layer QD lasers grown upon a 3-degree off-axis substrate exhibited a lower threshold current density than their on-axis substrate counterparts.

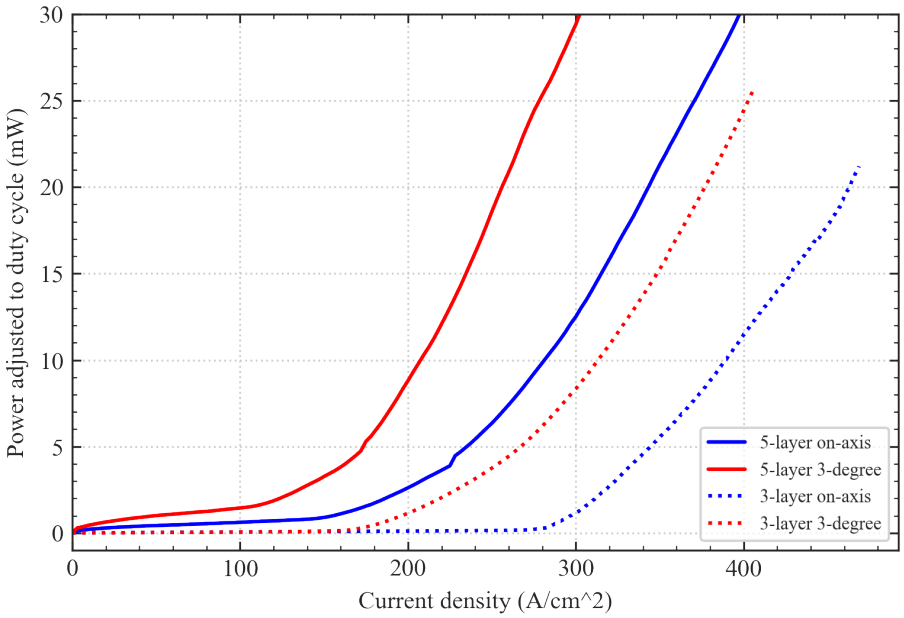

Fig 3. 7 Light power output vs pulsed current density for 4mm broad area laser of 3&5-layer samples at different substrate misorientation angle

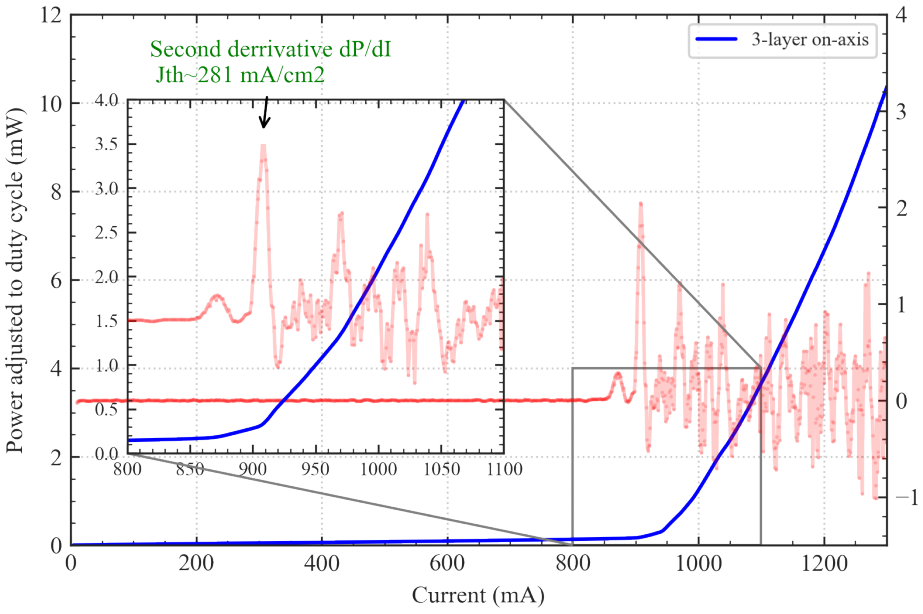

Fig 3. 8 Light power output vs pulsed current for 4mm broad area laser of 3-layer on-axis samples. The J_{th} of the laser device is obtained from maximum point of $\frac{d^2P}{dI^2}$

Sample	Threshold Current density (A/cm²)
5-layer on-axis	~180
5-layer 3-degree	~110
3-layer on-axis	~281
3-layer 3-degree	~210

Table 3.2 Summary of threshold current density obtained by pulsed LI measurements using methods described from Fig 3.8 at room temperature

These results clearly indicate that the off-axis substrates lead to a significant reduction in laser threshold current. In particular, the 5-layer 3-degree sample has the lowest J_{th} at room temperature of ~110A/cm^2. Compared to on-axis samples, the J_{th} of 3-layer and 5-layer QD samples is reduced by ~70A/cm^2 on 3-degree off-axis substrate, and it appears from the results that this reduction is independent of QD layer stacking.

To further analyse the performance of the QD lasers on different substrates, pulsed LI & lasing spectrum of different cavity lengths of 5-layer on-axis & 3-degree off-axis samples' broad-area laser are measured. Fig 3.9 plots the optical emission spectrum for each of the 4 broad area laser samples at 4mm cavity length and with pulsed current injection at 1.2xJ_{th}. The method for spectrum measurements is defined in Chapter 2. In Fig 3. 9, the spectrum has 2 distinct groups, with the 3-layer samples exhibiting lasing at shorter lasing wavelength of ~1050nm and the 5-layer samples exhibiting lasing at ~1130nm. The peak wavelength is almost identical for both 3-degree substrates compared with their on-axis counterparts, as we saw in the PL measurement (Fig 3. 4). The emission from the 5-layer samples is ~80nm red shifted compared with the 3-layer samples, in good agreement with the RT-PL measurements results. This suggests the red shift in wavelength results from the stacking of an increased number of QD layers.

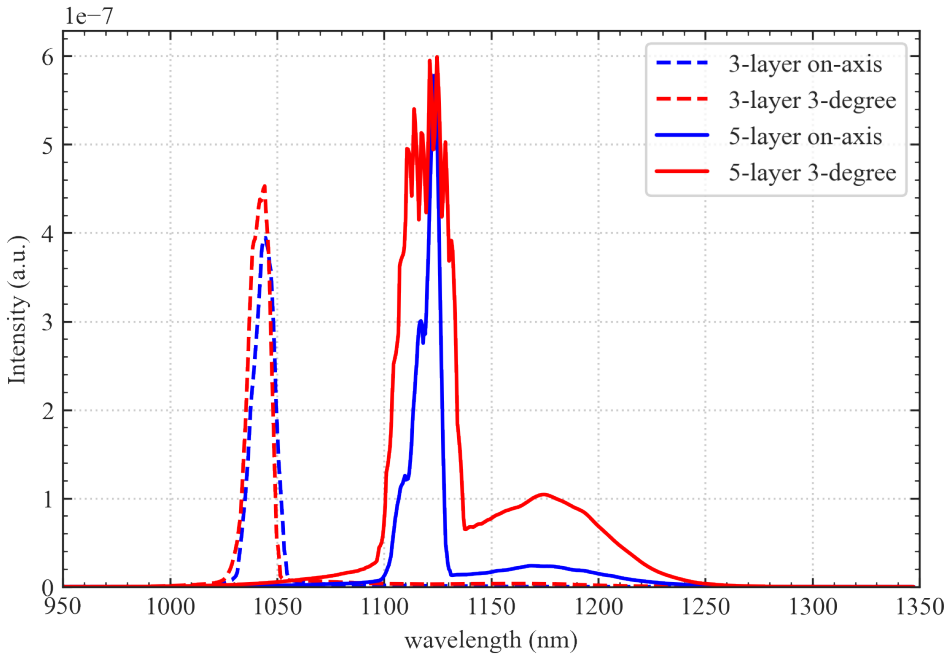

Fig 3. 9 Room temperature Emission spectrum at 1.2xJ_{th} for broad-area lasers of 3-layer and 5-layer QDs at different substrate orientations

The stacking in the 5-layer samples also results in an inhomogeneous broadening of the linewidth compared with the 3-layer sample. Such broadening of linewidth is also observed in RT-PL (Fig 3. 4). This might due to a wider distribution of dot size during higher stacking of QD layers[18], [51]. We also observed multiple separated peaks on the lasing spectrum (apart from the higher intensity shoulder) of 5-layer samples whereas the 3-layer samples exhibited a single-peak emission spectrum like the single layer QD PL shown in Fig 3.3. This implies the 3-layer samples have higher uniformity of the QD. The longer wavelength shoulder on the 5-layer samples emitting at ~1160nm could be some amplified spontaneous emission from the ground state of QD, and lasing is occurred at shorter wavelength (~1100nm), suggesting possible excited state lasing for these sample at 1.2xJ_{th}. This will be discussed further in the mesa diode EL measurement, where different quantum dot states are observed. From the spectral measurements, we can conclude that the 3-degree substrate has little to no effect on the emission wavelength which is beneficial for controlling the wavelength of QD laser.

Although we observed a significant improvement in J_{th} on 3-dgeree compared to the on-axis substrate sample in the LI measurements above, such improvements can be explained by many reasons and also, we need to exclude individual device error in the measurement. To investigate the properties of the devices further, the threshold current density in lasers with different cavity lengths was obtained using the same methods described in Fig 3. 8. This is then used to determine the internal quantum efficiency as described in Chapter 2. The internal quantum efficiency η_i and internal loss α_i of 5-layer on-axis and 3-degree are obtained from the pulsed LI measurements shown in Fig 3. 10. Thus, we can compare the optical performance of these lasers more precisely between different substrates.

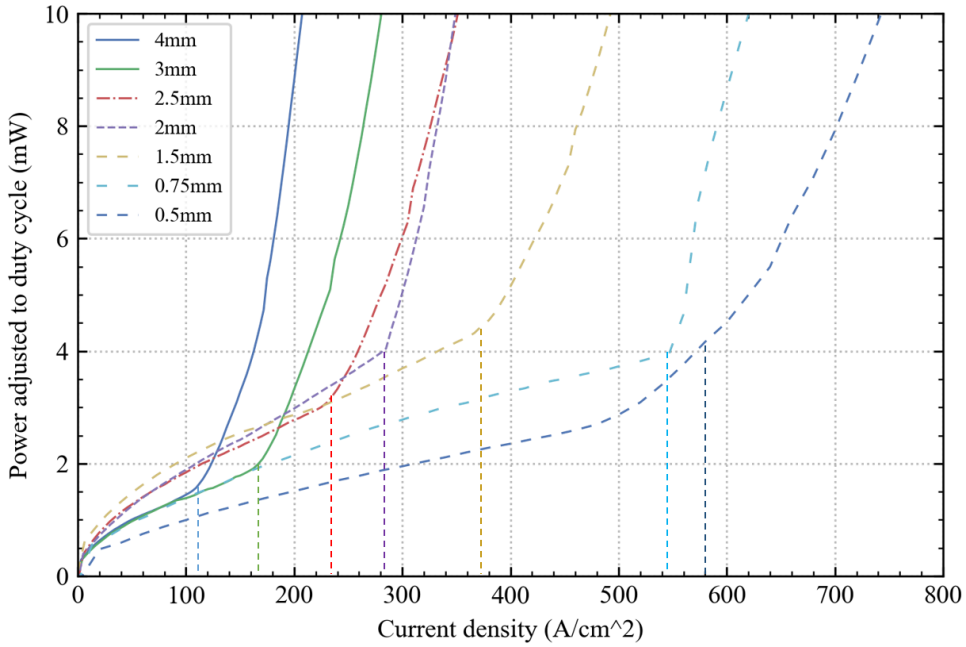

Fig 3. 10 Pulsed LI measurement for 5-layer 3-degree sample broad area laser cavity length from 4mm to 0.5mm

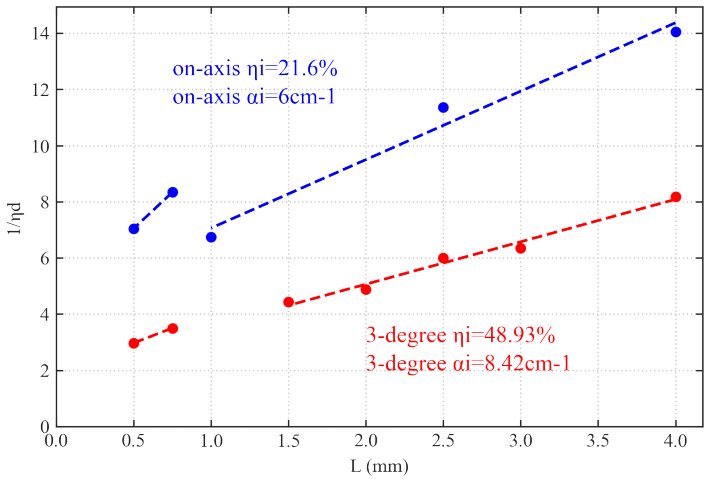

Fig 3. 11 Calculation of internal loss (α_i) and internal quantum efficiency (ηi) from the length LI measurement for 5-layer 3-degree and on-axis substrate sample

Fig 3. 11 shows the $1/\eta_d$ plotted against the cavity length. As previously described in Chapter 2, the external quantum efficiency (η_d) is calculated from the threshold current density & slop of the curve after the lasing. From Fig 3.11, the internal quantum efficiency η_i is obtained from the intercept of the line with the y-axis, and the loss in the laser α_i is extracted from the slope. The change in slope of the line observed in Fig 3. 11 indicates a shift from ground-state to excited-state lasing. In Fig 3. 11, the 5-layer 3-degree sample has a η_i of ~48.93% and the on-axis sample has ηi of ~21.6%. Thus, there is a large increase of 2.25 times in internal quantum efficiency for lasers grown on 3-degree substrate.

To analyse the origin of such improvements, the relationship between the threshold current density and internal quantum efficiency can be derived from the steady-state carrier rate equation model [132]:

$$\frac{N_{th}}{\tau_D} = \frac{\eta_i I_{th}}{qV} = \left(r_{sp} + r_{nr} + r_l\right) \quad (3.2)$$

Where I_{th} is the threshold current, τd is carrier lifetime, N_{th} is the carrier density at threshold current. The r_{sp}, r_{nr}, r_l are the spontaneous emission rate, non-radiative auger recombination rate and auger recombination rate. Rearranging the Equation 3.2:

$$I_{th} = \frac{qN_{th}V}{\tau_D \eta_i} \quad (3.3)$$

From Equation 3.3, that J_{th} is inversely proportional to the η_i. The η_i is related to the material defect levels in the active region. However, in the previous LI measurements (Fig 3. 7), the 61% reduction in J_{th} of the 3-degree sample is much less than the increase in ηi as seen in Fig 3. 11. This implies there are other factors introduced which might offset the increase in η_i. Since the Equation 3.3 shows that the threshold carrier density N_{th} and carrier life time τ_d also determine the J_{th} of laser. The carrier lifetime τ_D, is in fact generally a function of carrier density N_{th}. In addition, assuming 1 or 2 electron-hole pairs per QD occupied at ground state (at low carrier injection). Then the carrier density N_{th} is a function of quantum dot density as well. Therefore, both N_{th} and τd are dependent on quantum dot density and thus J_{th} depends on the quantum dot density as well. It is likely that the quantum dot density is another factor that could significantly affect the J_{th} of our QD lasers.

The threshold gain versus threshold current density can also obtained by length dependent LI using the methods described in literature[133].

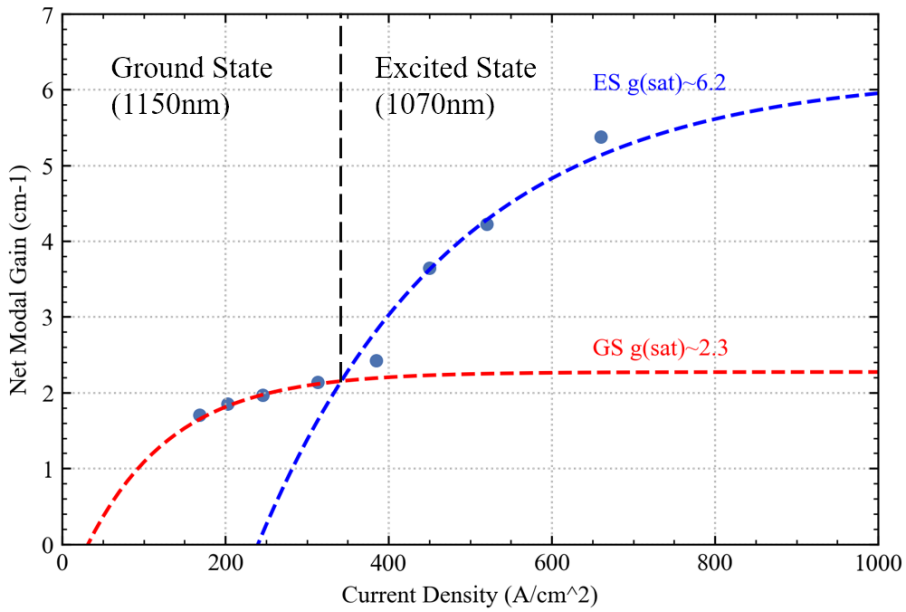

Fig 3. 12 Net modal gain for 3-degree 5-layer QD lasers versus current density. The dotted curves are fitted using equation 3.4.

Fig 3. 12 shows the net modal gain of 3-degree 5-layer QD samples as a function of current density. The curve is fitted using an empirical equation (3.4) [133]:

$$g = g_{sat}\left[1 - e^{\left(-A\frac{J_{th}-J_t}{J_t}\right)}\right] \quad (3.4)$$

Where g_{sat} is saturation modal gain, A is the fitting parameter, J_{th} is threshold current density, J_t is the transparent current density. In Fig 3. 12, the ground state (1150nm) net modal gain for 3-degree 5-layer QD sample is saturated at ~2.3/cm and the excited state (1070nm) net modal gain is saturated at ~6.2/cm. Considering the internal loss of ~8.4/cm obtained in the Fig 3. 11, the modal gain for ground state is thus ~10.8/cm and ~14.6/cm for excited state. However, these results are only fitted within a limited data range. Therefore, the obtained net modal gain results need to be further verified by the multi-section gain measurements which provides more detailed analysis of gain spectrum of QD laser grown on different substrate.

To further investigate the origin of the increased performance of QD lasers on the 3-degree substrate, we also carried out the multi-section gain measurements on the 5-layer QD lasers on different substrates using the method described in Chapter 2.

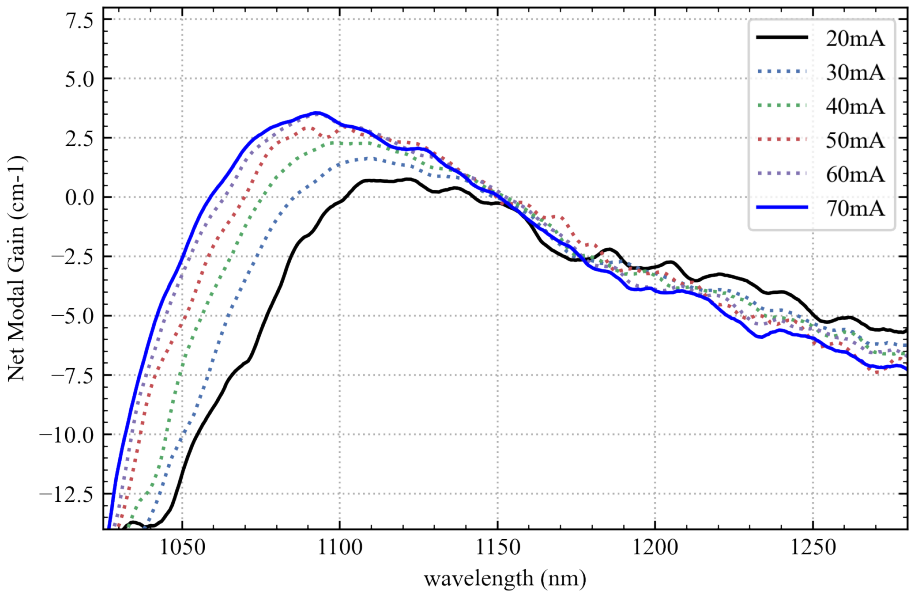

Fig 3. 13 Room temperature gain spectrum obtained from multisection laser of 5-layer on-axis sample at an injection current of 20mA to 70mA

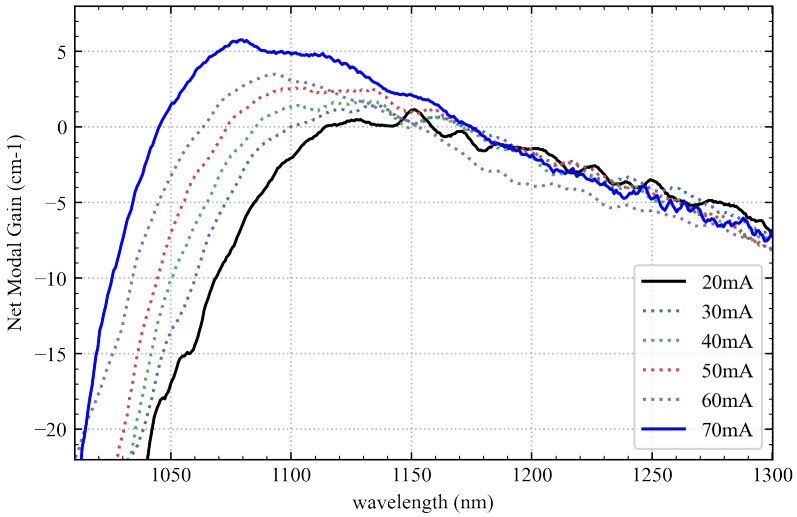

Fig 3. 14 Room temperature gain spectrum obtained from multisection laser of 5-layer 3-degree sample at an injection current of 20mA to 70mA

In Fig 3. 13 & Fig 3. 14, the gain spectrum of 5-layer samples was plotted against different substrates with injection current increased from 20mA to 70mA (equivalent to ~1.3 J_{th} to ~4.5 J_{th}). As shown in Fig 3. 13, the maximum gain for 5-layer on-axis sample occurs at ~1150nm at low injection current and the gain peak shifts towards a shorter wavelength (~1090nm) as injected current increases. The intensity of the gain peak (~1140nm) at 20mA (low injection current) begins to saturate as injection current increases, indicating possible ground state QD gain saturation at high injection current. Similar behaviour is observed in 5-layer 3-degree off-axis sample (Fig 3. 14) where the maximum gain is shifted towards shorter wavelength (~1070nm) as injection current increased. The gain spectrum has a general spectral width of ~100nm at room temperature at 70mA as shown in Fig 3. 15. This inhomogeneous broadening can be related to the spacing between states, where individual electronic transitions are indistinguishable. This implies the gain spectral consists of both GS and ES emission of dots at high current injection. Such behaviour is also observed on InGaAs dots at similar wavelength where the ground state and exited state of QD are intermixing[134].

The gain spectrum of 3-layer and 5-layer samples at an injection current of 70mA is compared in Fig 3. 15. Here we can see the 3-layer on-axis peak gain occurs at ~1060nm and the 5-layer

samples' peak gain is red-shifted by ~35nm compared with the 3-layer sample. This is consistent with the PL (Fig 3. 4) and EL (Fig 3. 9) measurements, which point to higher occupancies of smaller size dots on 3-layer samples comparing with the 5-layer samples. The gain spectrum shown in Fig 3. 15 for 5-layer 3-degree sample is higher than the on-axis sample across a wide spectrum range. The maximum gain of the 5-layer, 3-degree off-axis sample is ~6/cm and ~4/cm for the on-axis substrate sample at same current injection. Thus, we have observed a ~50% increase in maximum gain for the 3-degree off-axis sample. Such increase in maximum gain for 3-degree substrate sample is the reason behind the reduction in threshold current density J_{th}. Theoretically, we could assume a linear relationship between gain and injected current density J. From the rate equation and the Einstein relation, we can express the gain with injected current density as[132]:

$$J = q\left(\frac{\gamma c}{\Gamma \bar{n}}\right) g \quad (3.5)$$

Where g is the gain, Γ is optical confinement factor, γ is the ratio between extra photon produced and total photon from spontaneous emission, c is the speed of light and $\bar{n}$ is reflective index of the media. The equation 3.5 can then be approximated as linear between gain and current density J at $J \leq J_{th}$ as shown in equation 3.6:

$$g = A(J - J_{th}) \quad (3.6)$$

Where A is the gain coefficient and J_{th} is threshold current density. For real devices, we can't simply use this linear relationship to describe the gain and injection current density J. The material doping, QD line broadening and thermal effects etc. will contribute to shifting the curve away from linearity at high injected current density and temperature[130]. Although we have a smaller increase in the gain compared with ~61% reduction in J_{th} of 3-degree off-axis sample shown in LI measurements (Fig 3. 8), the approximation suggests the increase in maximum gain for the 3-degree off-axis sample will results in a reduction in J_{th}. This implies that the increase in quantum dot density, which is the likely reason behind the improvement of the gain also results in a corresponding reduction in J_{th}.

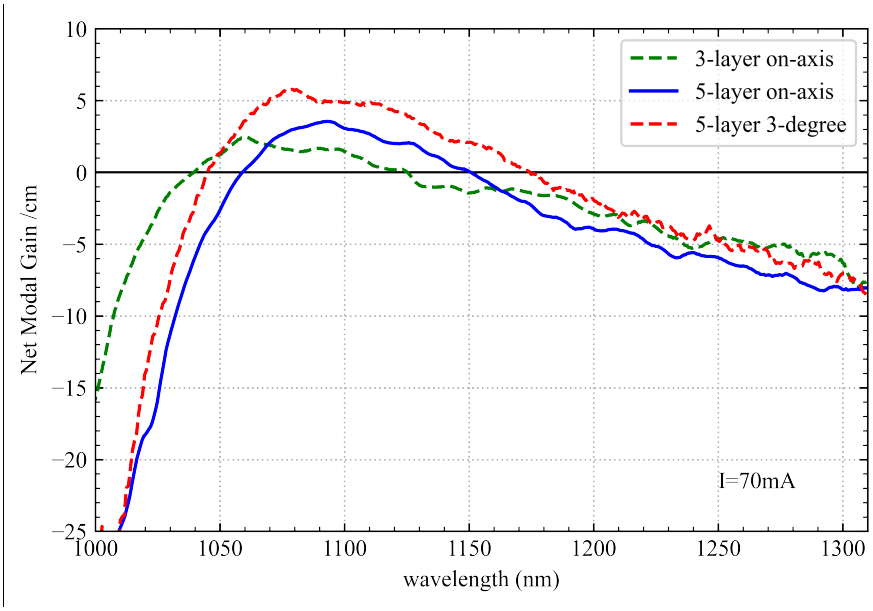

Fig 3. 15 Room temperature gain spectral obtained from 3-layer on-axis, 5-layer on-axis and 3-degree at an injection current of 70mA

The internal loss α_i which converges at longer wavelength gain spectrum in Fig 3. 15, shows that the α_i for 5-layer 3-degree off-axis sample is ~8.2±1/cm, for the on-axis is ~6.5±1/cm. These values are consistent with the calculated internal loss previously obtained from length-depended characterisation of ηi (Fig 3. 11). The internal loss consists of absorption of photons and scattering, etc., caused by the defects in the active region. The 3-layer QD sample has the lowest internal loss of ~6±1/cm, as shown in Fig 3. 15 and thus could implies a possible lower defect level compared to the 5-layer sample where stacking of QD layer increases the defects significantly. The increase in internal loss for 5-layer 3-degree substrate could be linked to the change of surface morphology in the active region and will be discussed later with respect to TEM results.

Therefore, the estimated net modal gain for 5-layer 3-degree is ~14.2±1/cm and on-axis is 10.5±1/cm, taking the internal loss of ~8/cm into account. These gain values are close to the net modal gain obtained from the length dependent LI measurements (Fig 3. 12). The calculated maximum net modal gain is lower than the state-of-art QD lasers in the literature where maximum model gain is ~55/cm for same current density [51], [131]. This is likely due to lower

quantum dot density of our QD sample which QD density is usually ~10^{10} to 10^{11} /cm^2 in literature[66].

Although the main reason behind the increase in threshold current density J_{th} is the improvement of gain of 3-degree substrate. There is also an increase in internal loss on 5-layer 3-degree off-axis sample compared with the on-axis sample, as shown in Fig 3. 11. Thus, the extracted characteristic temperature (*To*) through temperature-dependent LI measurements can be used as an indirect comparison of the defect level between different samples. The *To* is obtained using methods described in Chapter 2 and recorded as a function of temperature between the 15°C to 20°C. The *To* value should be as high as possible for a temperature stable performance of a reliable laser. In the Fig 3. 16, the stacking of QD considerably reduces the *To* from 77.3K for the 3-layer QD sample to 32.7K for a 5-layer QD sample. This implies bigger self-heating issue presents on these 5-layer samples. One possible explanation would be the higher overall defects when the number of stacked QD layers increases. These defects in the active region will act as additional carrier traps and non-radiative recombination centres, increasing the losses in the active region. The carrier will recombine at these traps and energy will be dissipated as heat which reduces the carrier available for population inversion[135].

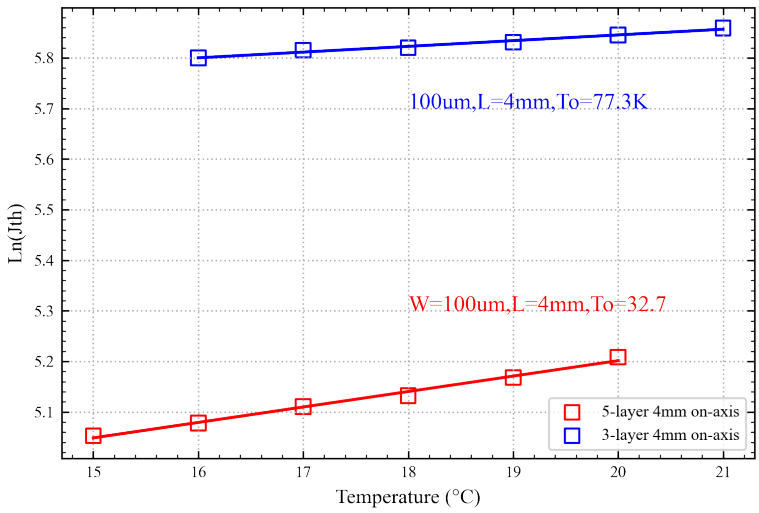

Fig 3. 16 Ln(J_{th}) versus temperature of 5-layer & 3-layer on-axis sample, slope is the characteristics temperature *To*. Temperature dependent LI is obtained from 100μm wide 4mm long laser device

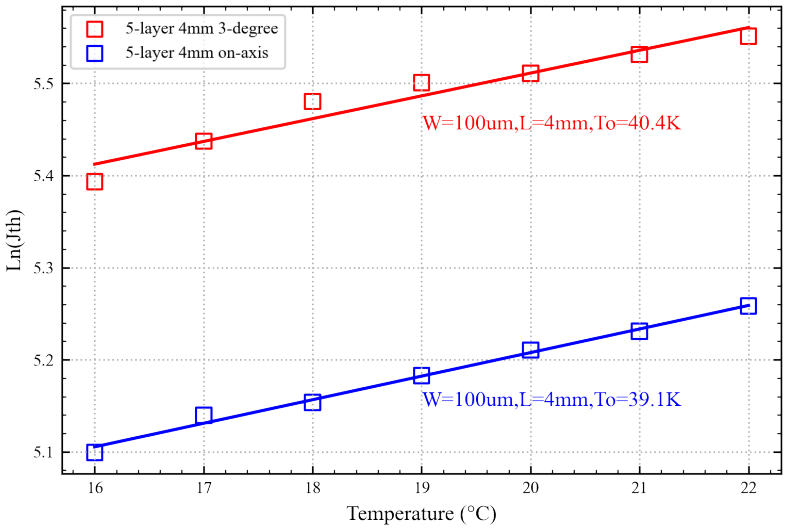

Fig 3. 17 Ln(J_{th}) versus temperature of 5-layer 3-degree & on-axis sample, slope is the characteristics temperature *To*. Temperature dependent LI is obtained from 100μm wide 4mm long laser device

In Fig 3. 17, there is only a slight increase of *To* from 39.1K to 40.4K on 3-degree substrate for 5-layer samples. The improvement is very small and such difference would be almost negligible which is within the measurement error of ~3%. This suggests that the 3-degree substrate doesn't have much effect on the characteristic temperature of the laser device and thus potentially the defect level. Although we observe a significant improvement in J_{th} and the gain on 3-degree substrate sample as discussed previously in the LI & gain measurements. The reduction of defect level is not likely to be the deciding factor that improves the performance of the QD laser between 3-degree and on-axis sample, as there is almost negligible improvements in the *To* on the 3-degree off-axis samples. Thus, the increase in quantum dot density (carrier density Nd) is the main reason behind the improvements in threshold current density of 3-degree off-axis sample.

In order to evaluate the quantum dot density, mesa diode EL measurements for 5-layer 3-degree off-axis and on-axis samples were taken and shown in Fig 3. 18 and Fig 3. 19. Mesa diode EL measurements allow us to better distinguish between different energy states of the QD ensembles.

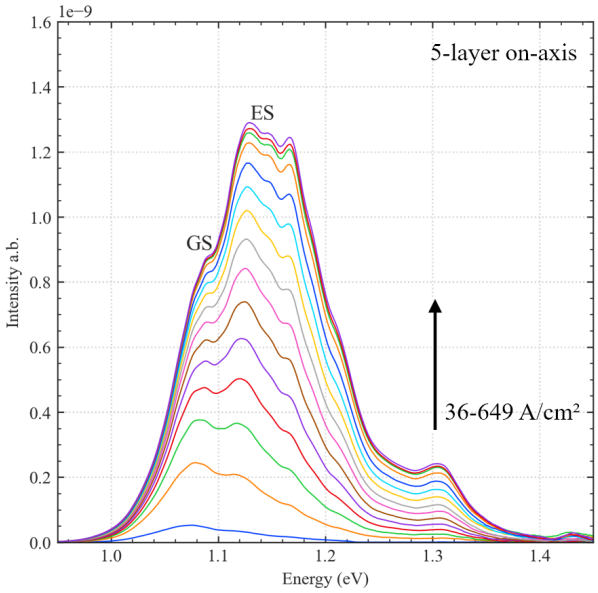

Fig 3. 18 Room temperature EL spectral obtained from 100μm of 5-layer on-axis sample at injection current density from 36mA to 649A/cm², GS emits at ~1.08eV and ES emits at ~1.13eV

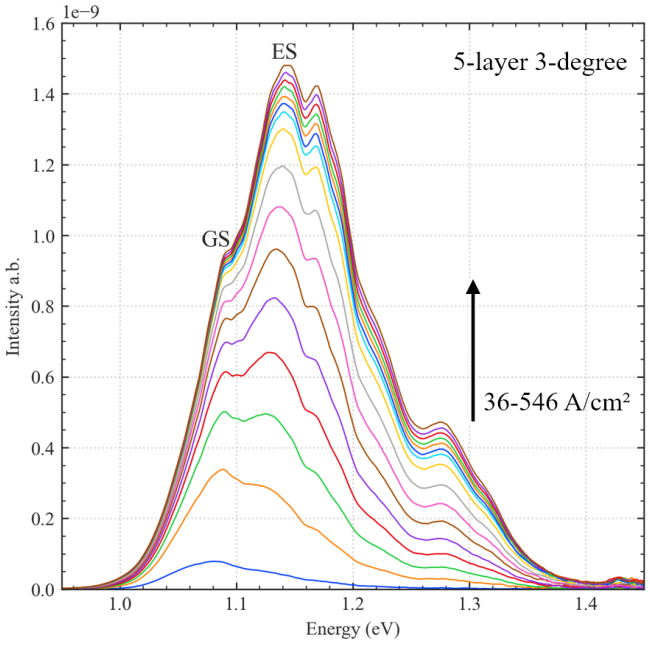

Fig 3. 19 Room temperature EL spectral obtained from 100μm of 5-layer 3-degree sample at injection current density from 36mA to 649A/cm², GS emits at ~1.09eV and ES emits at ~1.13eV

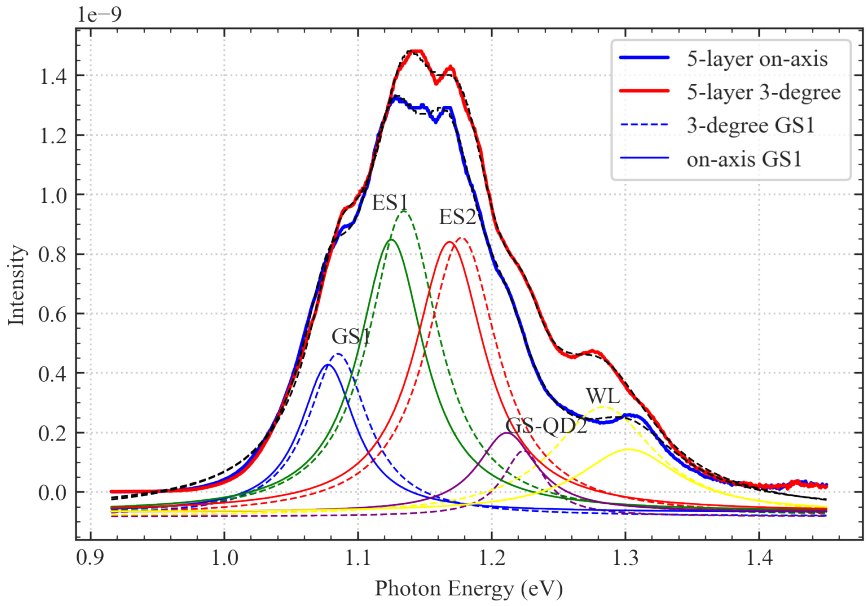

Fig 3. 20 Comparison of EL spectral for 5-layer QD laser 100μm mesa diode at different substrate with the fitted gaussian components for different QD states on on-axis(solid line) and 3-degree off-axis(dotted line) substrate sample at same current density.

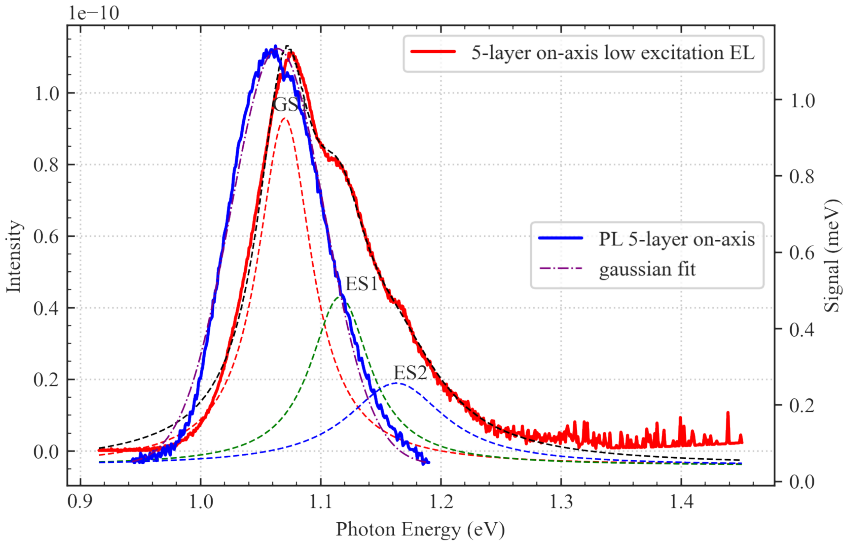

Fig 3. 21 Comparison of low excitation (50A/cm^2) mesa diode EL spectrum (red) for 5-layer on-axis QD laser with the RT-PL spectrum (blue). Dotted line shows the fitted gaussian component for mesa diode EL spectrum and dot-dashed line shows the gaussian fit for RT-PL.

Sample	Peak Intensity (x10^{-11})	Peak Centre (eV)	FWHM (eV)
3 Deg-off GS1	4.71	1.09	0.055
3 Deg-off ES1	10.3	1.13	0.064
3 Deg-off wetting layer	3.84	1.28	0.094
on-axis GS1	3.88	1.08	0.050
on-axis ES1	8.63	1.12	0.060
on-axis wetting layer	1.41	1.30	1.12

Table 3.3 Summary of Fitted gaussian peak for mesa EL spectrum (Fig 3.20) of 5-layer QD laser at different substrate.

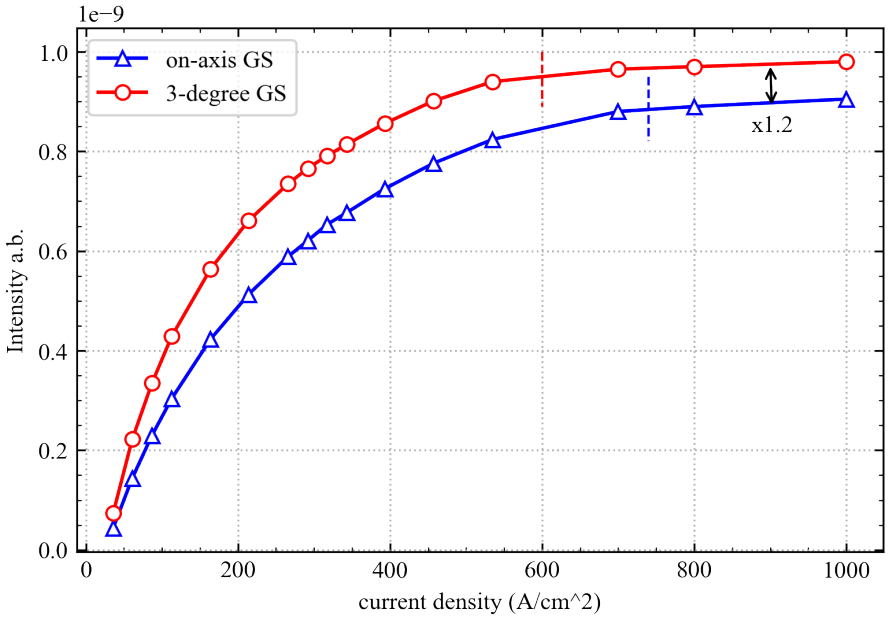

Fig 3. 22 Ground state peak intensity vs current density for 5-layer QD laser 100μm mesa diode at different substrate. The straight line shows the start of ground state saturation

The measurement setup is described in Chapter 2 and the light is collected from the top surface of the mesa diode at a constant temperature to avoid self-heating issue. The intensity is plotted against the photon energy instead of the emission wavelength for easier identification of different energy states.

In Fig 3. 18 and Fig 3. 19, there is a shift of peak from lower photon energy (longer wavelength) to higher photon energy (shorter wavelength) as injection current increased in both 5-layer samples. This indicates a transition from the ground state to the first excited state of quantum dot as injection current increases, where the ground state peak saturates at high injection current density[127]. Fig 3. 20 shows the mesa diode EL measurements for both substrate samples at same injection current density. The mesa diode EL recorded from the 3-degree off-axis and on-axis substrate sample has very similar ground state (~1.09eV) and excited state (~1.13eV) photon energy as shown in Fig 3. 20. Gaussian fit analysis for the EL measurement on the 3-degree and on-axis samples was also carried out and plotted in Fig 3. 20. Table 3.3 summaries the fitted gaussian components for 5-layer on-axis and 3-degree off-axis samples. The GS1 QD for both substrate samples centred at ~1.08eV and ~1.09eV (corresponding to ~1148nm). The separation between GS1 and ES1 on the gaussian fit for EL spectrum shown in Fig 3. 20 is ~40meV for both substrate samples. Fig 3. 21 compares the low-excitation EL spectrum of 5-layer on-axis sample with the RT-PL of 5-layer on-axis sample. A Gaussian fit is performed on both EL and PL spectrum. The GS of low excitation EL is at ~1.07eV (~1158.7nm) which is consistent with the PL gaussian peak of ~1.063eV (~1166nm) since RT-PL spectrum can be treated as EL spectrum at very low excitation. There is no wetting layer emission in low excitation EL spectrum (Fig 3. 21) since carrier will fill the energy state of QD first.

In Fig 3. 20, the ES1 for both substrate samples cantered at ~1.12eV (correspond to ~ 1107nm) which is same as the previous lasing EL spectrum of 5-layer samples (Fig 3. 9). There is a very small shift (~0.008eV) in photon energy in all energy states for the 3-degree off-axis sample compared with the on-axis sample. This implies that the 3-degree substrate may have smaller size QDs than the on-axis substrate. However, such difference in QD size is very small (corresponds to ~8nm) and thus can be related to a very small change in surface morphology

of GaAs spacer. The FWHM of both GS1 and ES1 peaks in 3-degree substrate is larger than the on-axis sample as shown in Table 3.3, suggesting the possible larger size distribution of 3-degree off-axis sample than the on-axis sample. The peak intensity of ES1 is ~2 times higher than the GS1 intensity for both substrate samples which is same as the double degeneracy theory of the excited state of quantum dot[136]. In Fig 3. 20, there is also a second excited sate peak (ES2) at ~1.17eV (corresponding to ~1059nm), which has a photon energy separation of ~5eV (~48nm) between ES2 and ES1. However, there is no ES2 lasing in the previous EL spectrum shown in Fig 3.9. But it can be expected that these QD laser to have lasing wavelength shifted to even shorter wavelength if the injected current density increased further than $1.2J_{th}$. Such behaviour is common for these InAs/GaAs QD lasers. There is a third excited state ES3 (GS-QD2) at (~1.25eV) appeared at longer shoulder of ES2 in both samples shown in Fig 3. 20. There is a possibility that the carriers are tunnelling between the GS of QD on second layer and thus intermixing with the ES3 state on the first QD layer with same photon energy. This peak is only observed at high excitation energy as shown in Fig 3. 18 & Fig 3. 19. The lower excited state of first layer QD starts to fill up and allows the carrier to recombine at GS of second layer QD but without recombined at ES3 of first layer QD[127], [137]. The large difference in intensity of fifth peak at (~1.28eV) is most likely due to the AlGaAs cladding layer, which corresponds to a wavelength of ~953nm. The fitted intensity for wetting layer on 3-degree off-axis sample is higher than on on-axis sample as shown in Table 3.3. This is likely due to the 3-degree substrate reduces the dislocation formed in the AlGaAs cladding layer by reducing the lattice mismatch between the substrate[138], [139]. There is also a shift in emission peak of wetting layer from ~1.30eV to ~1.28eV as shown in Fig 3. 20. This implies that the 3-degree substrate sample may relax the strain on the AlGaAs wetting layer which results in change of the bandgap of the AlGaAs.

Fig 3. 22 shows the ground state saturation curve for both substrate samples obtained from the GS peak intensity in Fig 3. 18 & Fig 3. 19. This allows the comparison of the carrier density of QD. At higher current injection, complete saturation of GS is observed in both on-axis and 3-

degree sample EL spectrum as the curve becomes parallel. Since the GS saturation intensity, I_{sat}, can be described by equation 3.7 [140]:

$$I_{sat} = \frac{2N}{\tau} \quad (3.7)$$

N is the quantum dot density, τ is the carrier lifetime. This can be used as a relative estimation of the quantum dot density difference between 2 samples, assuming all the quantum dot GS are occupied by 2 electron-hole pairs (in low injection current density). The GS saturation intensity of 3-degree sample is ~1.2 times higher than on-axis sample at complete saturation. The fitted peak intensity for 3-degree sample GS1 is ~20% higher than the GS1 for on-axis sample as well which is in good agreement with the Ground State saturation intensity curve shown in Fig 3. 22. This suggests a ~1.2 times higher quantum dot density for the 3-degree off-axis substrate sample. However, the ratio of internal quantum efficiency between different substrate samples obtained in Fig 3. 11 is much higher than the ratio of GS saturation intensity in Fig 3. 22. This is probably due to internal quantum efficiency measured from the length dependent LI is a mixture of excited states and the ground states as discussed in gain measurements section which results in a higher quantum efficiency than expected.

However, in EL measurements, only the carrier in the ground state were compared and these are directly related to the quantum dot density. Moreover, some light may not be fully collected by the apparatus in EL measurements due to unavoidable dispersion of light in the air which is larger than the lens diameter. Thus, only a relative comparison on QD density can be obtained from EL measurements. Therefore, further analysis of the quantum dot density and surface morphology is obtained from the TEM images of 5 layer 3-degree and on-axis sample.

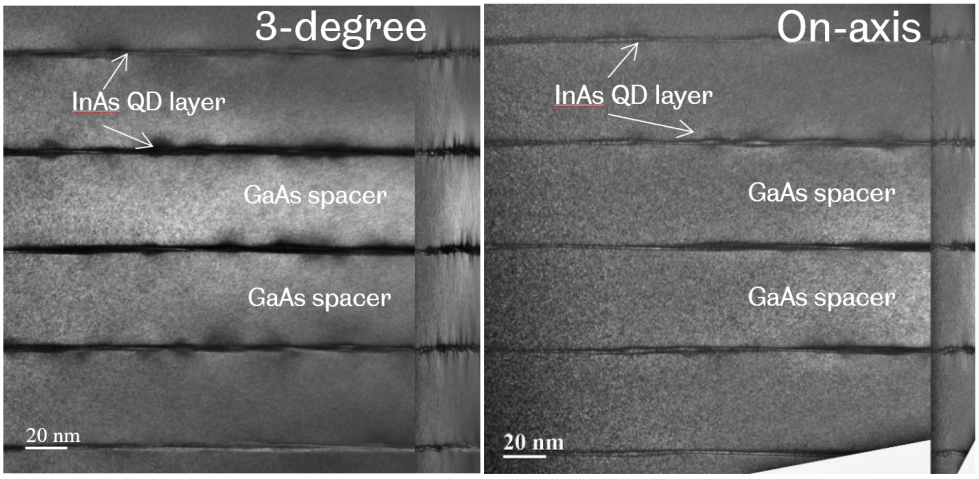

Fig 3. 23 Bright field TEM image of 5-layer QD laser at different substrate done by Dr. Richard. The image on left shows more QD formed on 3-degree substrate.

Fig 3. 23 shows the TEM images of both 5-layer 3-degree and on axis substrate laser samples. The InAs QD is embedded between the 50nm GaAs spacer layer. In Fig 3. 23, there are fewer QDs on the first QD layer than on other QD layers for both substrates, indicating that the problem is not due to substrate differences. One guess is the 200nm GaAs layer below the first QD layer which has a different surface strain compared to the other 50nm GaAs spacer above. The strain field produced by the first layer QD has an effect on the upper QD layers and their size. This implies that we would achieve an even lower J_{th} with more QD grown on the first layer by changing the strain of the 200nm GaAs waveguide layer.

	5-layer on-axis QD	5-layer off-axis QD	Error bar
QD counts	12.4	15	±2
Average QD density ($x10^9/cm^2$)	5.5	4.6	±0.4

Table 3.4 Summary of QD counts and average density of 5-layer QD laser over fixed area grown on different substrate.

In Table 3.4, the estimated average dot density is ~5.5±0.4x10^9/cm² for 3-degree sample and ~4.6±0.4x10^9/cm² for on-axis sample using the methods by counting the QDs of each layer over a fixed area with methods described in literature[141]. Comparing with the on-axis substrate, there is roughly ~20±8% increase in the density of dot for QD grown on 3-degree substrate. This ratio is about the same as the increase in the GS saturation intensity of 3-degree sample as shown in Fig 3. 22. However, these numbers are an order of magnitude lower than the QD density in the literature [142]. This explains the reason for insufficient ground state gain of these lasers, and further optimization of growth parameters is needed to improve the dot density.

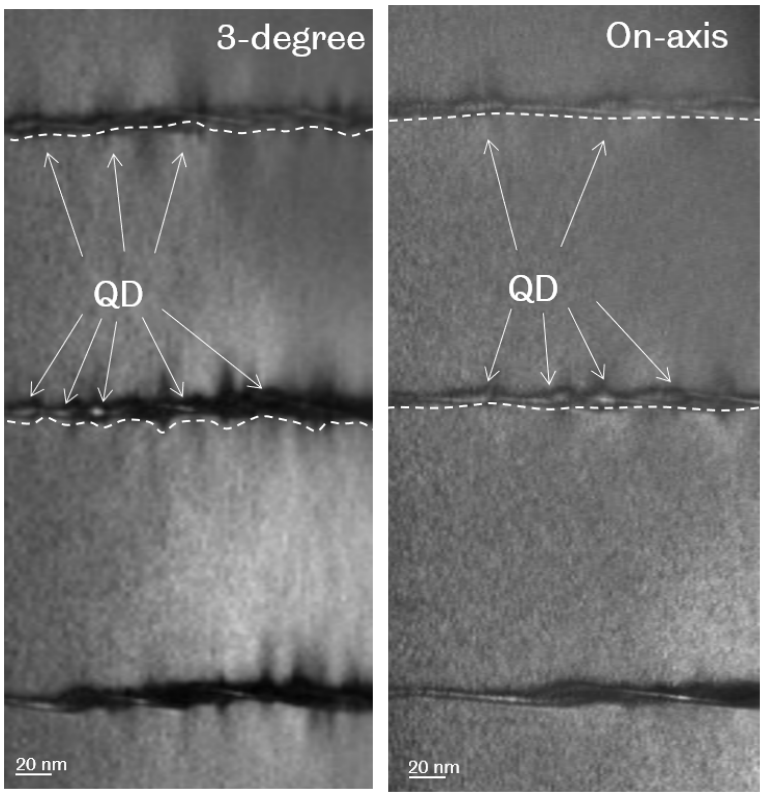

Fig 3. 24 Zoomed bright field TEM image of 5-layer QD sample on different substrate by Dr. Richard. Right image shows the closer steps formed under the QD layer with more QD formed at these step edges in 3-degree substrate sample. Extra bumpiness is observed on 3-degree substrate as indicated by dotted lines

From the zoomed cross-section TEM image Fig 3. 24, there are steps formed roughly 50nm apart under each QD layer (as indicates by the dotted lines). Quantum dots are grown at these steps' edges. In contrast, the lines shown in TEM image of on-axis sample (right) is smoother

without steps formed underneath the QD. More QDs were formed at the edge of these steps. These steps are densely formed in 3-degree sample, resulting in a smaller separation of dots in the 3-degree substrate.

Based on the mesa diode EL measurements and TEM image so far, 3-degree substrate shows higher quantum dot density than on-axis sample. The array of steps formed on GaAs spacer layer improves the surface morphology as well as reduces the lattice mismatch which provides preferential nucleation sites for the QDs. The increase of density of dots for 3-degree substrate also results in lower threshold current density and higher gain which is confirmed by the LI and gain measurements.

3.5 Future work towards high density QD laser

For our current laser grown on the on-axis and 3-degree substrate, there is an exited state lasing for these lasers, which is due to insufficient ground state gain. This is likely due to lower density of dots for these devices. The highest quantum dot density is ~5.5x10^9/cm² and this is about one magnitude lower than the state-of-art laser in the literature[142]. In order to improve the density of dots and thus the gain and reduce the J_{th}, direct approaches such as growth of higher stacks of QD layer is worth investigating. But the accumulation of defects and strain prevents the growth of higher stacking of QD layers. Methods to reduce the strain and defects should be considered to compensate for such effects. A higher degree off-axis substrate could be used to reduce the strain in the buffer layer and could allowing higher density of dots. However, such increase of dot density would have a limit. Another way of reducing the strain during the growth of QD is by incorporating the $In_{0.15}GaAs$ strain relaxing layer (SRL)[64], [65]. The $In_{0.15}GaAs$ SRL will also increase the emission wavelength which is necessary for reaching the telecom application at 1.3µm[143]–[146].

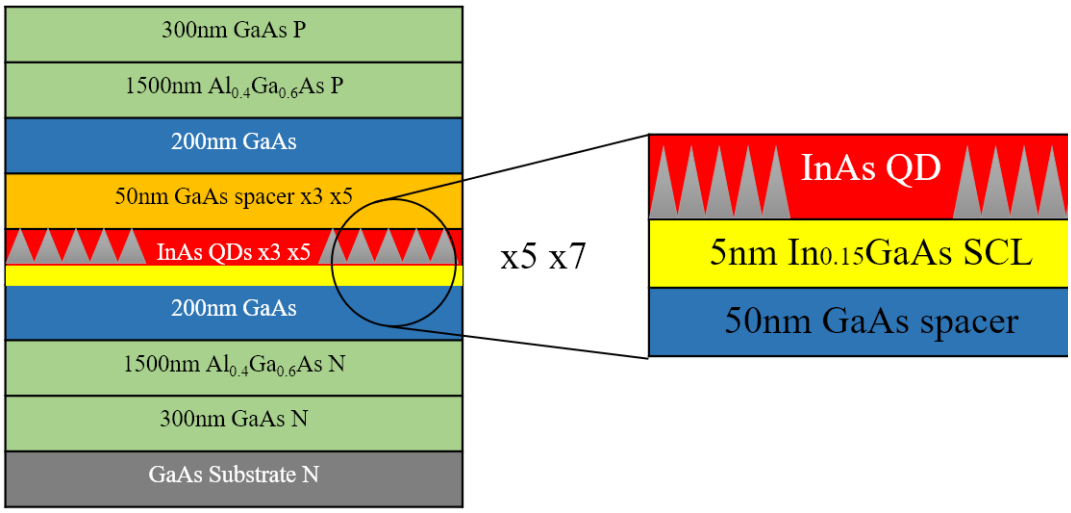

Fig 3. 25 new structure for 1.3µm QD laser with 5nm InGaAs SCL incorporation

The proposed new laser structure shown in Fig 3. 25 adds 6nm LT - In0.15GaAs (SRL Capping layer) into current 1.1µm laser structure and the rest of structures remain the same. The $In_{0.15}GaAs$ provides a strain balance effect between InAs QD and GaAs spacer layer which

could reduce the lattice mismatch (thus strain) and larger size QD can be formed. However, calibration of QD PL sample growth is required before the growth of actual QD laser structure in order to obtain optimum growth parameters such as indium composition, thickness of InGaAs SRL, etc. The GaAs spacer thickness can be further reduced after the incorporation of SRL which should improve the overall quantum dot density and reduce the threshold current density for the laser. Last but not least, the QD structure on higher degree off-axis substrate such as 6-, 9- and 12-degree towards (110) substrates can be grown in the future which provides a complete analysis of the effect of off-axis substrate on the density of QD. Together with the above strain releasing methods, a much higher density of QD can be achieved than current QD structure and this would be another step towards the final silicon integration of these QD lasers. In future, it would be interesting to compared the quantum dot density on GaAs (311)B planes as well, but such a high degree off-axis would be difficult to integrate with standard silicon substrates. Finally, further investigation into the heterogenous integration of these InAs/GaAs QD lasers on silicon platform, utilising higher degree off-axis substrates would be interesting to explore in future growth.

3.6 Conclusion

In conclusion, this chapter demonstrates that the MOCVD growth of InAs/GaAs QD lasers on 3-degree GaAs substrates outperforms those on on-axis GaAs substrates. The spectral measurements show lasing at 1.1μm at room temperature with the lowest J_{th} of 110A/cm^2 achieved on 3-degree substrates, and is comparable to the state-of-the-art GaAs QD laser at the same wavelength [31]. On a 3-degree substrate, lower threshold current density and higher maximum gain are achieved. The off-axis substrate has no effect on the emission wavelength of the device, but the 3-degree substrate has a higher internal quantum efficiency than the on-axis substrate. The increase in performance of the QD laser is mostly due to a ~20% increase in dot density on 3-degree substrate sample which is obtained from the mesa diode EL measurements and TEM images. The array of steps formed by a 3-degree substrate improves the surface morphology of the GaAs spacer and acts as additional nucleation sites which favours the formation of higher dot density.

However, the ground state gain for both 3- and 5-layer devices is insufficient for lasing, and the lasing is mainly due to excited states. The ground state lasing could be achieved by increasing the density of quantum dots further. Although the most obvious way to obtain higher density dot is to change the S.K QD growth parameters such as temperature, V/III ratio, etc. However, the off-axis substrate could also be taken into consideration as it has very little effect on the emission wavelength of QD laser. Theoretically, a higher degree of off-axis substrate could further improve surface morphology, resulting in a higher dot density. Therefore, further growth of sets of off-axis substrates, such as 6, 9, and 12-degree substrates, is necessary for obtain optimal quantum dot density for the QD laser.

3.7 reference

[99] M. Henini and M. Bugajski, 'Advances in self-assembled semiconductor quantum dot lasers', *Microelectronics J*, vol. 36, no. 11, pp. 950–956, Nov. 2005, doi: 10.1016/J.MEJO.2005.04.017.

[100] M. S. Skolnick and D. J. Mowbray, 'Self-assembled semiconductor quantum dots: Fundamental physics and device applications', *Annu Rev Mater Res*, vol. 34, pp. 181–218, 2004, doi: 10.1146/ANNUREV.MATSCI.34.082103.133534.

[101] Dusanowski, M. Gawełczyk, J. Misiewicz, S. Höfling, J. P. Reithmaier, and G. Sęk, 'Strongly temperature-dependent recombination kinetics of a negatively charged exciton in asymmetric quantum dots at 1.55 μ m', *Appl Phys Lett*, vol. 113, no. 4, Jul. 2018, doi: 10.1063/1.5030895.

[102] N. F. Hasbullah *et al.*, 'Dependence of the electroluminescence on the spacer layer growth temperature of multilayer quantum-dot laser structures', *IEEE J Quantum Electron*, vol. 45, no. 1, pp. 79–85, 2009, doi: 10.1109/JQE.2008.2002671.

[103] H. Y. Liu *et al.*, 'Improved performance of 1.3 μm multilayer InAs quantum-dot lasers using a high-growth-temperature GaAs spacer layer', *Appl Phys Lett*, vol. 85, no. 5, pp. 704–706, Aug. 2004, doi: 10.1063/1.1776631.

[104] C. L. Walker *et al.*, 'The role of high growth temperature GaAs spacer layers in 1.3-μm In(Ga)As quantum-dot lasers', *IEEE Photonics Technology Letters*, vol. 17, no. 10, pp. 2011–2013, Oct. 2005, doi: 10.1109/LPT.2005.854393.

[105] N. Arpatzanis *et al.*, 'Effect of rapid thermal annealing on the noise properties of InAs/GaAs quantum dot structures', *J Appl Phys*, vol. 102, no. 5, 2007, doi: 10.1063/1.2775536.

[106] T. Yang, J. Tatebayashi, K. Aoki, M. Nishioka, and Y. Arakawa, 'Effects of rapid thermal annealing on the emission properties of highly uniform self-assembled InAs/GaAs quantum dots emitting at 1.3 μm', *Appl Phys Lett*, vol. 90, no. 11, 2007, doi: 10.1063/1.2713135.

[107] C. Dion, P. Desjardins, N. Shtinkov, F. Schiettekatte, P. J. Poole, and S. Raymond, 'Effects of grown-in defects on interdiffusion dynamics in InAsInP (001) quantum dots subjected to rapid thermal annealing', *J Appl Phys*, vol. 103, no. 8, 2008, doi: 10.1063/1.2905317.

[108] S. Bietti, L. Esposito, A. Fedorov, A. Ballabio, A. Martinelli, and S. Sanguinetti, 'Characterization and Effect of Thermal Annealing on InAs Quantum Dots Grown by Droplet Epitaxy on GaAs(111)A Substrates', *Nanoscale Res Lett*, vol. 10, no. 1, pp. 1–7, Jun. 2015, doi: 10.1186/s11671-015-0930-3.

[109] T. P. Pearsall, B. I. Miller, R. J. Capik, and K. J. Bachmann, 'Efficient lattice-matched double-heterostructure LED's at 1.1 μm from GaxIn1−xAsyP1−y', *Appl Phys Lett*, vol. 28, no. 9, p. 499, Aug. 2008, doi: 10.1063/1.88831.

[110] A. S. Brown, U. K. Mishra, J. A. Henige, and M. J. Delaney, 'The effect of InP substrate misorientation on GaInAs-AlInAs interface and alloy quality', *J Appl Phys*, vol. 64, no. 7, p. 3476, Jun. 1998, doi: 10.1063/1.341482.

[111] A. Gomyo, S. Kawata, S. Tohru, S. Iijima, and S. Hino, 'Large (6°) Off-angle effects on sublattice ordering and band-gap energy in Ga0.5In0.5P grown on (001) GaAs infstrates', *Jpn J Appl Phys*, vol. 28, no. 10 A, pp. L1728–L1730, Oct. 1989, doi: 10.1143/JJAP.28.L1728/XML.

[112] Y. He *et al.*, 'Dislocation distributions and tilts in Al(Ga)InAs reverse-graded layers grown on misorientated GaAs substrates*', *Chinese Physics B*, vol. 26, no. 3, p. 038102, Mar. 2017, doi: 10.1088/1674-1056/26/3/038102.

[113] K. Li *et al.*, 'Effects of substrate miscut on the quality of In0.3Ga 0.7As layers grown on metamorphic (Al)GaInP buffers by metal-organic chemical vapor deposition', *Applied Physics Express*, vol. 6, no. 6, p. 065502, Jun. 2013, doi: 10.7567/APEX.6.065502/XML.

[114] K. Li *et al.*, 'Effects of substrate miscut on the quality of In0.3Ga 0.7As layers grown on metamorphic (Al)GaInP buffers by metal-organic chemical vapor deposition', *Applied Physics Express*, vol. 6, no. 6, p. 065502, Jun. 2013, doi: 10.7567/APEX.6.065502/XML.

[115] K. A. Lozovoy, A. G. Korotaev, A. P. Kokhanenko, V. v. Dirko, and A. v. Voitsekhovskii, 'Kinetics of epitaxial formation of nanostructures by Frank–van der Merwe, Volmer–Weber and Stranski–Krastanow growth modes', *Surf Coat Technol*, vol. 384, Feb. 2020, doi: 10.1016/J.SURFCOAT.2019.125289.

[116] S. A. Teys, 'Different growth mechanisms of Ge by Stranski-Krastanow on Si (111) and (001) surfaces: An STM study', *Appl Surf Sci*, vol. 392, pp. 1017–1025, Jan. 2017, doi: 10.1016/J.APSUSC.2016.09.124.

[117] A. (orcid:0000-0001-8320-7354) Krysa, *Growth and characterisation of InAsP/AlGaInP QD laser structures*.

[118] A. Ponchet, 'Shape transition in InAs nanostructures formed by Stranski-Krastanow growth mode on InP (001) substrate', *Appl Phys Lett*, vol. 114, no. 17, pp. 173102-, Apr. 2019.

[119] M. Buffolo *et al.*, 'Degradation of 1.3 μm InAs Quantum-Dot Laser Diodes: Impact of Dislocation Density and Number of Quantum Dot Layers', *IEEE J Quantum Electron*, 2020, doi: 10.1109/JQE.2020.3033041.

[120] B. Shi *et al.*, 'MOCVD grown low dislocation density GaAs-on-V-groove patterned (001) Si for 1.3 μ m quantum dot laser applications', *Appl Phys Lett*, vol. 114, no. 17, Apr. 2019, doi: 10.1063/1.5090437.

[121] D. Panda *et al.*, 'Optimization of dot layer periodicity through analysis of strain and electronic profile in vertically stacked InAs/GaAs Quantum dot heterostructure', *J Alloys Compd*, vol. 736, pp. 216–224, Mar. 2018, doi: 10.1016/j.jallcom.2017.11.086.

[122] G. M. Lewis, J. Lutti, P. M. Smowton, P. Blood, A. B. Krysa, and S. L. Liew, 'Optical properties of InP⁄GaInP quantum-dot laser structures', *Appl Phys Lett*, vol. 85, no. 11, p. 1904, Sep. 2004, doi: 10.1063/1.1794379.

[123] A. A. El-Emawy *et al.*, 'Formation trends in quantum dot growth using metalorganic chemical vapor deposition', *J Appl Phys*, vol. 93, no. 6, p. 3529, Mar. 2003, doi: 10.1063/1.1543647.

[124] D. Guimard *et al.*, 'Ground state lasing at 1.30 microm from InAs/GaAs quantum dot lasers grown by metal-organic chemical vapor deposition', *Nanotechnology*, vol. 21, no. 10, 2010, doi: 10.1088/0957-4484/21/10/105604.

[125] T. Yang, M. Nishioka, and Y. Arakawa, 'Optimizing the GaAs capping layer growth of 1.3 μm InAs/GaAs quantum dots by a combined two-temperature and annealing process at low temperatures', *J Cryst Growth*, vol. 310, no. 24, pp. 5469–5472, Dec. 2008, doi: 10.1016/J.JCRYSGRO.2008.09.173.

[126] H. Z. Song, Y. Tanaka, T. Yamamoto, N. Yokoyama, M. Sugawara, and Y. Arakawa, 'AlGaAs capping effect on InAs quantum dots self-assembled on GaAs', *Phys Lett A*, vol. 375, no. 40, pp. 3517–3520, Sep. 2011, doi: 10.1016/J.PHYSLETA.2011.08.021.

[127] E. C. le Ru, A. J. Bennett, C. Roberts, and R. Murray, 'Strain and electronic interactions in InAs/GaAs quantum dot multilayers for 1300 nm emission', *J Appl Phys*, vol. 91, no. 3, pp. 1365–1370, Feb. 2002, doi: 10.1063/1.1429797.

[128] A. S. Somintac *et al.*, 'Confined photocarrier transport in InAs pyramidal quantum dots via terahertz time-domain spectroscopy', *Optics Express, Vol. 23, Issue 11, pp. 14532-14540*, vol. 23, no. 11, pp. 14532–14540, Jun. 2015, doi: 10.1364/OE.23.014532.

[129] M. Suwa, T. Andachi, T. Kaizu, Y. Harada, and T. Kita, 'Polarization characteristics of electroluminescence and net modal gain in highly stacked InAs/GaAs quantum-dot laser devices', *J Appl Phys*, vol. 120, no. 13, Oct. 2016, doi: 10.1063/1.4964446.

[130] A. Salhi *et al.*, 'Linear increase of the modal gain in 1.3 μm InAs/GaAs quantum dot lasers containing up to seven-stacked QD layers', *Nanotechnology*, vol. 19, no. 27, pp. 275401–275401, Jul. 2008, doi: 10.1088/0957-4484/19/27/275401.

[131] P. Caroff *et al.*, 'High-gain and low-threshold InAs quantum-dot lasers on InP', *Appl Phys Lett*, vol. 87, no. 24, pp. 1–3, 2005, doi: 10.1063/1.2146063.

[132] 'Quantum Wells, Wires and Dots : Theoretical and Computational Physics of Se...: EBSCOhost'. https://web.p.ebscohost.com/ehost/detail/detail?vid=0&sid=18269f74-cb93-41b6-a797-bd840b96a850%40redis&bdata=JnNpdGU9ZWhvc3QtbGl2ZQ%3d%3d#AN=141706&db=nlebk (accessed Aug. 14, 2022).

[133] A. E. Zhukov *et al.*, 'Gain characteristics of quantum dot injection lasers', *Semicond Sci Technol*, vol. 14, no. 1, pp. 118–123, 1999, doi: 10.1088/0268-1242/14/1/020.

[134] P. M. Smowton, E. Herrmann, Y. Ning, H. D. Summers, P. Blood, and M. Hopkinson, 'Optical mode loss and gain of multiple-layer quantum-dot lasers', *Appl Phys Lett*, vol. 78, no. 18, pp. 2629–2631, Apr. 2001, doi: 10.1063/1.1366652.

[135] D. J. Mowbray, *Analysing radiative and non-radiative recombination in InAs QDs on Si for integrated laser applications*.

[136] Y. Zhou *et al.*, 'High-power dual-wavelength lasing in bimodal-sized InGaAs/GaAs quantum dots', *Opt Express*, vol. 24, no. 25, pp. 29321–29328, Dec. 2016, doi: 10.1364/OE.24.029321.

[137] Y. Sin, S. Lalumondiere, W. Lotshaw, and S. C. Moss, 'Carrier dynamics in self-assembled InAs QD laser structures and broad-area InAs QD lasers grown by molecular beam epitaxy', *Prehosp Disaster Med*, vol. 1635, no. 3, Nov. 2014, doi: 10.1557/OPL.2014.103.

[138] H. W. Yu *et al.*, 'Effect of substrate misorientation on the material properties of GaAs/ Al0.3Ga0.7As tunnel diodes', *Appl Phys Lett*, vol. 97, no. 23, Dec. 2010, doi: 10.1063/1.3525158.

[139] S. O'Hagan, 'The effect of substrate orientation on the properties of low temperature molecular beam epitaxial GaAs', *J Appl Phys*, vol. 82, no. 5, pp. 2400–2404, Sep. 1997.

[140] S. Raymond, X. Guo, J. L. Merz, and S. Fafard, 'Excited-state radiative lifetimes in self-assembled quantum dots obtained from state-filling spectroscopy', *Phys Rev B*, vol. 59, no. 11, p. 7624, Mar. 1999, doi: 10.1103/PhysRevB.59.7624.

[141] R. Beanland, 'Dark field transmission electron microscope images of III–V quantum dot structures', *Ultramicroscopy*, vol. 102, no. 2, pp. 115–125, Jan. 2005, doi: 10.1016/J.ULTRAMIC.2004.09.003.

[142] T. Amano, T. Sugaya, and K. Komori, '1.3-μm InAs quantum-dot laser with high dot density and high uniformity', *IEEE Photonics Technology Letters*, vol. 18, no. 4, pp. 619–621, Feb. 2006, doi: 10.1109/LPT.2006.870143.

[143] H. Y. Liu *et al.*, 'Long-wavelength light emission and lasing from InAsGaAs quantum dots covered by a GaAsSb strain-reducing layer', *Appl Phys Lett*, vol. 86, no. 14, pp. 1–3, Apr. 2005, doi: 10.1063/1.1897850.

[144] J. Tatebayashi, M. Nishioka, and Y. Arakawa, 'Over 1.5 μm light emission from InAs quantum dots embedded in InGaAs strain-reducing layer grown by metalorganic chemical vapor deposition', *Appl Phys Lett*, vol. 78, no. 22, pp. 3469–3471, May 2001, doi: 10.1063/1.1375842.

[145] J. Tatebayashi, M. Nishioka, and Y. Arakawa, 'Over 1.5 μm light emission from InAs quantum dots embedded in InGaAs strain-reducing layer grown by metalorganic chemical vapor deposition', *Appl Phys Lett*, vol. 78, no. 22, p. 3469, May 2001, doi: 10.1063/1.1375842.

[146] J. Tatebayashi, M. Nishioka, and Y. Arakawa, 'Luminescence in excess of 1.5 μm at room-temperature of InAs quantum dots capped by a thin InGaAs strain-reducing layer', *J Cryst Growth*, vol. 237–239, no. 1-4 II, pp. 1296–1300, Apr. 2002, doi: 10.1016/S0022-0248(01)02048-6.

Chapter 4: Design, Simulation and Growth of 1.55µm InAs/InGaAs/InP Quantum Dot laser by Droplet Epitaxy using MOCVD

4.1 Introduction

Quantum dots and quantum well materials have been utilised in various optoelectronic applications over many years. MOCVD and MBE are the two most important epitaxy tools for quantum dot and quantum well growth. Although the growth of self-assembled QD has been studied extensively since the early 1990s[99], the growth of high-quality and long-wavelength dots using MBE is still challenging, and it is even more difficult to achieve the same quality dots using MOCVD because of MOCVD's higher growth temperature requirements of MOCVD. The S.K. growth method is a well-known epitaxy technique for growing self-assembled quantum dots, although the lattice mismatch restricts the selection of epitaxy material systems. This chapter focuses on a novel QD growth technique known as droplet epitaxy (DE). It is based on the Volmer-Weber growth model in forming group III droplets, which are then crystallized into quantum dots. This process does not rely on lattice mismatch in quantum dot formation[148]. This allowing easier control over the size distribution, density, and optical quality of the QDs. The strain coupling effect of QDs in stacked dot layers is also reduced by DE, allowing a thinner spacer between each QD layer, which increases the overall gain of the active region[90]. Another advantage of droplet epitaxy is the removal of the wetting layer in DE, as opposed to S.K. growth[149]. The wetting layer that is present in the S.K. growth is a disadvantage in the growth of QDs as it serves as a competitive channel for carriers, which

reduces the QD optical gain and thus can also affect the dynamic properties of the laser[150]. Therefore, wetting-layer-free DE QD is very promising for highly efficient QD-based laser devices.

In this thesis, the possibility of incorporating InAs quantum dots into quantum dot laser devices via droplet epitaxy was investigated. There have been reports of droplet epitaxial growth of quantum dots for single and entangled photon emitters, solar cells, and QLED[15], [26], [149], [151], [152]. However, there are no demonstrations of the growth of QD laser diodes utilising DE at 1.55μm telecom wavelength. The closest report of the DE laser is lasing at ~980 nm on GaAs substrate, and only low-temperature lasing operation has been achieved. The J_{th} of the QD laser is also much higher than that of similar S.K grown QD laser devices[153]. In this research, the aim is to achieve longer telecom wavelengths of 1.55μm, which is even more challenging than achieving DE QD lasing on GaAs materials for shorter wavelength.

Since the current design of QD laser structures mostly compatible with the conventional S.K growth, which typically have fixed active region layer composition choices due to fixed lattice mismatch requirements driving the S.K growth mechanism, but the DE growth procedure does not. Therefore, the DE QD process requires a new design of the laser active region and capping layer composition to ensure maximum compatibility. In this chapter, through careful design, simulation, and growth calibration, a new QD laser structure tailored to the new DE QD method established in Sheffield was proposed. The active region of the QD laser structure was composed of 3x, 5x, and 7x stacks of InAs QDs grown by DE on a 5 nm InGaAs interlayer that was directly grown on a 35 nm InP barrier layer[85]. For optimisation purposes, QD laser structures and identical QW laser structures in which the InGaAs interlayers act as QWs were grown simultaneously for comparison. The samples were then fabricated into 4 mm long, broad-area lasers for basic electrical and optical characterization. The emission wavelength of these QD/QW laser samples was successfully tuned to ~ 1530 nm, which was close to the desired wavelength of 1550 nm. Unfortunately, no lasing was observed in either the QW or the QD samples. To optimise the performance of the QD/QW lasers, samples with different Zn doping concentrations and waveguide materials were grown, and the possible issues caused by the growth were analysed. If further increases in the QD density and a decrease in the defects

accumulated during the growth of QD layers can be achieved, there is a strong potential for room-temperature lasing of QD lasers at 1.5µm using this DE approach in MOCVD.

4.2 Droplet Epitaxy of InAs QD on InGaAs interlayer for 1.55µm emission

The S.K. growth method has dominated the growth of self-assembled InAs QD on InP or GaAs substrates for many years. However, the droplet epitaxial growth of QDs has several advantages over S.K growth. For example, there is a more symmetrical shape of individual QDs formed by droplet epitaxy (DE) compared to S.K growth, as evidenced by the AFM image of InAs QDs grown by S.K and DE in Fig 4. 1. This is especially useful in the case of single photon emitters[81], [154], where, due to the elongated or pyramidal shape of the quantum dots formed by S.K, their mean fine-structure splitting (FSS) is approximately two times greater than that of DE (4.5 µeV)[149].

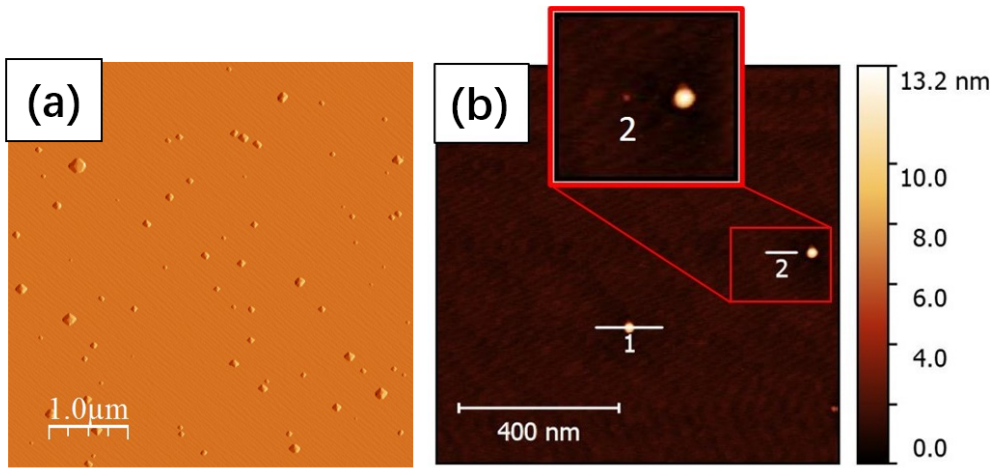

Fig 4. 1 (a) The AFM image of S.K growth of InAs QD on GaAs substrate, individual QDs are in pyramid shape. (b) the AFM image of droplet epitaxy of InAs QD on InP substrate, individual QDs are more round-like[182]

In droplet epitaxy, the dot density is, in principle, independently controlled through the formation of indium droplets. The growth temperature for indium droplets is typically between 150 and 500ºC and their size and density are strongly dependent on temperature, with lower temperatures giving higher densities. In MBE, growth temperatures close to the room temperature can be achieved. However, in the case of MOCVD, the lowest temperature and highest droplet density are determined by the cracking temperature of the TriMethyl Indium

used as the precursor for indium deposition, and are thus limited to approximately 400 ºC[155]. Thus, the growth of high-density DE InAs QDs for laser diodes using MOCVD remains a challenge, and careful investigation of the DE QD growth parameters is needed.

The benefit of DE, such as quantum dot (QD) growth on either lattice-matched or mismatched nanostructures, which does not depend on the strain and lattice mismatch between the epilayer and substrate, is beneficial for various optoelectronic applications. The strain-free quantum dots formed by DE are expected to exhibit superior laser device performance compared to conventional S.K growth. However, as discussed earlier, the DE method for QD laser devices has received little attention, and few studies have been conducted. The earliest demonstration of a laser utilizing DE focused primarily on GaAs quantum dots on an AlInAs substrate, with an emission wavelength of 980 nm, which is outside the telecom range. Initial investigations showed that lasing was only observed at 77 K, with a threshold current density of 6.2 kA/cm^2[41]. For the DE of 3-layer GaAs/AllnAs QD laser on a Si substrate, the lowest CW operation was up to 100 K with a J_{th} of approximately 3.9 kA/cm^2[156]. Such a high J_{th} for lasers grown by DE is primarily due to the low quantum dot density in the active region, which is insufficient for lasing. Thus, it is important to obtain high-density DE QD to achieve room-temperature lasing in this project.

Using droplet epitaxy, the maximum InAs quantum dot density demonstrated was 7x10^{10}/cm^2 on GaAs (311), although S.K growth can achieve a higher density of ~6x10^{11}/cm^2 on GaAs (100)[44], [53]. The density of the DE InAs QD can be increased by stacking more QD layers and thus reducing the J_{th} of the laser device to obtain similar performance as S.K QD. Because the strain coupling effect of the stacked QD layers is also reduced in DE, the space between the QD layers can be further reduced and thus improve the optical gain in the active region. To date, the highest reported InAs quantum dot (QD) density by droplet epitaxy is ~10^{11}/cm^2, which is achieved on an InAlAs/InP(111) substrate. Although this may still be lower than that of InAs QDs grown using S.K. growth at the same wavelength[83], [155], [157], it shows the potential for laser applications using DE. Moreover, the additional advantages of DE QDs, such

as increased QD uniformity and removal of the strain effect during the formation of the dot, still make DE QDs attractive for laser applications, despite the lower density of the QD. For example, in the droplet epitaxy of a GaAs/AlInAs QD laser structure, a 2 nm GaAs 2D-layer is grown on top of the AlInAs buffer layer at 580 °C prior to the deposition of GaAs QD, followed by a 4-minute high-temperature post-annealing procedure at 750 °C. The final GaAs quantum dot laser has an extremely narrow linewidth of 20 meV at 77 K[156]. The same technique can be applied to InAs QD grown on InP substrates.

Although DE is considered to have an advantages in not forming a strain-driven wetting layers, such as is formed in the SK method, there is, in fact, formation of a 2D *quasi-wetting layer* [151], [155]. Following the formation of indium droplets, these Indium droplets are crystallized into quantum dots upon exposure to Arsine[84], [87], [89], [90]. However, the surface underneath the dots is also exposed to the arsine, and if that surface is InP, there is likely an As-P exchange process leading to the formation of an InPA layer that can be a few nanometres thick[85]. Thus, a quasi-wetting layer was formed. This quasi-wetting layer (not a wetting layer, because it is not formed by the S.K. process) can compete with the QDs and reduce the available gain. The carriers could tunnel from the QD to this 2D layer, resulting in modifying the transition energy of the QD. Therefore, it can also change the emission wavelength and linewidth of the QD laser device. By introducing an InGaAs 'interlayer' on which the DE dots are grown, such As-P exchange can be suppressed and no longer forms a 2D quasi-wetting layer. Therefore, the DE InAs dots that grew on top of the InGaAs QW showed higher density and uniformity[85].

Dr. Elisa Sala *et al.* at Sheffield University developed a novel DE growth of InAs QD on an InP (001) substrate by MOCVD, but with a 5 nm lattice-matched $In_{0.53}Ga_{0.47}As$ interlayer between the QD and InP substrate/buffer. The growth on the $In_{0.53}Ga_{0.47}As$ interlayer increased the QD density on InP(100) up to $1x10^{10}$ cm^{-2} and it is possible to fine-tune the emission wavelength between 1.5 and 1.8 µm by controlling the InGaAs layer thickness[85], [158]. In advance of the growth of QD laser diode structures, sets of samples shown in Fig 4. 2 were

grown for structural and optical characterisation of the dots and for optimisation of the growth conditions for QD wavelength, linewidth, and density.

For the growth of Droplet epitaxy InAs QD. The AsH_3 and PH_3 were used as group V precursors, whereas TMIn and TMGa were used as group III precursors. The initial growth structure consisted of a 300 nm InP buffer layer grown at a substrate temperature of 600ºC on an InP(100) substrate. On top of the InP buffer layer, a 5 nm $In_{0.53}Ga_{0.47}As$ layer lattice-matched to InP were grown. Finally, indium droplets were deposited at 400ºC and 1.4 µmol/min at constant In flow. The Indium deposition time varied from 15 s to 40 s. To crystallize the droplets into QDs, they were exposed to an As flow rate of 24 µmol/min at 520 ºC using previously optimised parameters[85], [155]. The QDs were then capped with 20 nm InP grown at the same temperature as the QD crystallisation process. Finally, an InP capping layer of 80 nm was deposited at a high temperature of 600 ºC. Fig 4. 2 shows the structure of the QD DE and the AFM images of a single-layer QD.

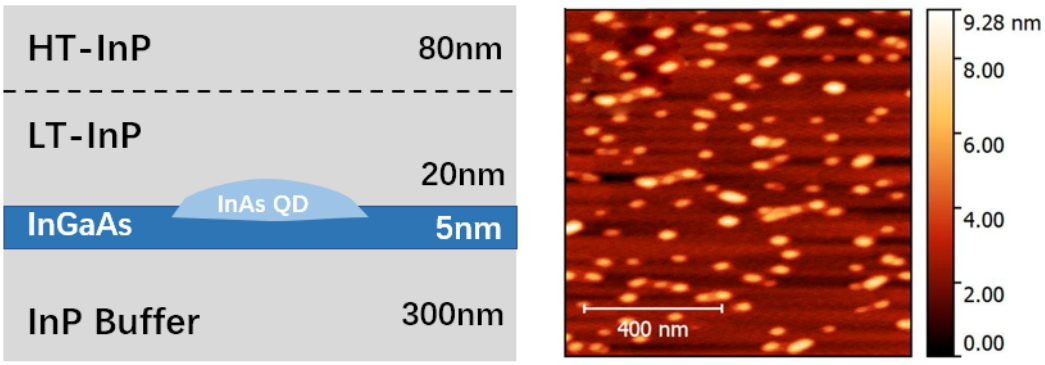

Fig 4. 2 (Left) Schematic diagrame of Droplet epitaxy of InAs QD grown on 5nm of InGaAs interlayer with 20nm of InP capping layer. (Right) AFM image of InAs QD grown on 5nm InGaAs interlayer using droplet epitaxy, The density of dots is ~10^{10} cm^{-2}.[182]

For growth on InGaAs, it was found that droplets only formed at a substrate temperature above 400 ºC, which is higher than the normal 320 ºC used for droplets directly deposited on InP[85]. This is because of the higher activation energy needed for the In droplets on the InGaAs layer

[85]. The effect of indium deposition time was also investigated between 20 and 40s at a constant TMI flow rate of 1.4 µmol/min in Fig 4. 3.

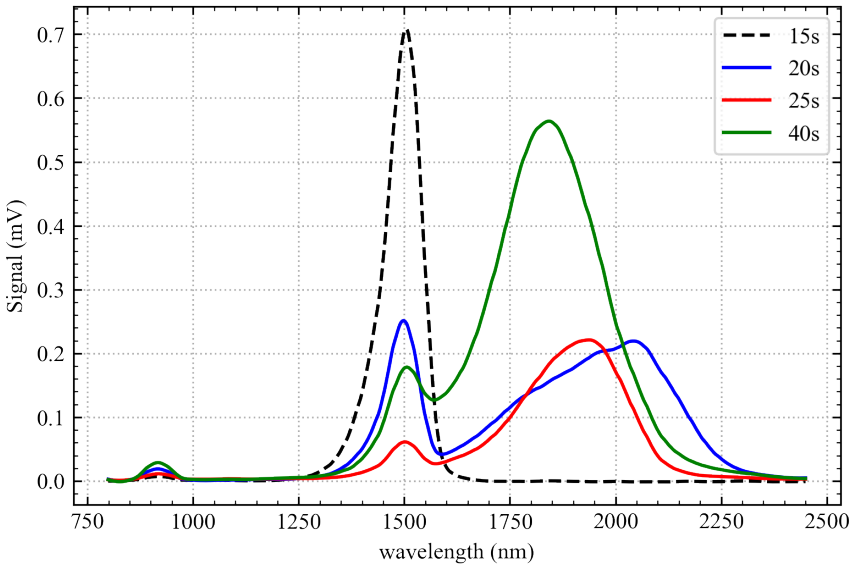

Fig 4. 3 Room temperature PL of InAs QD on 5nm InGaAs layer samples with different indium deposition time.The In flow rate is kept at constant 1.4 µmol/min. The 15s PL shows only 5nm of InGaAs QW with no InAs QD formation. [182]

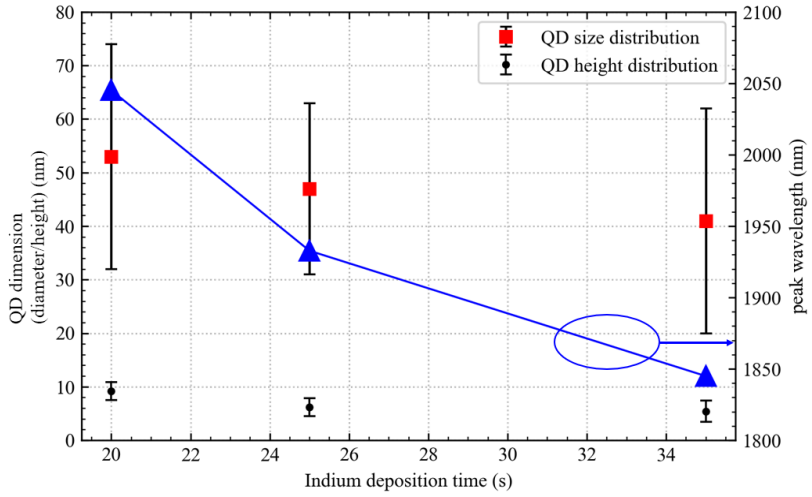

Fig 4. 4 Droplet epitaxy of InAs QD diamter and PL peak wavelegnth versus the indium deposition time between 20~40s at constant In flow rate of 1.4 µmol/min

Fig 4. 3 illustrates the room-temperature PL of droplet epitaxy of InAs QD on a 5 nm InGaAs interlayer with varying indium deposition times. The sharp 1500 nm peak at 15s an indium deposition time in Fig 4. 3 corresponds to emission from the 5 nm InGaAs interlayer, where no droplet is formed. As shown in Fig 4. 3, QDs were only formed when the indium deposition time increased from 20s to 40s. The observed QD PL emission decreased from ~ 2100 nm to ~ 1840 nm with increasing deposition time. In addition, there is an increase in the peak intensity as the deposition time increased to 40 s. The quantum dot density increased from ~$6x10^{8}$ cm^{-2} to ~$1x10^{10}$ cm^{-2} as the In-deposition time increased from 20 to 40 s. However, the peak wavelength was also blue-shifted, which indicates smaller QDs were formed. This is likely due to a change in the surface energy of the 5 nm InGaAs interlayer, which inhibits the diffusion of the In droplet, resulting in the formation of smaller droplets. These results are promising for the use of DE InAs QD as the active region in the laser structures. Fig 4. 4 illustrates the effect of indium deposition time on the size and emission wavelength of the QD, as determined by RT-PL measurements in Fig 4. 3. The size distribution of QD on InGaAs varies between 15 and 55 nm, which is smaller than that of QD deposited directly on InP[85], [155]. As shown in Fig 4. 4, when the indium deposition time was increased from 20s to 35s, the average QD size decreased from 53 nm±21 nm to 41 nm± 21 nm. The height of the QD was reduced from 10 nm ± 2 nm to 5 nm ± 2 nm. Since the 5 nm InGaAs interlayer grown underneath the DE InAs QD inhibits the diffusion of the In droplet, it results in the formation of smaller In droplets. The increase in the growth temperature of the InGaAs layer, which provides an excellent growth interface for the In droplets, is another reason for this[85], [158], [159].

To confirm the formation and quality of the QDs grown using this method, TEM measurements were performed on the selected samples. Fig 4. 5 shows the TEM images of a DE InAs QD sample grown on InP and on a 5 nm InGaAs surface. The TEM image (A) in Fig 4. 5 shows a very good surface morphology of the QD on the InGaAs interlayer, and no dislocations or defects were observed. In contrast, on the InP, there is an InPAs 2D-layer formed between the InAs QD and InP substrate in the TEM image (B) in Fig 4. 5.

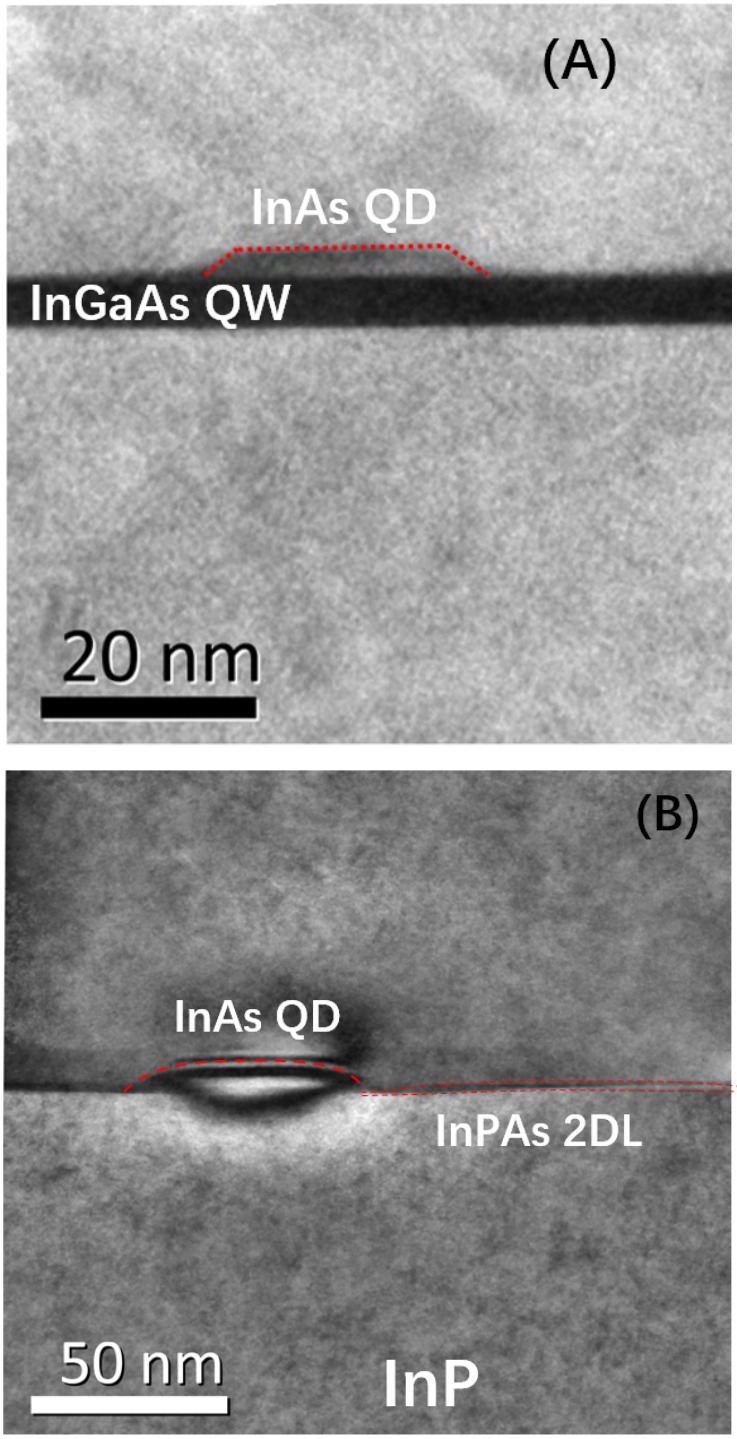

Fig 4. 5 (A) Bright field TEM image of Droplet epitaxy of InAs QD on 5nm InGaAs QW interlayer.[182] (B) TEM image of droplet epitaxy of InAs QD directly on InP. There is a formation of 2D-layer of InGaAs. Red lines are drawn for better illustration.

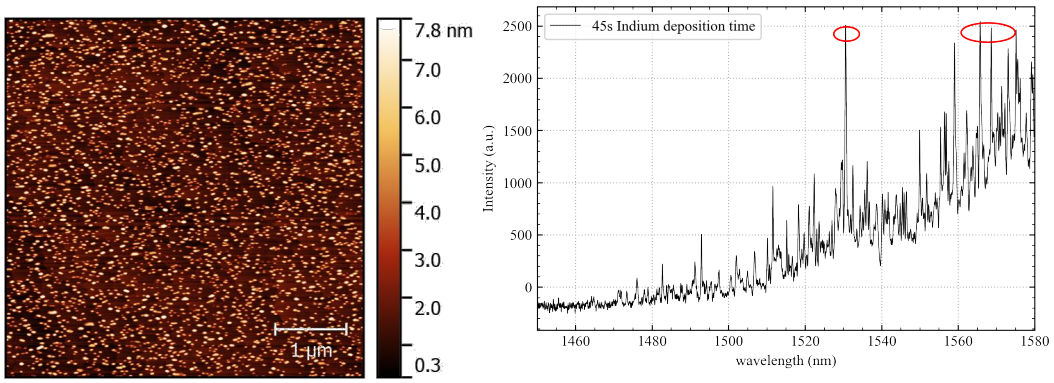

Fig 4. 6 AFM(Left) images, LT-µPL(Right) spectrum of Droplet epitaxy of InAs QD on 5nm InGaAs QW for 45s Indium deposition time. Red circle indicates a bimodal distribution of QD peaks.

In order to further confirm dot formation, AFM measurements and low-temperature micro-PL spectra were obtained from the InAs QD samples. Fig 4. 6 shows the AFM and LT-PL of QDs formed with 45s of In deposition for droplet epitaxy of InAs quantum dots on 5 nm InGaAs. LT-PL was performed at 4 K with a spatial resolution of 5µm and spectral resolution of 25 µeV. The AFM clearly showed dot formation and indicated a dot density even higher than 35s. In the microPL, there are a number of bright and distinct QD emission lines between 1530 and 1580 nm, which is within the desired 1.55µm range. The quantum dot density obtained from the AFM image is ~$1.5x10^{10}$ cm^{-2} (Fig 4. 6 left). Although the DE density is lower than the dot density for 1.55µm QD lasers grown using S.K growth, it is within range of the S.K growth and could provide enough carriers for population inversion, especially if stacked[61].

After establishing the initial single layer droplet epitaxy of QD growth and achieving high density dots with calibrated the emission wavelengths to the range of 1.5-1.6µm, the next step was to design a suitable QD laser structure that could directly implement droplet epitaxy QDs as the active region material.

4.3 Design, Growth and Wavelength tuning of new 1.55µm QD laser structure for droplet epitaxy

In this thesis, the aim was to design a new QD laser structure emitting in the 1.5µm range that incorporates the droplet epitaxy of InAs QD grown on InGaAs interlayers. One of the most important parameters of a laser structure is the active region material, which affects the lasing wavelength of the laser diode as well as its threshold current density. To date, the longest wavelength of these InAs QD on GaAs substrate lasers is still restricted to the 1.4µm range, which is shorter than the 1.55µm telecom band we seek to achieve. However, it is much simpler to achieve longer wavelengths on an InP substrate than on a GaAs substrate. Therefore, the InP substrate was used for droplet epitaxy of the QD laser structure which allows a smaller band-gap (E_g) lattice-matched material to grow on top[153], [160].

For QD laser structures emitting in the ~1.55µm range, there are various active region material options. The material composition, E_g, and emission wavelength suitable for the QD laser structures around ~1.55µm range were summarized in Table 4.1[14], [35], [69], [70], [72]. Although these materials have successfully achieved lasing with S.K-grown InAs QD lasers, laser structures grown by droplet epitaxy using these material systems have not yet been reported. However, these QD laser structures can still be used as references for the growth of our DE QD lasers. Because the performance of the semiconductor laser device highly depends on the quality of the epilayers, the lattice mismatch between the epilayer must be as small as possible to reduce dislocation formation and provide a smooth growth surface for the active region. Thus, the material compositions shown in Table 4.1 are all lattice-matched to InP.

Material	Eg (eV)	Emission wavelength of QD (um)
$In_{0.53}AsGa_{0.47}$	0.74	~1.6-1.8
$In_{0.52}Al_{0.29}Ga_{0.19}As$	1.07	~1.58
$In_{0.83}Ga_{0.17}As_{0.38}P_{0.62}$	1.17	~1.5-1.6

Table 4.1 summarise of activer region material for InAs QD laser active region emitting ~1.5µm on InP substrate

Since the Droplet epitaxy of InAs QD is grown on the InGaAs interlayer, it is essential to ensure good lattice matching between the InGaAs interlayer and rest of epilayer. Fig 4. 7 shows the transition wavelength plotted against the lattice constant of common III/V materials. For the InGaAs material lattice matched to InP, a Ga composition of x=0.47 was used, and E_g = 0.74 eV ,which corresponds to a transition wavelength of ~1.7µm.

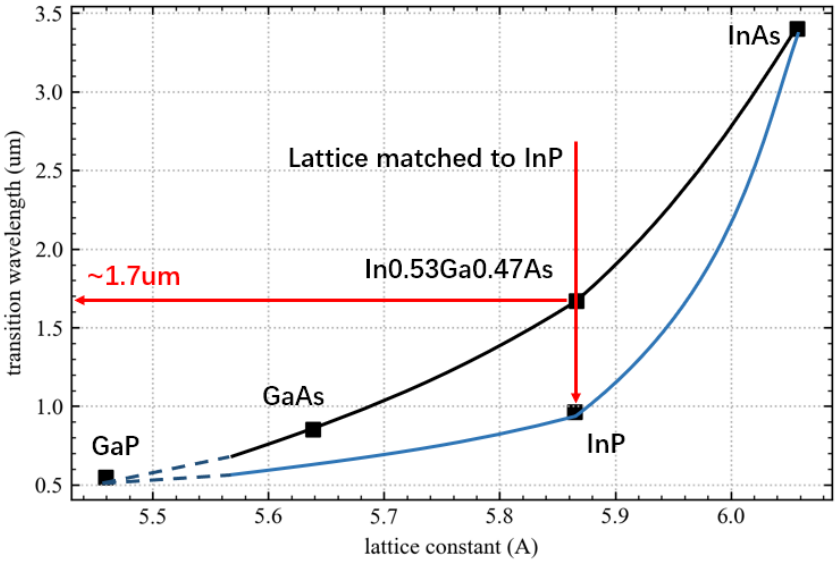

Fig 4. 7 transition wavelength plotted agianst the lattice constant of commin III/V material, arrow shows the $In_{0.53}Ga_{0.47}As$ lattice matched to the InP with emission wavelength ~1.7µm

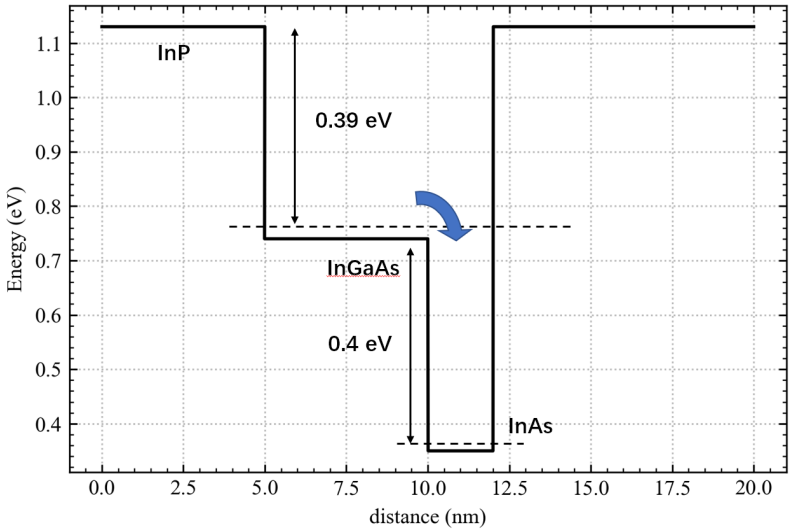

Fig 4. 8 Simulated transiton energy for 2nm InAs after 5nm of $In_{0.53}Ga_{0.47}As$ lattice matched to the InP. The transition energy for ground state of InAs is 0.35eV.

Fig 4. 8 shows simulated the transition energy between coupled InAs dot and InGaAs QW band structure. Using Rsoft, a software capable of finite difference method calculation, the different states of InAs QD and $In_{0.53}Ga_{0.47}As$ QW were simulated. The results indicate that the ground-state transition energy for the 5 nm thick $In_{0.53}Ga_{0.47}As$ QW is 0.74 eV and 0.36 eV for the 5 nm thick InAs QD. The ΔE_g between the $In_{0.53}Ga_{0.47}As$ and InP is 0.39 eV, which shows a good carrier confinement effect with incorporation of the InGaAs QW. In the literature, 15-layer of $In_{0.53}As\ Ga_{0.47}$/InP QW laser have been reported to emit at a wavelength of ~1.57µm with a threshold current of ~40mA although the lasing operation is at 200k[161]. In QD laser case, with InAs QD grown on top of the InGaAs interlayer, the interlayer acts as an additional carrier injection channel, which should increase the quantum efficiency of the active region by allowing a faster carrier relaxation time of the carrier[162].

After confirming the material selection for the active region layer, the waveguide layer material needs to be considered. To achieve high optical confinement, the cladding layer material typically has a lower refractive index $\bar{n}$ than that of the active-region material. In theory, there should be typically $\Delta\bar{n}$ between doped cladding and active region of approximately 3–7% to

provide good optical confinement[163]. In a real device, the E_g of a material is usually inversely proportional to the refractive index. Thus, the upper/lower cladding layer material should have a higher E_g than the active region and should be lattice-matched with InP for a low defects level. Therefore, the choice of waveguide material is limited to $Al_{0.48}In_{0.52}As$, $In_{0.52}Al_{0.29}Ga_{0.19}As$, and $In_{0.83}Ga_{0.17}As_{0.38}P_{0.62}$ which are all lattice-matched to InP and have a higher band gap than the InAs QD active region. Table 4.2 summarises the refractive index of these materials.

Material	$\bar{n}$
$In_{0.53}Ga_{0.47}$ As	~3.6
$In_{0.52}Al_{0.29}Ga_{0.19}As$	~3.3
$In_{0.83}Ga_{0.17}As_{0.38}P_{0.62}$	~3.27
$Al_{0.48}In_{0.52}As$	~3.2

Table 4.2 summarise of refrative index of waveguide material which lattice matched to the InP substrate.

The $Al_{0.48}In_{0.52}As$ and $In_{0.52}Al_{0.29}Ga_{0.19}As$ are 2 common cladding materials for QD laser structures reported in literature.[14], [34], [70], [161], [163] Here, the $Al_{0.48}In_{0.52}As$ was chosen as the cladding material in the Separate Confinement Heterostructure. Because it has the highest E_g ~1.44 eV and thus should provide good optical & carrier confinement. The heavily doped InP upper and lower cladding layers were used as carrier injection regions. The p- and n-doped InP cladding regions reduce the leakage current caused by carrier drift and hole diffusion.

To further improve the optical confinement in the active region, an additional waveguide layer with a high refractive index layer in the separate confinement heterostructure (SCH) is typically placed between the active region and the $Al_{0.48}In_{0.52}$ As-doped cladding layer. The waveguide layer has a positive effect on decreasing J_{th} and optical mode confinement by ensuring that most of the modes overlap with the gain section of the laser. Typically, the waveguide material is identical to the barrier material, providing a suitable surface morphology for active region growth. Since the $Al_{0.48}In_{0.52}As$ was chosen as the cladding material, both $In_{0.53}Ga_{0.47}As$ and InP are suitable for waveguide-layer materials as they have a lower E_g than $Al_{0.48}In_{0.52}As$ which

could permit carrier injection into the active region. Fig 4. 9 shows the initial proposed QD laser structure with InAs QD on the 5 nm InGaAs interlayer as the active region and 100nm of InGaAs as the waveguide layer. Fig 4. 10 shows the simulated confinement factor using FIMMWAVE software for the QW laser with the p-doped InP upper cladding thickness varying from 1μm to 1.6μm.

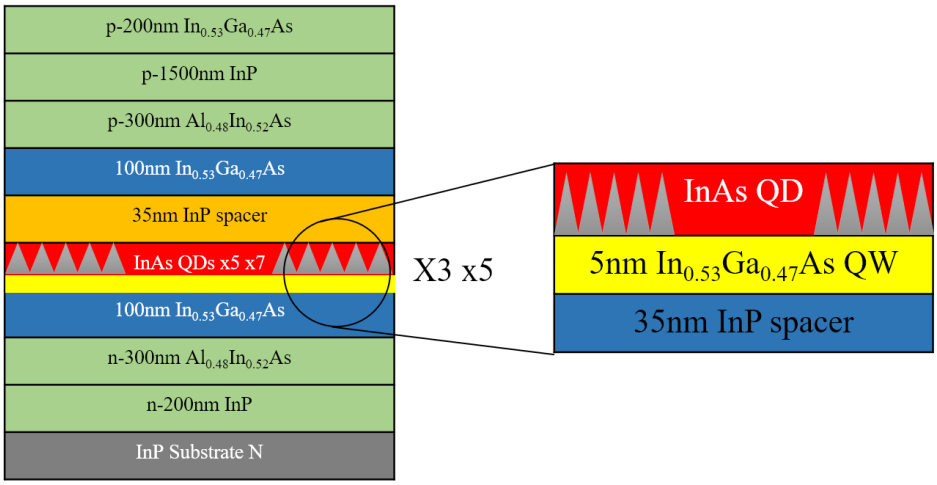

Fig 4. 9 Structure of new QD laser structure consists of droplet epitaxy of InAs QD on 5nm of $In_{0.53}Ga_{0.47}As$ QW as active region

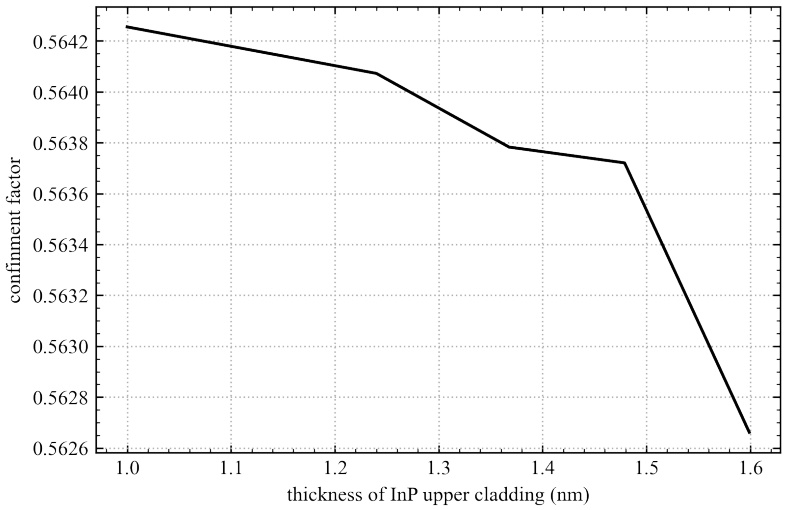

Fig 4. 10 Simulated confinment factor versus thickness of p-doped InP upper cladding material which lattice matched to the InP substrate.

Fig 4. 10 suggests that the thickness of the InP cladding layer had very little effect on the confinement factor (0.2 %), thus affecting only the electrical properties of the laser. However,

too thick an InP upper cladding layer could increase the laser diode resistance and introduce self-heating issue. Here the 1.5µm upper cladding InP with a p-doping density of $1x18^{18}/cm^3$ was selected in the initial QD structure, and is the same as other studies[14], [33], [69], [162]. The 35 nm InP barrier thickness was obtained from the optimised capping thickness for the droplet epitaxy of InAs QD[85]. In the literature on similar QW laser structures, the InGaAs QW thickness was approximately 10 nm[164]. However, considering the already optimised dot density in the droplet epitaxy of QDs, the 5 nm $In_{0.53}Ga_{0.47}As$ interlayers were placed in the active region of the proposed QD laser structure to maintain the same QD density as before.

The stacking of DE QDs on 5 nm InGaAs interlayers was calibrated through PL measurements. The PL structure used for stacking calibration is shown in Fig 4. 11. The In droplet was deposited at 400°C with a constant flow of In at 1.4 µmol/min for 45s. Then a 20 nm InP capping layer was grown at 520°C. The doping concentration for the InP lower cladding was $2x10^{18}$ and n-AlInAs is $1x10^{18}/cm^3$.

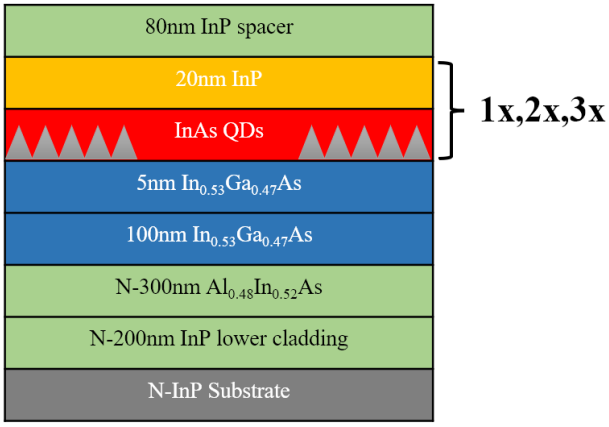

Fig 4. 11 Structure for Room temperature PL of 2 stacked QD strucure on 100nm of InGaAs layer

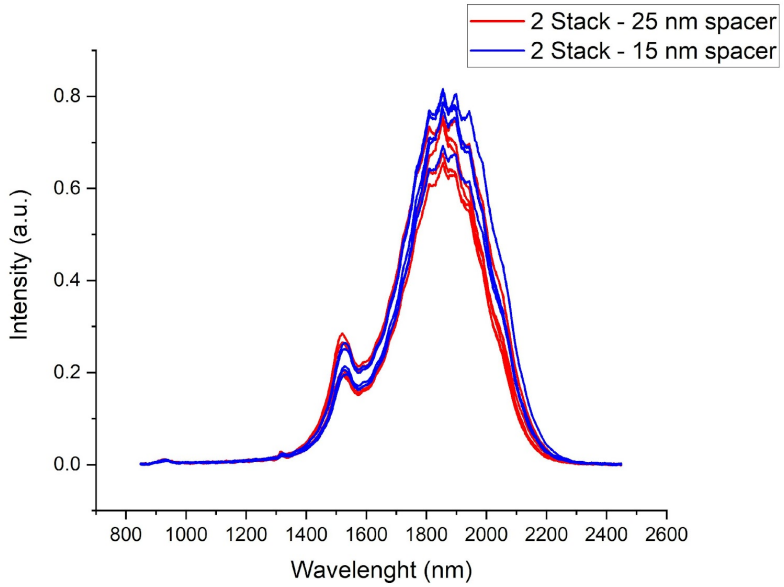

Fig 4. 12 Room temperature PL of 2 stacked QD strucure shown in Fig 4.11 with InP spacer layer of 25nm and 15nm

The test PL structure comprises a 1x, 2x, 3x, and 5x stacked InAs QD layers. The initial stacking was accomplished with a 15 nm InP spacer and a 20 nm InP capping layer positioned above the QD layer. Fig 4. 12 illustrates the RT-PL of two stacked QD layers with 25 nm and 15 nm InP spacers. The PL results demonstrate a slight increase in the PL intensity for the 15 nm InP spacer. As shown by the peak intensity of RT-PL, the overall QD density was enhanced with a thinner InP spacer. The PL peak at 1500 nm shown in Fig 4. 12 originates from the 5 nm InGaAs QW layer underneath the InAs QD. Multiple peaks in the InAs QD PL at ~1890 nm indicate inhomogeneous broadening of the QDs in the active region. The small peak at approximately 1300 nm is caused by the AlInAs cladding layer. Fig 4. 13 illustrates the RT-PL of three stacked QD layers versus two stacked QD layers with a 15 nm InP spacer.

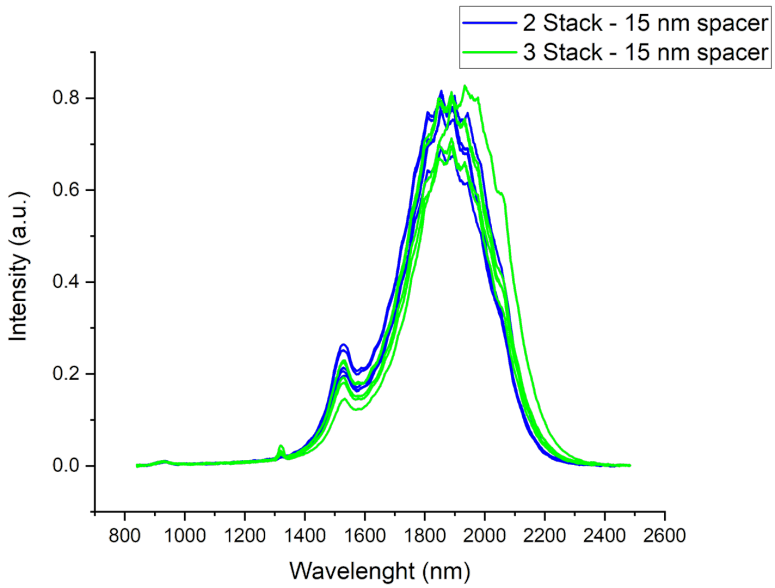

Fig 4. 13 Room temperature PL of 2 stacked vs 3stacked QD layer with InP spacer layer at 15nm

The PL intensity showed no significant improvements between the 3-stack and 2 stack of QD. This is likely due to the accumulation of strain and defects, which reduce the optical efficiency of the stacked QDs, indicating the need for further optimisation of the stacking process. There is a ~ 20 nm red-shift in the peak wavelength for 3-stacked QD layers. This implies that larger QD were formed as the QD layers were stacked.

For the initial growth of the InP capping layer and AlInAs cladding layer, the V/III ratio was maintained at 400. Fig 4. 14 illustrates the Nomarski images of the samples grown with V/III ratios of 400 and 50 for the PL test structure. The high V/III ratio (400) of the AlInAs causes significant surface roughness, evidenced by the small dots on the surface, which degrades the surface morphology of the active region. Similar round defects were observed in the InAs/GaAs QD sample due to a high V/III ratio of the capping and cladding layers [55], [57].

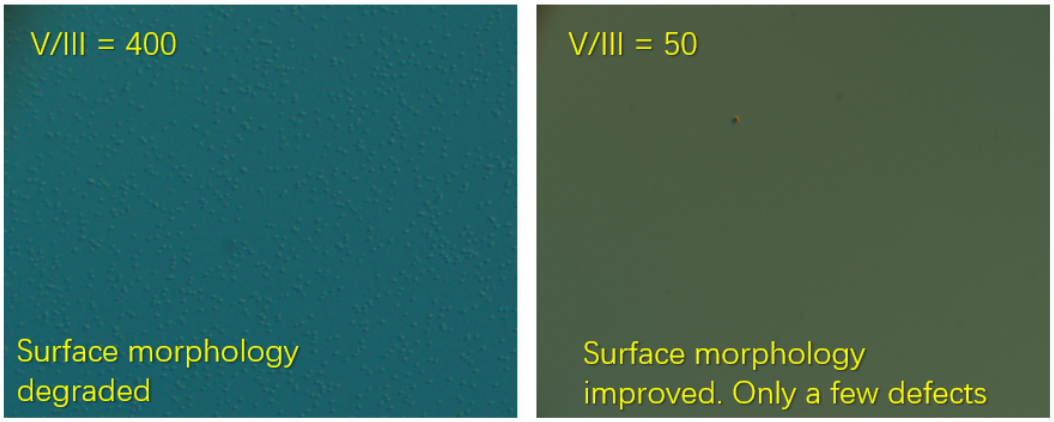

Fig 4. 14 10x Nomarski image for AlInAs layer with V/III ratio decreased from 400 to 50. Less defects are observed as V/III ratio decreased

As the V/III ratio of AlInAs decreased to 50, the surface morphology improved with fewer circular defects became visible. Moreover, the V/III ratio of the AlInAs cladding layer also influences the Zn doping density. With a reduced V/III ratio of 50, the minimum Zn doping density that growth could achieve on the AlInAs was $9x10^{17}/cm^3$ under constant Zn flow. The AlInAs cladding layer should have a lower doping density than the InP upper and lower cladding to promote carrier injection into the active region.

4.3.1 Results and Discussion

Following the stacking of DE QD and calibration of cladding layer doping density, full QD laser structures with 3-layer and 5-layer QD were grown using the MOCVD machine on a 2-inch Si doped InP substrate. The initial grown QD laser structure is shown in Fig 4. 9. First, a 200 nm n-doped InP buffer layer was grown with a doping density of $2x10^{18}/cm^3$. Second, the 300 nm AlInAs lower cladding layer was grown on top and n-doped with Si at a doping density of $1x10^{18}/cm^3$. Then, a 100 nm InGaAs waveguide layer was grown at 620 ºC on either side of the active region. The active region consists of DE InAs QD deposited on top of a 5 nm layer of $In_{0.53}Ga_{0.47}As$ interlayer lattice-matched to InP spacer. The 3-layer and 5-layer DE QD were deposited using the same growth parameters as the PL structure. The DE QD were then capped with 20 nm of InP grown at the same temperature as the QD. Then, a high temperature 15 nm InP capping layer was deposited between each QD layer at 610 ºC. The 300 nm AlInAs upper cladding layer was p-doped with Zn at a doping density of $9x10^{17}/cm^3$ and grown at 610 ºC. On top of the p-AlInAs, 1500 nm of the InP upper cladding layer (doped at $2x10^{18}/cm^3$) were grown and finish with a 200 nm p-InGaAs ($2x10^{18}/cm^3$) contact layer on top. The initial 3-layer and 5-layer QD samples were fabricated into broad-area lasers of 4 mm length with ridge widths of 100µm, 80µm, and 50µm for basic device characterisation.

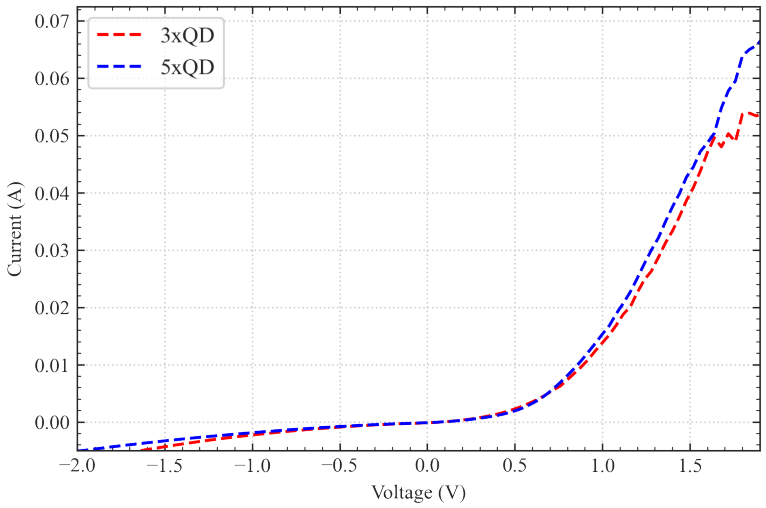

Fig 4. 15 IV characteristics of initial 3x, 5x layer of QD sample measured from 4mm broad area laser

Fig 4. 15 shows the IV characteristics of the initial grown QD samples. The turn-on voltage is ~0.6V for all the samples. The calculated on-state resistance for each sample is ~13.4 ohms which is consistent across the samples. The identical resistance values show the uniform fabrication quality of all the samples, which is essential for comparison. In addition, the cleaving quality of these broad-area laser samples was investigated using scanning electron microscopy (SEM), as shown in Fig 4. 16

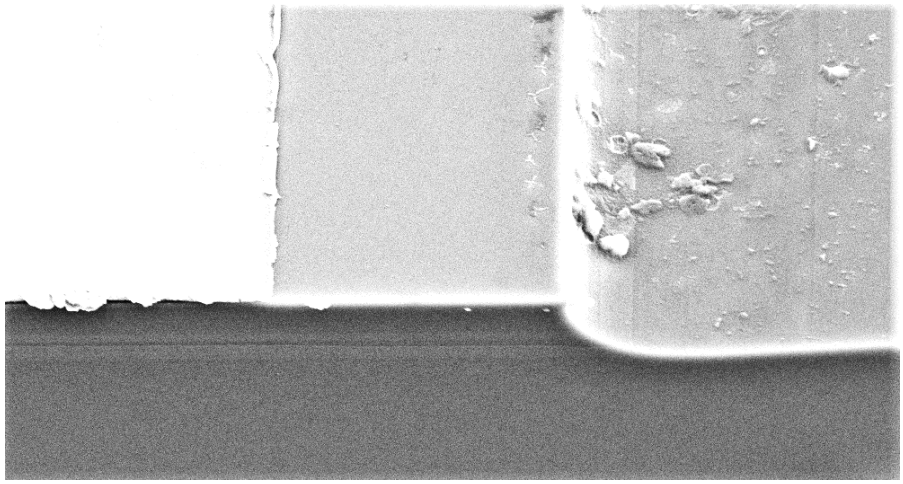

Fig 4. 16 SEM image of broad area laser of Sample 5xQW. The cleaved facet is clean without any damage

The SEM image shows a good quality of cleaving and thus eliminates the possible damaged facet on these samples, which might prevent lasing.

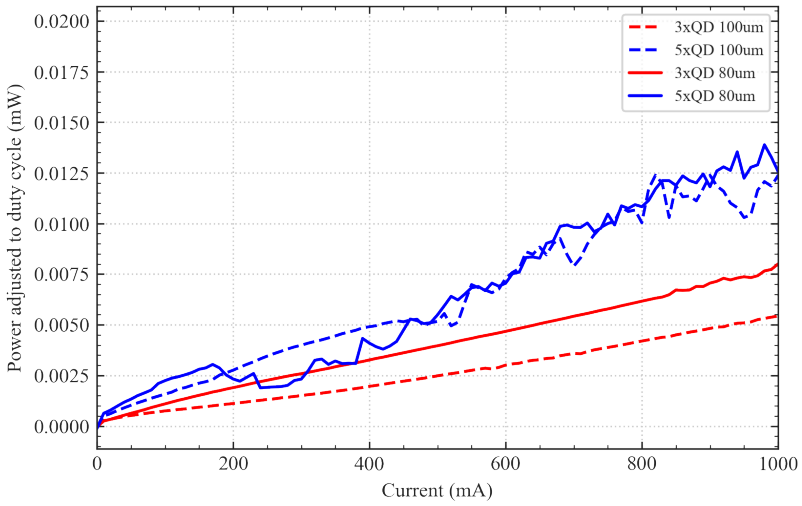

Fig 4. 17 Pulsed LI spectral of 3x, 5x QD & QW samples with pulsed width of 1µs and duty cycle of 1%

Fig 4. 17 illustrates the pulsed LI measurements at room temperature for the 4 mm 100/80µm broad area laser of the 3x and 5x QD samples. The applied pulsed current ranged from 0 to 1000mA (corresponding to a J of ~500A/cm^2). All the initial growth QD samples displayed SLED-like LI spectral characteristics and no signs of lasing. This result implies that there is either insufficient gain in the active region or very high optical loss. To investigate this issue further, 100 µm mesa diodes EL measurements of the 3xQD Sample were performed. Using this vertical geometry for EL measurements, free carriers or other absorption processes were eliminated in the doped AlInAs layers because the interaction length was negligible.

Fig 4. 18 illustrate the EL spectra of 100µm 3xQD mesa diodes at injection current densities of 10mA (low injection) and 100mA (high injection), corresponding to J of 0.12kA/cm^2 and 1.2kA/cm^2. The sharp cut-off in the spectra at 1.7µm was due to the InGaAs detector limit. At a high injection current (100mA), the 3xQD sample had a peak wavelength of approximately 1650 nm, with multiple peaks being observed. The FWHM of the 3xQD EL spectrum at 100mA injection was ~ 159 nm. This is mainly due to the large inhomogeneous broadening of QDs. The small peak at ~ 1400 nm likely corresponds to the excitation of the AlInAs cladding layer.

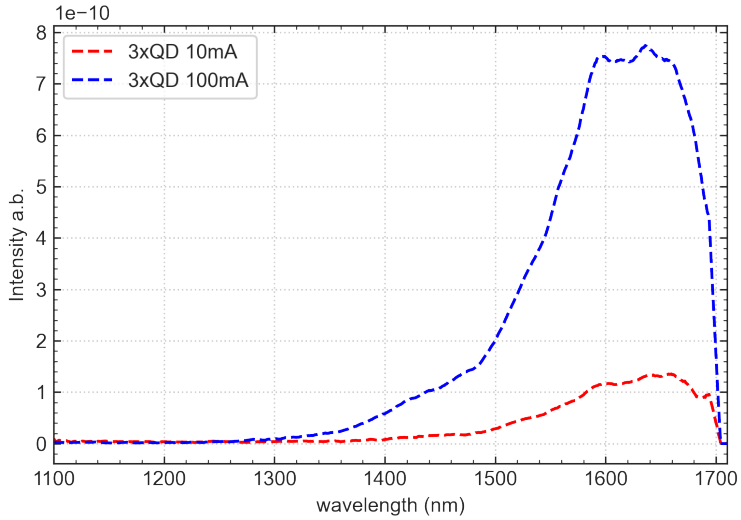

Fig 4. 18 Room temperature mesa diode EL spectrum of 3xQD samples at 10mA and 100mA current injection. The injected current corresponds to J of 0.12kA/cm^2 and 1.2kA/cm^2

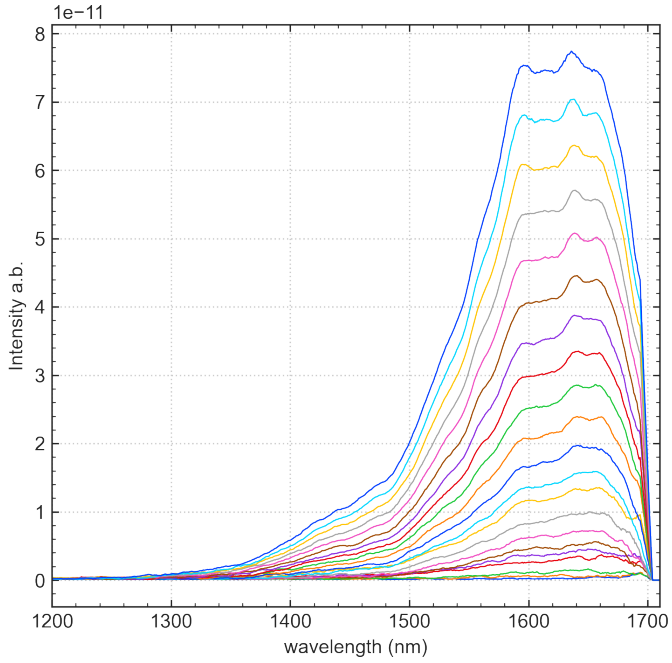

Fig 4. 19 Room temperature mesa diode EL spectrum of 3x QD samples from 0mA and 100mA current injection. Correspond to J from 0 to 1.2kA/cm^2

In Fig 4. 19 the mesa diode EL spectrum of the 3x QD sample was plotted in smaller injection current steps. Most importantly, the 5 nm InGaAs interlayer peak is evident in all spectra from low to high current densities. This suggests that there is poor transfer of injected carriers from

the InGaAs to the QDs, which may also be the origin of the poor dot efficiency (and consequently gain) in these structures. One explanation is that the carrier only recombined at the waveguide layer, resulting in less carrier injected into the InAs QD owing to the lower E_g of the InGaAs waveguide layer than the InP barrier layer.

To further tune these QD lasers emission from 1.6μm to 1.5μm to meet the desired telecom wavelength window. The growth parameters of the DE QD need to be been further optimised. However, as discussed in Section 4.1, the current DE growth of QD has already been optimised for high density dots. Therefore, growth parameters should be carefully adjusted without reducing the dot density too much. Thus, a change in the waveguide material from InGaAs to InP was proposed to improve the quantum efficiency of the QD laser. This ensures minimum effect on the DE QD density. The lower InP bandgap could increase the transfer of injected carriers from the waveguide to the QDs in the active region. Fig 4. 20 illustrates the revised QD structure incorporating the aforementioned optimisation techniques. The 100 nm InGaAs waveguide layer was replaced by an InP waveguide layer. New QD structures with 100 & 200 nm InP waveguide layers were also grown to investigate the effect of waveguide thickness on the optical and electrical properties of the QD laser structure. The Zn doping of the p-doped AlInAs layer was decreased to $5x10^{17}/cm^3$ to eliminate any Zn diffusion into the active region. The InP upper cladding thickness was also reduced from 1.5 μm to 1.2 μm to further reduce the resistance of the laser diode and thus reduce any self-heating issue. Additionally, a higher number of stacked QD layers (5x, 7x) were grown to increase the gain of the active region and decrease J_{th}.

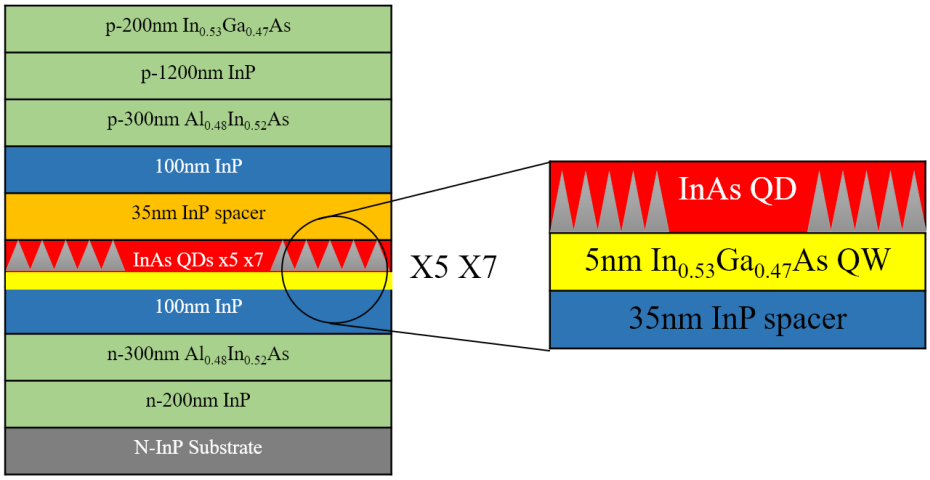

Fig 4. 20 Revised structure for QD/QW laser grown. The active region consists of 5x, 7x stacked droplet epitaxy of InAs QD on 5nm of $In_{0.53}Ga_{0.47}As$ QW

Structure	Thickness	Temperature	Doping density
InP	20nm+80nm	610°C	
InAs QD	2ML	520°C	
$In_{0.53}Ga_{0.47}As$	5nm	610°C	
$In_{0.53}Ga_{0.47}As$ or InP	100nm	610°C	
N-$In_{0.52}Al_{0.48}As$ cladding	300nm	630°C	$2x10^{18}/cm^3$
N-InP buffer layer	200nm	610°C	$1*10^{18}/cm^3$

Table 4.3 RT-PL structure for DE InAs QD on 5nm of $In_{0.53}Ga_{0.47}As$ QW grown on top of 100nm of $In_{0.53}Ga_{0.47}As$ and also on 100nm InP layer

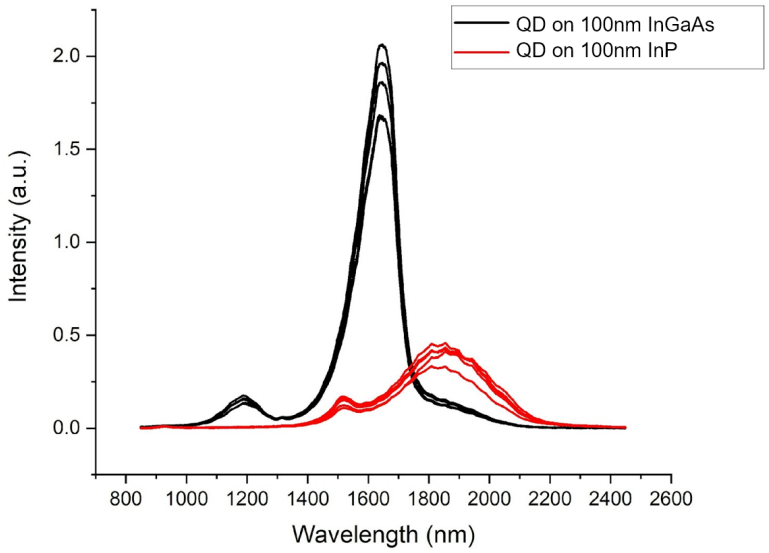

Fig 4. 21 RT-PL of droplet epitaxy of InAs QD on 5nm of $In_{0.53}Ga_{0.47}As$ interlayer grown on top of 100nm of $In_{0.53}Ga_{0.47}As$ (black) and 100nm of InP (red)

Before the growth of the optimised QD laser structure (Fig 4. 20), RT-PL was obtained from the PL structure shown in Table 4.3. In Fig 4. 21, the dominant PL peak at ~ 1600 nm in QDs grown on the 100 nm InGaAs sample (black) is most likely due to the bulk 100 nm InGaAs layer, with a small tail of QD emission peaking around ~ 1890 nm. This is significantly lower than that observed when the QDs were grown on the 100 nm InP layer (red). The spectrum of QD sample grown on the 100 nm InP (red) shows that the QD emission is predominantly at ~ 1890 nm. The smaller emission peak at ~1500nm is likely due to the 5 nm InGaAs interlayer under the dots (this peak is swamped by the bulk InGaAs layer in the QDs on the 100 nm InGaAs spectrum). The PL results implies that the presence of a 'bulk' InGaAs waveguide region in the initial QD structure traps the carriers and competes with the dots in the active region for the gain. The PL results clearly indicates that QD grown on the InP waveguide layer could achieve a higher quantum efficiency.

Next, the revised full QD laser structure, as shown in Fig 4. 20, was grown with identical parameters for InAs QD droplet epitaxy as before. 7x stacked QD layer samples were grown to

increase the gain of the active region and decrease J_{th}. Pulsed optical spectra measurements on the 4 mm broad area laser were carried out on these QD lasers. Fig 4. 22 compares the optical EL spectrum between the initial 5xQD sample and the new optimised 7xQD sample under pulsed conditions at the same current injection.

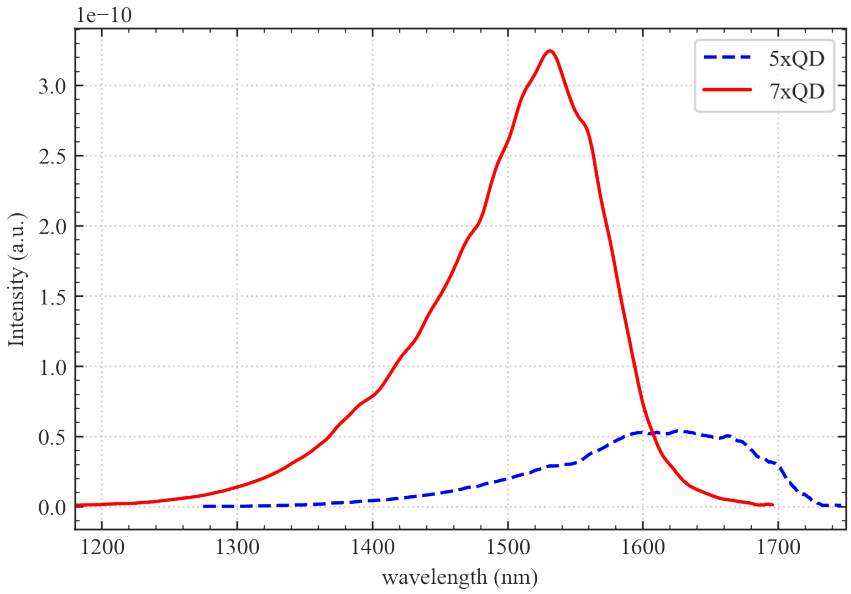

Fig 4. 22 Room temperature pulsed EL spectrum of 4mm broad area laser fabricated from initial Samples 5xQD and optimised Sample 7xQD.

In the EL spectrum of Samples 7xQD (Fig 4. 22), which use InP as waveguide layer material and a slightly higher growth temperature of the InP capping layer, a shorter emission wavelength of ~ 1530 nm was achieved. Previous Sample 5xQD (using InGaAs as waveguide material) spectrum is dominated by the bulk InGaAs waveguide at an emission of ~ 1600 nm, consistent with the RT-PL results shown in Fig 4. 21. The significant blue-shift in the emission wavelength of the 7xQD indicates successful tuning of the wavelength of the QD lasers close to the aimed 1.5μm range. Moreover, the 5 times increase in peak intensity of the 7xQD EL sample implies that more carriers are confined in the 7xQD than the 5xQD, as shown in Fig 4. 22. This is likely due to more carriers recombined in the smaller size QD, which mostly been trapped in the InGaAs bulk waveguide before (not recombined in the QD). In addition, the InP waveguide also provide better lattice match with the InP spacer underneath the DE QD, which

could favourite the formation of smaller size QD. However, the reason for lack of lasing in these QD samples is difficult to identify. For example, the potential high doping or dopant diffusion in the structures , such as Zinc, is known to show strong diffusion in MOCVD growth. Thus, reference QW laser structures were grown to investigate the possibility of diffusion of interstitial Zn into the active region, which could severely impact laser performance and preventing the lasing operation.

4.4 Design, Simulation and Growth of 1.5µm InGaAs/InP QW laser structure

4.4.1 QW laser structure simulation

The initial reference QW structure (Fig 4. 9) was simulated using the Rsoft LaserMod before the actual growth of the full QW/QD laser structure. The software can simulate the band diagrams, refractive index, optical modes, LIV, and optical spectrum gain of the laser structure. An appropriate estimation of the optical confinement and lasing capabilities of the structure in 1D and 2D simulations can be performed. The simulation outcomes will be used as a benchmark for future QD/QW optimisation. The QW thickness and barrier thickness are two of the most important parameters affecting the QW laser performance. The thickness of the quantum wells defines the emission wavelength, as it affects the energy state of the QW. Carriers will tunnel out of the QW if the well thickness is too small which prevent the formation of quantized state density[164]. Moreover, the barrier thickness of the QW layer must be sufficient thick to prevent carrier coupling between QW layers. However, an excessively thick barrier layer could increase the laser's on-state resistance and results in higher J_{th}. The number of QWs must also be optimised to allow sufficient gain to overcome the cavity loss and achieve lasing at room temperature. Multiple Quantum Well (MQW) lasers typically contain 5–15 QWs in the active region[132], [162], [165], [166]. In theory, the higher the number of QWs, the greater the gain, and the lower the threshold current density. Fig 4. 23 and Fig 4. 24 illustrates the band structure and refractive index of the initial 7xQW laser structure with InGaAs as waveguide material (Fig 4. 9). The results were simulated with a thickness of 5 nm/35 nm for the $In_{0.53}Ga_{0.47}As$/InP QW laser active region. A 100 nm InGaAs was used as the waveguide material.

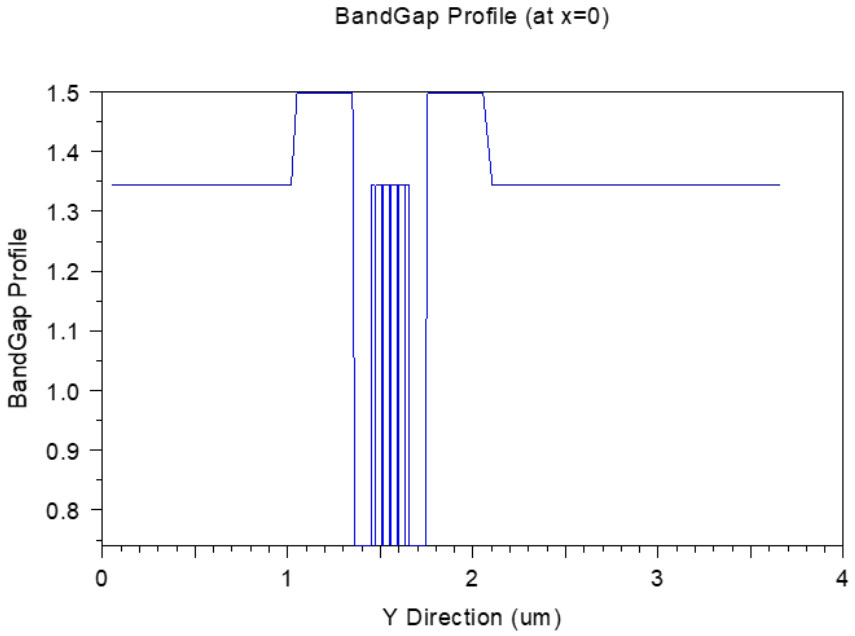

Fig 4. 23 Simulated band structure for 7xQW structure with InGaAs waveguide shown in Fig 4.9. The active region is consists of 5nm of $In_{0.53}Ga_{0.47}As$ and 35nm InP Barrier.

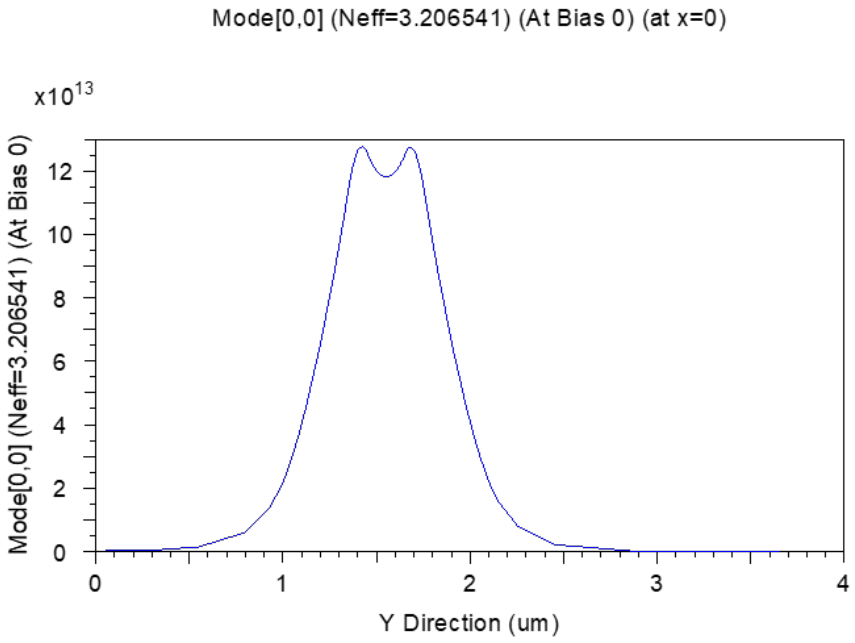

Fig 4. 24 Simulated mode profile for 7xQW structure shown in Fig 4.9.

In Fig 4. 24, the mode was confined to the active region with a calculated confinement factor of ~0.43. To further increase the confinement factor, one method is to increasing the quantum

well thickness. Fig 4. 25 shows the simulated confinement factor of lasers with $In_{0.53}Ga_{0.47}$ As QW thickness varied from 2 to 10 nm, and the InP barrier thickness was maintained at 35 nm. The 35 nm barrier thickness is obtained from the optimized capping thickness for droplet epitaxy of InAs QD[85].

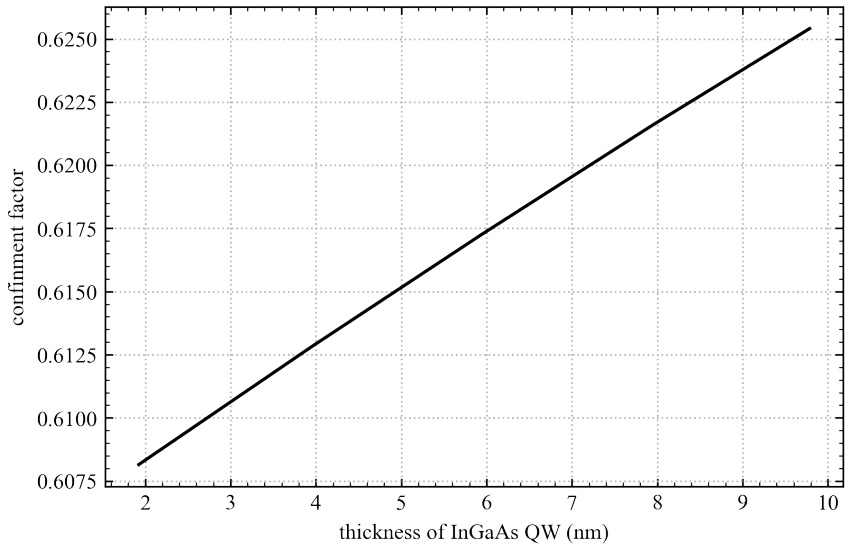

Fig 4. 25 Simulated confinment factor for QW thickness varied from 2-10nm, with InP barrier maintained at 35nm

According to the simulation results, the confinement factor increases as the QW thickness increases. This is expected, as the total area of the active regions expands. In the literature on similar InGaAs/InP QW structures, the QW thickness was approximately 10 nm[164]. The estimated λ of the InGaAs QW in the active region was ~1.6μm.

Using Rsoft LaserMod, a 2D simulation of the reference 7xQW laser structure with a 20μm ridge width and a 4 mm long laser device was performed. The LI curve and the optical emission spectrum of the simulated 7xQW laser structure are shown in Fig 4. 26 and Fig 4. 27. In Fig 4. 26, the simulation showed a threshold current of ~68mA (corresponding to a J_{th} of ~85A/cm^2). The simulated optical spectrum (Fig 4. 27) shows the initial 7xQW laser structure should have an emission wavelength of ~1.56μm.

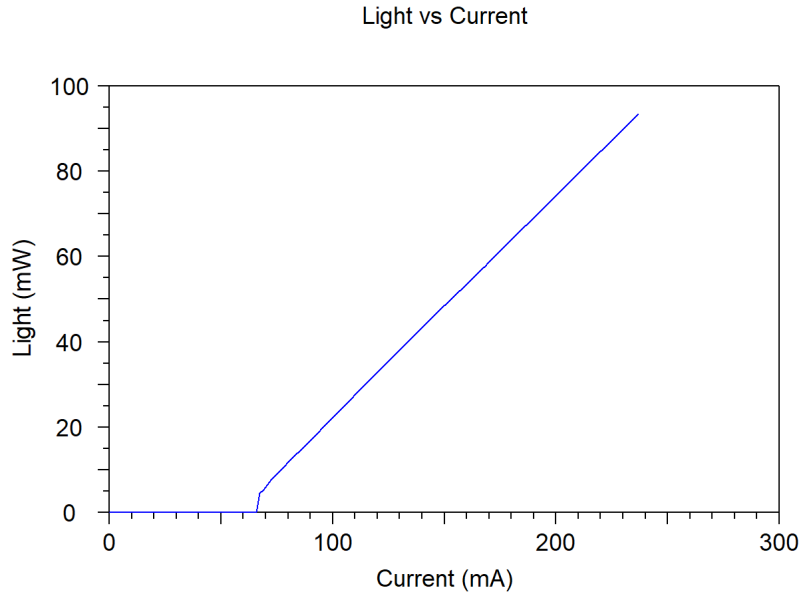

Fig 4. 26 2D Simulated LIV for 7xQW strucure shown in Fig 4.9 with 20um ridge width and 4mm cavity length.

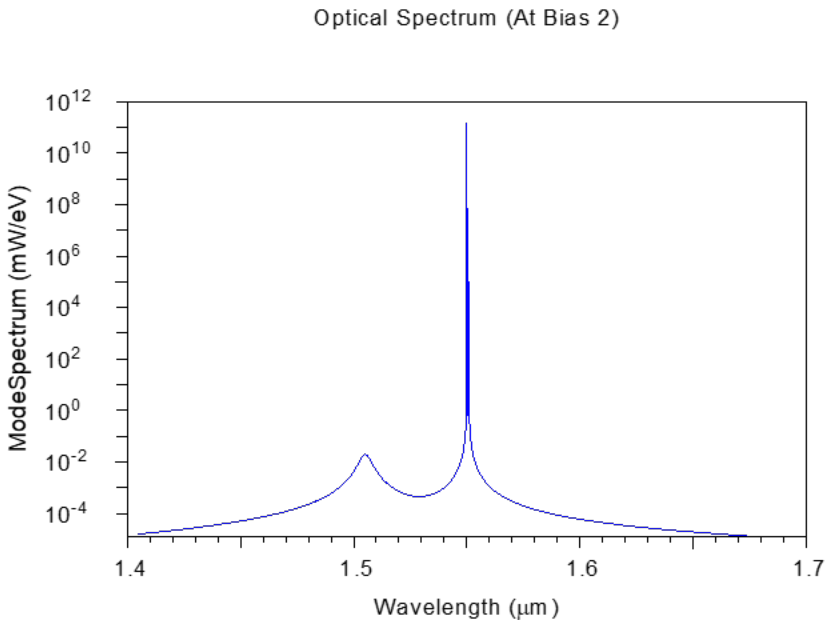

Fig 4. 27 Simulated optical spectrum for 7xQW strucure shown in Fig 4.9 with 20um ridge width and 4mm cavity length.

In previous Section 4.3, the growth of the initial 3x, & 5x InAs/InP QD laser structures with InGaAs as waveguide material showed no lasing on all samples. One possible explanation is that the J_{th} of these devices, if they lase at all, could be a few orders of magnitude higher than

the simulation results shown in Fig 4. 26, owing to the low quantum efficiency of the active region. A similar 15 stack QW laser structure in the literature is reported to show lasing at low temperatures (even with higher number of QW than the 5xQW we grown)[168]. This suggests that the number of QW should be increased to reduce the J_{th} of the current QW laser to achieve room temperature lasing. The second issue that impedes the performance of the QD laser is the carrier trapped by the InGaAs waveguide, which is not injected into the QD. This was proven by the higher EL measurements (Fig 4. 22) of the optimized 7xQD with InP as waveguide material compared with the initial 5xQD at the same current density.

Thus, to further investigate the issue of no lasing in these QD laser samples. A new reference QW laser structure with 100 nm & 200 nm of InP waveguides and 7x InGaAs/InP QW as the active region was simulated prior to the actual QW laser growth. Fig 4. 28 illustrates the 2D simulation of the new 7xQW laser structure's band structure and mode profile. Fig 4. 29 & Fig 4. 30 illustrates the simulated LI and the optical spectrum of the optimised 7xQW laser.

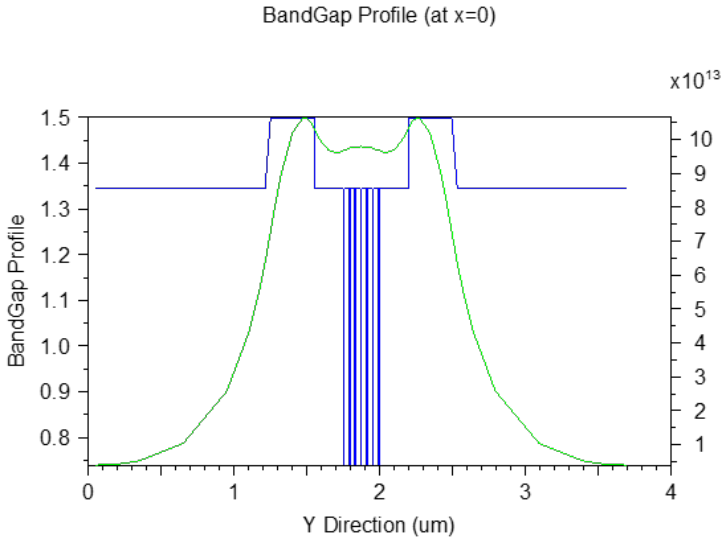

Fig 4. 28 Simulated band structure and mode profile for 7x $In_{0.53}Ga_{0.47}As$/InP QW with 100nm of InP waveguide layer.

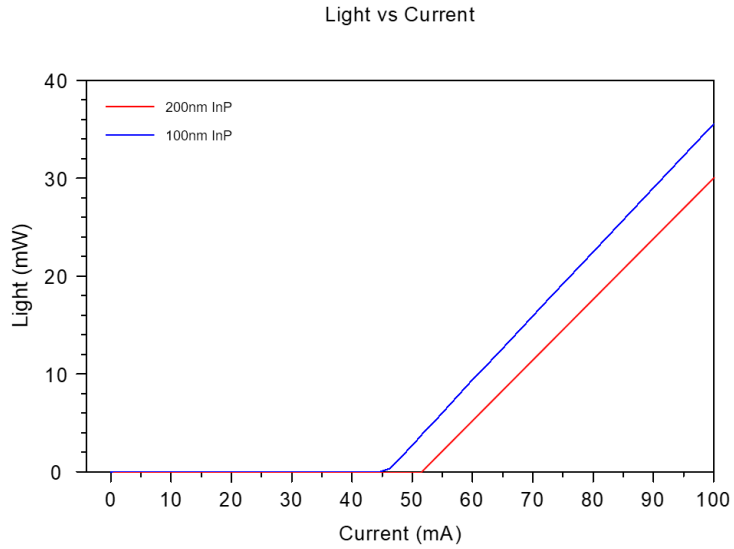

Fig 4. 29 Simulated LI for 7x $In_{0.53}Ga_{0.47}As$/InP QW with 100nm &200nm of InP waveguide layer.

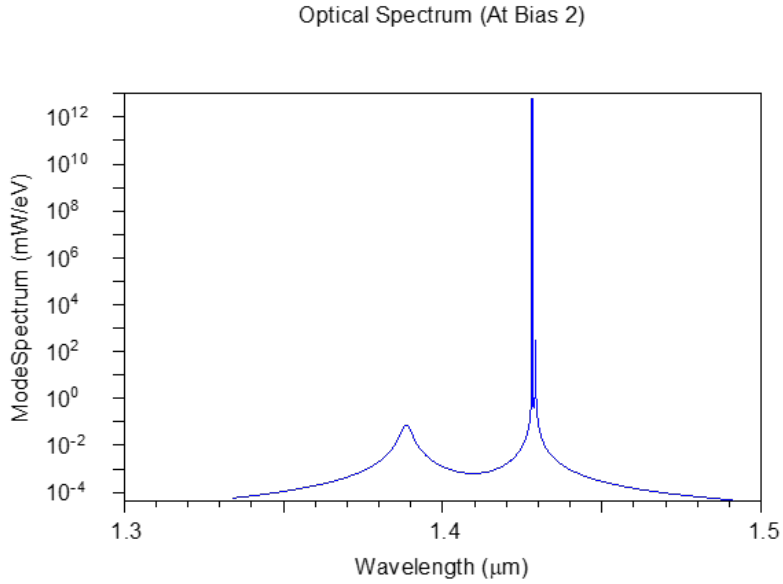

Fig 4. 30 Simulated optical spectrum for 7x $In_{0.53}Ga_{0.47}As$/InP QW with 100nm of InP waveguide layer.

Fig 4. 29 shows the simulated J_{th} of the optimised 7xQW is ~50A/cm^2 for a 4 mm long 20 µm ridge-width laser diode, which is lower than the initial 7xQW laser simulation LI results shown in Fig 4. 26. The optical spectrum shown in Fig 4. 30 also suggests that the InP waveguide layer blue-shifts the emission wavelength by ~1.43 µm which is closer to the desired 1.5 µm. Once the simulation results confirm the lasing of these QW structures, the reference QW structures

with both InP and InGaAs as waveguide materials were grown simultaneously with the DE QD lasers to ensure identical growth conditions.

4.4.2 Results and Discussion

Following the simulation of the reference QW laser structure, full QW laser structures were grown. For the QW laser structures, the same growth parameters and structure as the DE QD laser were used, but without the incorporation of the InAs QD layer. The samples were fabricated into broad-area lasers of 4 mm length with ridge widths of 100µm , 80µm, and 50µm for basic device characterisation. Various QW laser samples were grown using the structure shown in Fig 4. 20. The grown QW samples were summarised in Table 4.4. Sample 5xQW-A is the initial QW structure with InGaAs as the waveguide material. Samples B and C are 5x and 7x QW samples grown in the same run with the waveguide material changed from InGaAs to InP and with the AlInAs cladding p-doping density decreased to $5x10^{17}/cm^3$. Sample D is a QW laser grown with the InP waveguide layer increased from 100 nm to 200 nm. In Sample D, the AlInAs Zn doping was reduced to zero, and the InP cladding layer Zn doping was reduced to $1x10^{18}/cm^3$ which further eliminates the possible Zn diffusion into the active region.

Sample-reference	Waveguide material	Waveguide thickness (nm)	AlInAs Zn doping density	InP-cladding layer Zn doping density
5xQW-A	InGaAs	100	$9 x10^{17}/cm^3$	$2 x10^{18}/cm^3$
5xQW-B	InP	100	$5 x10^{17}/cm^3$	$2 x10^{18}/cm^3$
7xQW-C	InP	100	$5 x10^{17}/cm^3$	$2x10^{18}/cm^3$
7xQW-D	InP	200	0	$1 x10^{18}/cm^3$

Table 4.4 summarise of QD & QW samples grown with different SCH layer material & Zn doping density

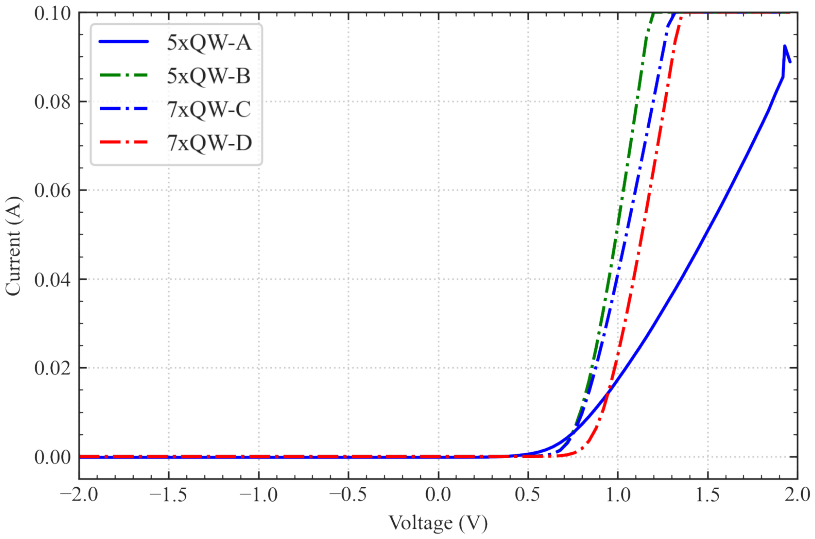

Fig 4. 31 IV characteristics of 4mm broad area laser fabricated from QW Samples A-D

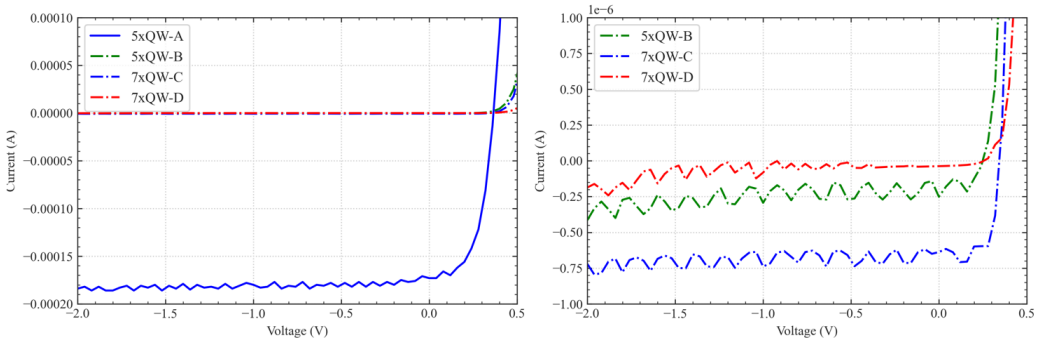

Fig 4. 32 Reverse IV characteristics of 4mm broad area laser fabricated from Samples A-D (left) and from Sample B-D (right)

Fig 4. 31 illustrates the IV properties of 4 mm broad area laser samples A, B, C and D. Sample B,C, D exhibit a turn-on voltage of 0.7V and Sample A has a turn-on voltage of 0.5V, which is consistent with the replacement of waveguide material from InGaAs to InP and the subsequent reduction in band-gap. In addition, the on-state resistances of samples B,C, and D exhibit good consistency at 5 Ω. The main difference between samples B, C, and D is the Zn doping density, which implies that AlInAs Zn doping has no effect on the resistance. Reverse IV for each QW sample is shown in Fig 4. 32. In Fig 4. 32 (left), the reverse leakage current of Sample 5xQW-

A is much higher than that of the other samples with InP as the waveguide material (~10^{-7}A). One possible explanation for this is that the InP waveguide provides a better lattice match with the InP barrier, which improves the quality of the active region. The lowest reverse leakage current was achieved by Sample 7xQW-D, as shown in Fig 4. 32 (right). This suggests that a thicker InP waveguide further reduces the reverse leakage current by reducing Zn diffusion into the active region.

Fig 4. 33 illustrates the measured pulsed LI curves for Samples A, B, C, and D at 1µs pulse width of 1% duty cycle. The temperature was maintained at room temperature and measurements were performed using the apparatus described in Chapter 2.

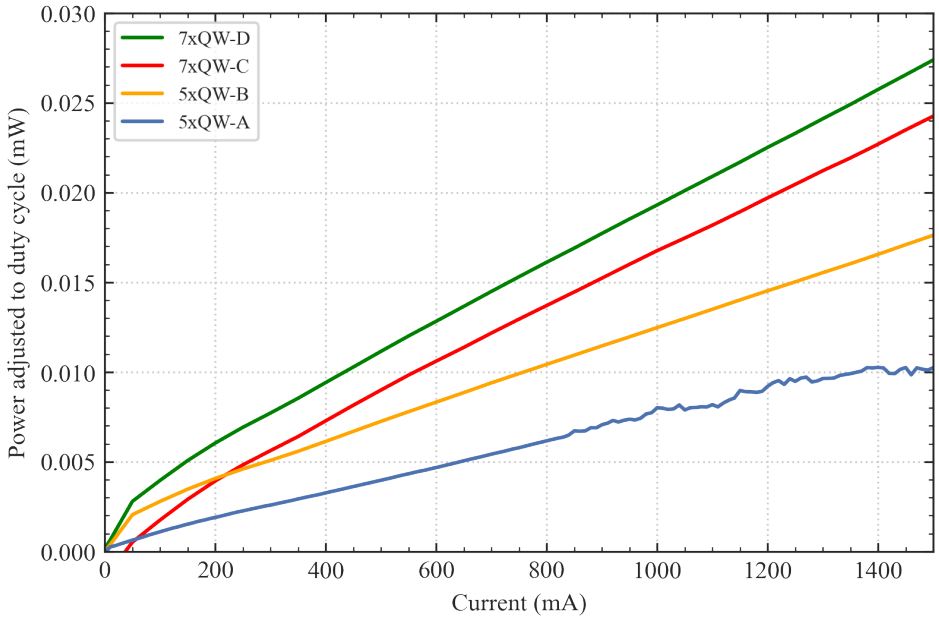

Fig 4. 33 pulsed LI characteristics of 4mm broad area laser fabricated from Samples A-D. The pulsed width is 1µs and duty cycle is 1%

From the LI spectra of the QW laser samples, there is an overall increase in the output power at the same current as the Zn doping in the AlInAs decreases from 9x10^{17} to 5x10^{17}/cm^3 and to zero (Samples B–D). The intensity of Sample 7xQW-D at ~1200mA increased approximately fivefold compared to that of Sample 5xQW-A. Such a large increase in intensity suggests that a higher quantum efficiency of the active region was achieved for the InP waveguide layer. The

InP waveguide material increased the number of carriers in the QWs, consistent with previous QD laser LI results. In Fig 4. 33, Sample 7xQW-D is ~1.4 times higher than sample 5xQW-C, which correlates well with the increase in the number of stacked QW layers (~1.4 times). The highest output intensity was achieved by Sample 7xQW-D, with Zn doping of AlInAs reduced to 0. This result clearly suggests that the diffusion of Zn should be kept at a minimum in future laser structure optimisation. However, none of the samples showed lasing at currents up to 1400mA (~700A/cm^2).

Because neither the QW nor QD laser LI results showed lasing, even at the injection current density nearly 10 times above the simulated value. This implies that the issue may be growth-related. Thus, the samples were analysed through SIMS for further investigation (all SIMS was carried out by Aystorm Scientific Limited, using a Depth Profiling SIMS analysis tool and calibrated control wafers). The Zn and Si doping concentrations as well as As counts are plotted against the measured SIMS depth for the Sample 7xQW, shown in Fig 4. 34.

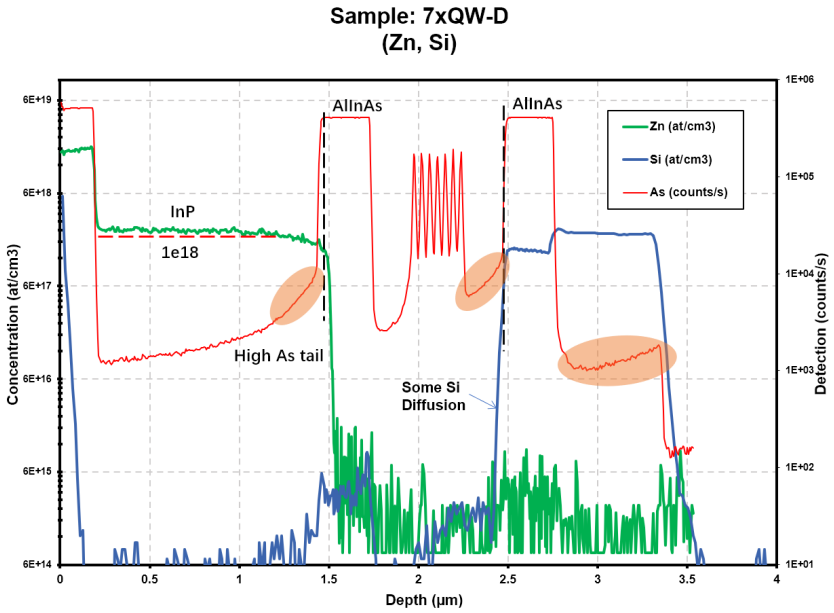

Fig 4. 34 SIMS analysis of Zn and Si doping concentration of Sample D (7xQW). The As counts are used for reference on the growth layer. The orange circle shows high As tail presents in the InP.

The Zn doping density of the p-InP upper cladding is $1.5x10^{18}/cm^3$, which is slightly higher than the required $1x10^{18}/cm^3$. However, because the actual activated Zn doping concentration could be lower than that measured by SIMS at these concentrations, this is not a major concern, as the Zn doping of InP normally becomes saturated at 1-2 $x10^{18}/cm^3$[169], [170]. For the undoped 300 nm AlInAs cladding region, as indicated by dashed line in Fig 4. 34, the Zn diffusion length from the InP cladding to AlInAs is ~ 60 nm. This implies that the diffusion of Zn atoms into the active region may occurred in all doped AlInAs Sample. There is also a Si diffusion of ~ 80 nm from n-AlInAs to the lower InP waveguide layer, suggesting that Si doping should be controlled as well. Therefore, further optimisation is required by incorporating graded doping into AlInAs for better carrier confinement and supress the diffusion of Zn and Si.

In Fig 4. 34, there is an unusual arsenic (As) peak in the lower InP waveguide layer and other InP layers (shown by orange circle). Because background As count is nearly identical for each SIMS analysis (~100 counts), the As present in the InP layer is real and the concentration is estimated to be 0.2% in InP, which is two times higher the background. Such an As tail can introduce additional defects that reduce the efficiency of the laser structure. Moreover, same As tail was present in all QW and QD laser SIMS samples. In Fig 4. 35, the As count was plotted against each growth run in different epitaxy layer. The SIMS samples were divided into different growth runs for better comparison.

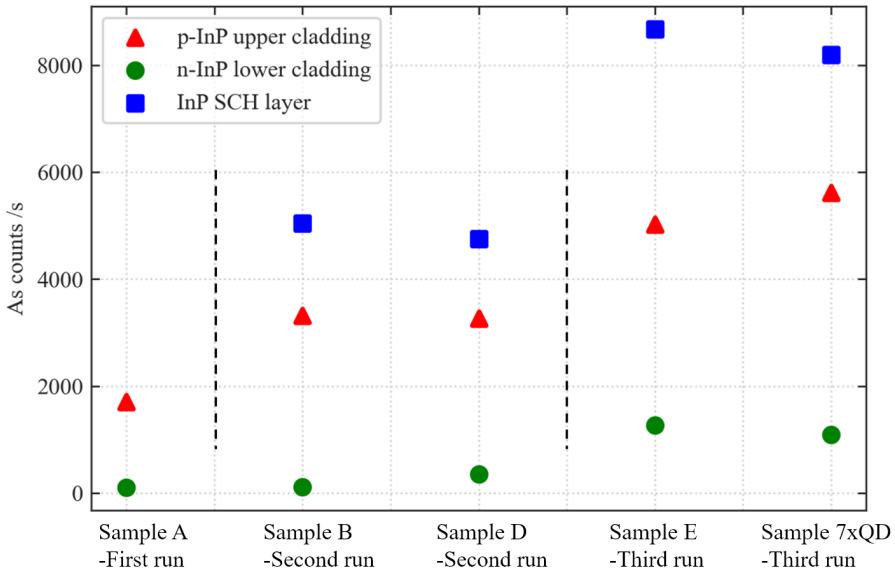

Fig 4. 35 Average As counts in the different InP layers collected from SIMS analysis of all samples grown by the same MOCVD reactor. The background As is ~100. Dashed line is separation of each growth run.

As shown in Fig 4. 35, the average As counts in all InP-containing layers increased from the first to the third growth-run. The As counts between the samples in the same growth-run is identical (both QD and QW). Despite doubling the thickness of the InP waveguide layer, the As tail in the third run exhibited a significant increase compared to the previous two runs. These results suggest that the issue is unrelated to the droplet epitaxy process of QD in the active region. In Fig 4. 35, the As counts (green dots) in the lower-cladding region increased in the third run, where the first growth run was similar to the second run. Since this is a pure InP buffer layer, no As elements should be present in the lower cladding region. This high As tail may be caused by the chamber memory effect where excess As is present in the background. Thus, further investigation via additional SIMS measurements of AlInAs and InP growth in the bulk is required.

In conclusion, based on the SIMS analysis shown in Fig 4. 34, high Zn diffusion was one of most significant growth-related issues in our QW and QD laser samples. To balance the zinc diffusion for good carrier injection in the laser, the Zn/Si doping in the AlInAs waveguide

should be controlled via graded doping and the doping density should be gradually reduced from $5x10^{17}/cm^3$ over the course of 60 nm. The second significant growth issue is the As diffusion, which also present in all the QD and QW samples grown. However, the reason for this high As tail is not yet understood and could link to the chamber memory effect. This can be reduced by grow a much thicker InP buffer layer prior to each ample growth.

Nonetheless, the absence of room-temperature lasing in the Sample 7xQW-D structure must also be investigated. The QW simulation results shown in Fig 4. 29 indicate that lasing is possible in these QW structures. The exact QW laser device could have a lower quantum efficiency than the ideal condition of the simulation because of the presence of other defects in the active region. Therefore, pulsed LI at a low temperature (77 K) of a 1 mm broad area laser of Sample-E 7xQW was carried out. Due to the 4-times reduction in the laser's physical dimensions compared to the 4 mm cavity, a higher injection current density on the 1 mm broad area laser can be achieved. The maximum J that can be applied to the device is $15kA/cm^2$, which should be sufficient to achieve lasing. For the low-temperature measurement setup, the device was measured in a helium cryostat cooled to 77K using the same pulsed current sources with a pulse width of 1µs and duty cycle of 1%. The output light of the laser was measured through the window of the cryostat using an InGaAs detector. Measurements at low temperatures supress any thermal carrier loss in the active region and increase the internal quantum efficiency of the laser, which should significantly reduce the threshold current density of the laser. Fig 4. 36 illustrates the low-temperature pulsed LI obtained for Sample-E 7xQW at 77 K.

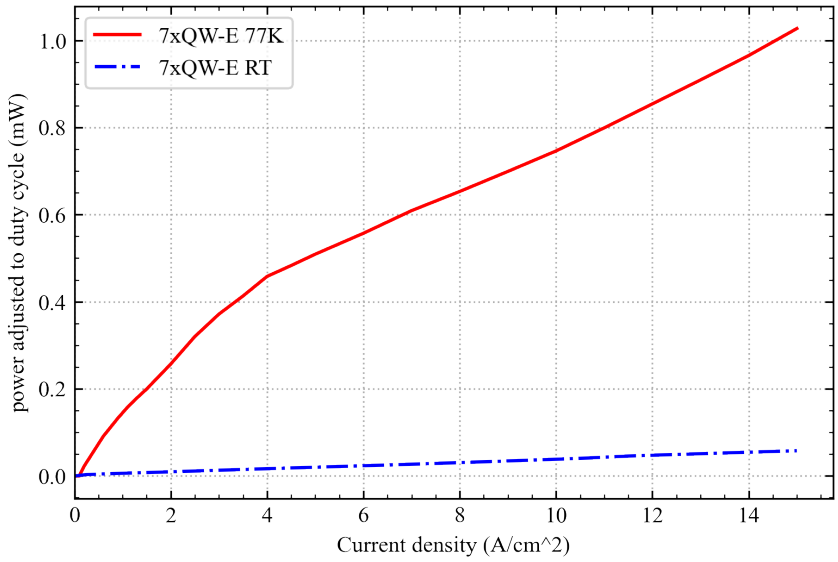

Fig 4. 36 Pulse LI of Sample-E 7xQW measured from broad area laser at 77K and room temperature

The LI spectrum at 77k represents an SLED-like spectrum with a slight increase in the slope as the current density increased. Although J_{th} should be significantly reduced at such low temperatures. There was still no sign of lasing, even at 77k. As shown in Fig 4. 36, the absolute LI intensity at 77 K was ~17.7 times greater than that at room temperature. Because the quantum efficiency increases in the active region at low temperatures, where defect-related losses are minimised. Therefore, the lack of lasing at low-temperature LI implies that either carrier injection into the QW is not sufficient to achieve population inversion or there is a lot of non-radiative recombination even at 77 K, which stops the lasing (likely due to the high As tail).

To increase the carrier confined in the QW, modification of the existing QW laser structure to achieve a higher quantum efficiency is required. This can be achieved by increasing optical confinement in the active region. One way of increasing the optical confinement in the structure is by changing the 100 nm InP waveguide layer to a higher refractive index material. Fig 4. 37 illustrates structures that can achieve room-temperature lasing using similar InAs QD on InAlGaAs QW, as demonstrated in numerous published works[14], [33], [35]–[37], [69], [165], [172], [173]. In the literature, InAs/InAlGaAs QD lasers have a threshold current of 40mA, room room-temperature lasing has been achieved at ~1.56 µm[162]. The reference QW laser

structure can be grown by removing the InAs QD layer from the structure shown in Fig 4. 37. The quaternary layer was selected to have a bandgap of ~1.07 eV (corresponding to ~ 1158 nm), which is lattice-matched to the InP. Since the E_g of $In_{0.528}Al_{0.238}Ga_{0.234}As$ is also lower than that of InP (1.344 eV). Thus, carriers should be more easily injected from the $In_{0.528}Al_{0.238}Ga_{0.234}As$ waveguide into the InGaAs QW compared to InP waveguide. Another benefit of the $In_{0.528}Al_{0.238}Ga_{0.234}As$ waveguide layer is that it has a refractive index of ~3.3, which is higher than that of AlInAs (~3.2). This suggests that the $In_{0.528}Al_{0.238}Ga_{0.234}As$ waveguide layer could also provide a higher optical confinement than InP, resulting in a higher carrier capture efficiency compared to the current InP waveguide layer and thus possible room-temperature operation.

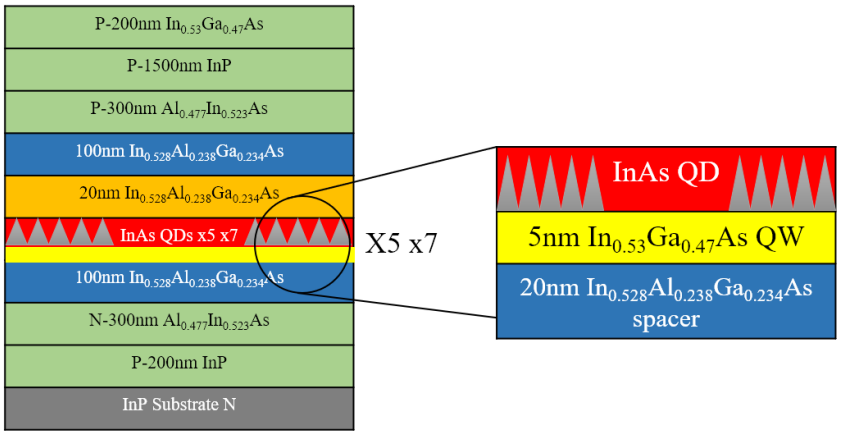

Fig 4. 37 Structure of QD laser with InAs QD on 5nm InGaAs QW with InAlGaAs as waveguide layer material[165].

A new QW laser structure with 5 nm InGaAs QW, 20 nm of $In_{0.528}Al_{0.238}Ga_{0.234}As$ barrier layer and 100nm of $In_{0.528}Al_{0.238}Ga_{0.234}As$ waveguide layer could be grown to achieve higher internal quantum efficiency than current QW laser structure. The reference QW laser structure is then simulated using the Rsoft LaserMod for design approval for future growth plan. The band structure and mode profile of the QW laser are shown in Fig 4. 38. The simulated LI is shown in Fig 4. 39.

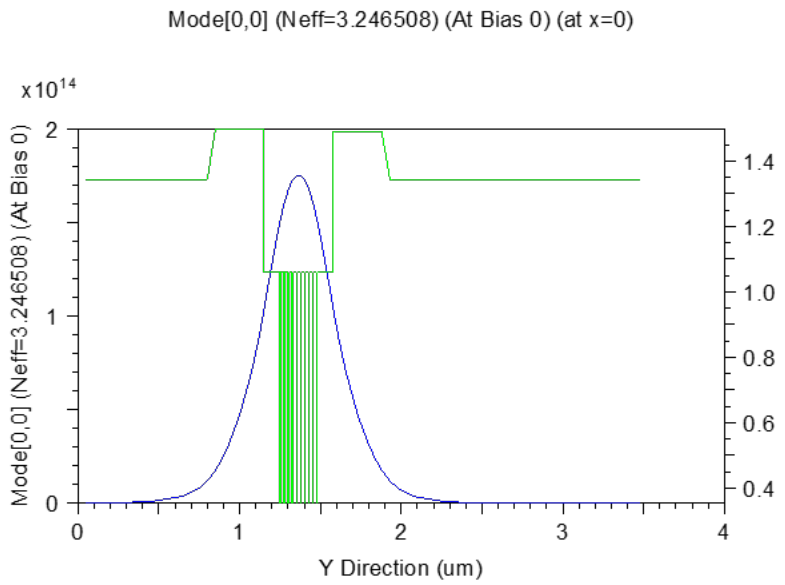

Fig 4. 38 Simulated band structure and mode profile of 10x 5nm InGaAs QW with InAlGaAs as waveguide layer

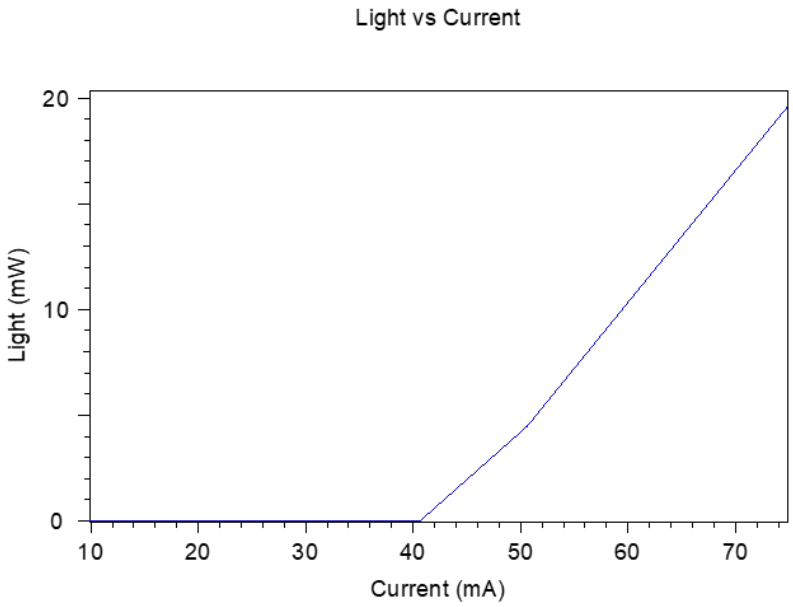

Fig 4. 39 Simulated LI of 10x 5nm InGaAs QW with InAlGaAs as waveguide layer

The structure exhibited excellent optical mode confinement at the centre of the active region, aligning the maximum optical gain with the active region. The LI spectral shows a threshold current of 40mA, which is lower than the previous LI simulation results of 7xQW shown in Fig 4. 29. This is likely due to the higher optical confinement of $In_{0.528}Al_{0.238}Ga_{0.234}As$, which

increases the gain of the laser. However, the inclusion of AlInGaAs as a waveguide in the active region could be challenging for MOCVD[174], and the aluminium-containing layers in the active region often results in a higher oxygen concentration, which reduces the quantum efficiency. Thus, the growth parameters must be carefully optimised for the $In_{0.528}Al_{0.238}Ga_{0.234}As$ layer.

Another method to increase the quantum efficiency of the active region is to increase the thickness of the QW. In the literature, the thickness of an InGaAs QW is typically 6–7 nm, and the barrier is approximately 8–10 nm for similar QW laser structures[45], [168], [175]–[181]. Because the InGaAs QW and InP barrier thicknesses of the QW structure are correlated with the growth structure of the DE InAs QDs. Therefore, the minimum thickness of the InP barrier was kept at 20 nm in grown QW structures. However, for future optimisation of the QW laser structure, the InGaAs QW thickness can be increased from 5 nm to 6 nm, 7 nm, etc. to obtain a higher confinement factor in the active region. In addition, a thicker InGaAs QW could reduce the strain field effect of the stacked QD layer and improve the surface morphology[144]. In summary, the growth issue related to the lack of lasing of the QW laser has been investigated through SIMS measurements and is likely due to the high As diffusion in the InP and high Zn doping in the AlInAs. To further increase the quantum efficiency and achieve lasing of the QW lasers, methods such as changing the waveguide material to AlInGaAs and increasing the InGaAs quantum well thickness can be considered in future optimisation. Once the aforementioned growth-related issues have been solved, the simulation results imply that there is a high possibility of achieving lasing for these QW laser structures. Thus, it can be used as a guide to optimise the current DE InAs QD laser structure.

4.5 Characterisation and Optimisation of Droplet Epitaxy of InAs/InP QD laser

In this section, the additional growth-related issue that prevents the DE InAs QD laser from achieving lasing is discussed. As mentioned in previous Section 4.4, a high As tail and diffusion of Zn were also present in the QD laser growth. However, other defects related to the DE process can further reduce the quantum efficiency of QD lasers. Thus, it is necessary to identify the origin of these additional defects. Fig 4. 40 illustrates the 10x zoomed Nomarski image for 1the PL structures of the 1x, 2x, and 3x QD layers.

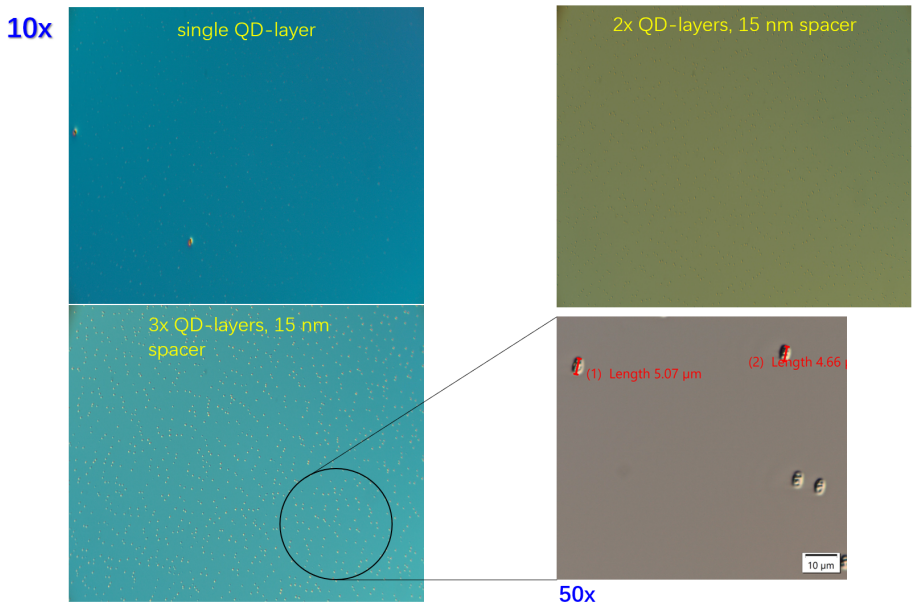

Fig 4. 40 10x zoomed Nomarski image for PL structure of 1x, 2x and 3x QD layer. The 50x shows the length of defects is ~5µm

The Nomarski image shows degradation in the surface morphology as the number of stacked layers increases from one to three. Round defects (~5µm in diameter) were observed on the entire surface of the sample. The density of these defects increases with a higher number of QD layers stacked, suggesting that it is also related to strain accumulation during stacking. Such circular defects are likely the result of the low-quality InP capping layer, indicating that the

V/III ratio may be too high. Similar round defects were present only in all the QD samples but not in the QW samples. This implies that the issue is only related to the droplet epitaxy growth of stacked QD. Therefore, the QD growth temperature, V/III ratio, and thickness of the capping layer must be optimised to reduce such defects in the future growth.

For the actual QD laser structure grown, the same parameters were used for InAs QD droplet epitaxy process in the active region. Samples grown using the QD laser structure outlined in Fig 4. 20 were summarised in Table 4.5. For comparison purposes, the AlInAs Zn doping density was reduced from $9x10^{17}/cm^3$ to $5x10^{17}/cm^3$ in one sample and left undoped together in another. The 3xQD (A) Sample used InGaAs as a waveguide layer material. Samples 5xQD (B) and 7xQD (C) were grown using the InP as waveguide layer. Sample 7xQD (C) had an InP waveguide thickness increased to 200 nm, the AlInAs Zn doping was reduced to zero, and the InP cladding layer Zn doping was reduced to $1x10^{18}/cm^3$.

Sample-reference	Waveguide material	Waveguide thickness (nm)	AlInAs Zn doping density	InP-cladding layer Zn doping density
3xQD-A	InGaAs	100	$9\ x10^{17}/cm^3$	$2\ x10^{18}/cm^3$
5xQD-B	InP	100	$5\ x10^{17}/cm^3$	$2\ x10^{18}/cm^3$
7xQD-C	InP	200	0	$1\ x10^{18}/cm^3$

Table 4.5 summarise of QD samples grown with different waveguide layer material, thickness & Zn doping density

The samples were fabricated into 4 mm long, 100µm, 80µm, and 50µm wide broad-area lasers for basic electrical and optical comparison. Fig 4. 41 shows the 10x Nomarski image of the 3xQD (A) and 7xQD (C) samples.

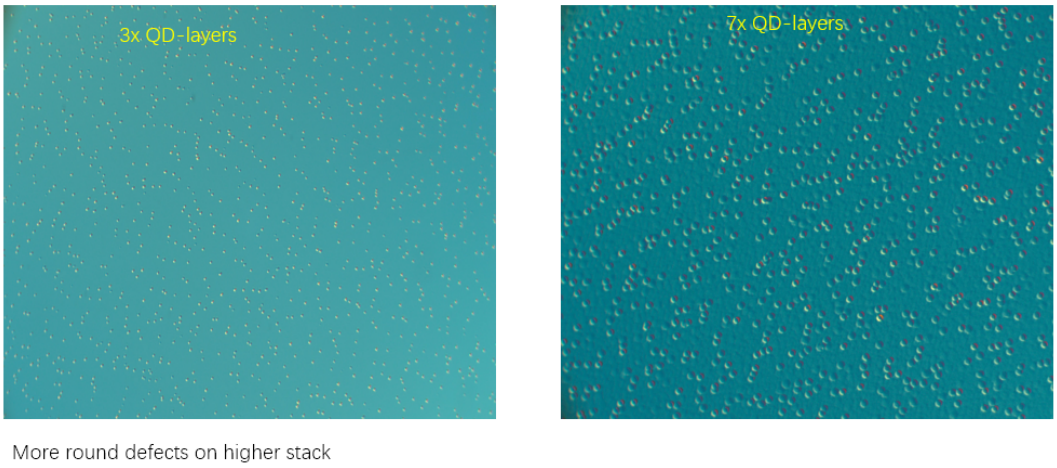

Fig 4. 41 Nomarski image of Sample (A) 3xQD on left , Sample (C) 7xQD on right.

Similar round defects in Fig 4. 40 were observed on both 3xQD and 7xQD samples Nomarski image, confirmed that this is due to droplet epitaxy of QD. The size of the defects also increased as the stacking of QD increased, probably because of the higher strain accumulation as stacking increased, altering the surface morphology of the InP capping layer. Thus, a thicker InGaAs QW can be used to reduce the strain field effect of the QD layer underneath to improve the surface morphology of the InGaAs QW[144], which could reduce the formation of round defects.

Fig 4. 42 illustrates the measured pulsed LI curves for samples A, D, and F at 1us pulse width of 1% duty cycle. The temperature was maintained at room temperature. From the LI spectra of samples A-C (dashed line), there is an overall increase in output power at the same current as the Zn doping in the AlInAs decreases from $9x10^{17}$ to $5x10^{17}/cm^3$ and to zero, which is identical to the LI results shown by the QW sample previously. The QD samples exhibited an S-LED-like spectrum with no sign of lasing. The maximum intensity of Samples B and C increased significantly compared to the initial grown 3xQD (with InGaAs as waveguide material). This large increase in intensity suggests that a higher quantum efficiency of the active region was achieved for the InP waveguide layer, which significantly increased the number of carriers in the QDs.

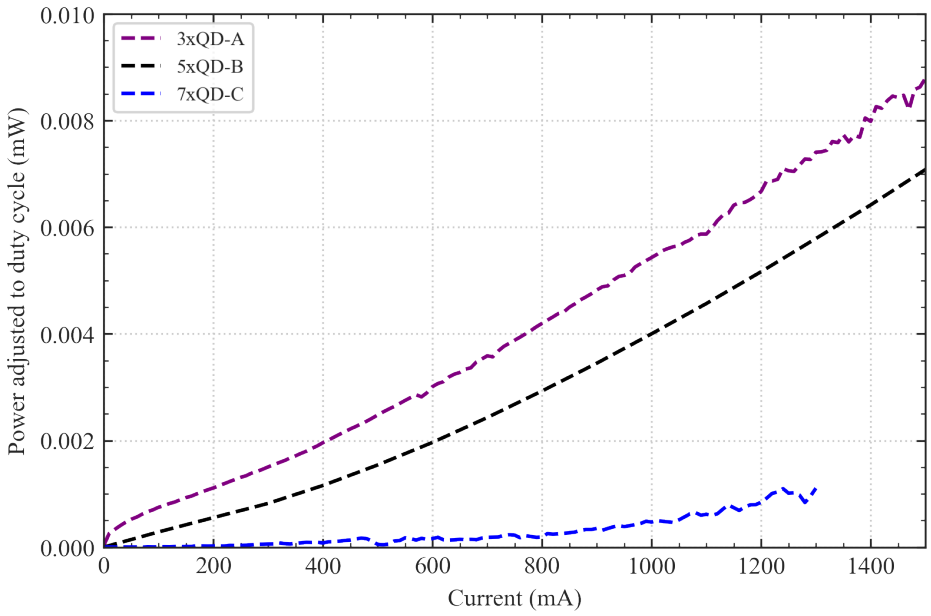

Fig 4. 42 pulsed LI characteristics of 4mm broad area laser fabricated from QD laser Samples A-C. The pulsed width is 1μs and duty cycle is 1%

The output intensity of the Sample 7xQW shown in Fig 4. 21 is approximately three times higher than that of the 7xQD samples (C) in Fig 4. 42 at the same injection current density. This suggests that circular defects discussed in Fig 4. 41 reduce the internal quantum efficiency significantly compared to the QW samples. Moreover, the low quantum dot density of the QD samples could be another reason behind. Therefore, SIMS analyses on Sample 3xQD-A and 7xQD-C were also performed to further identify the additional issue of low quantum efficiency of these QD samples.

In addition to the presents of high As tail observed in the QW samples, shown in the previous section, high oxygen impurities were also presents in the 3xQD and 7xQD Samples. Fig 4. 43 shows the oxygen SIMS analysis of Sample-C 7xQD and Sample-A 3xQD.

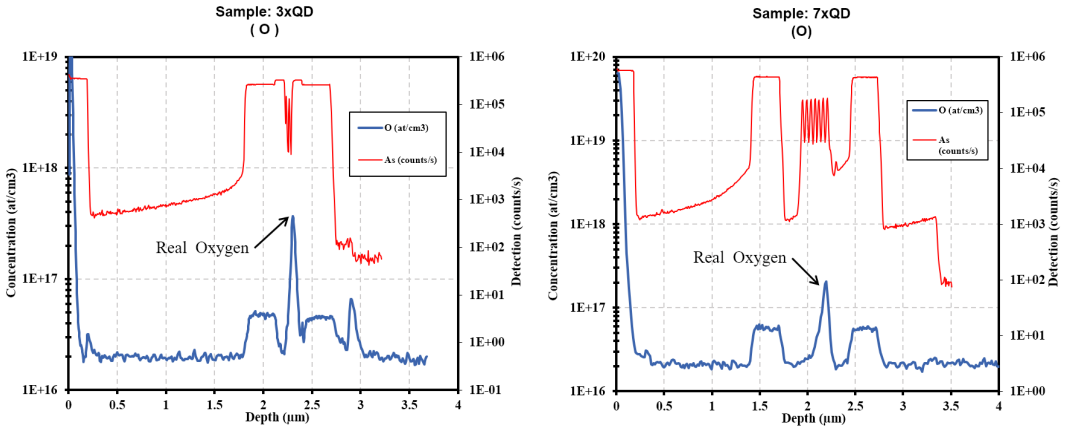

Fig 4. 43 SIMS analysis of oxygen impurity concentration of Sample F (7xQD) & A(3xQD). The As counts are used for reference on the growth layer. The arrow shows high oxygen presents in the active region

In Fig 4. 43, the oxygen content in the AlInAs cladding is ~5x10^{16}/cm^3 which is likely due to the high concentration of aluminium, which is close to the detector background noise. However, the oxygen peak concentration in the active region of Sample 3xQD is ~3x10^{17}/cm^3 which is ~15 times higher than the normal background oxygen level. Although the oxygen concentration was slightly lower in Sample 7xQD (~2x10^{17}/cm^3). It was still ~10 times higher than that of the background oxygen level. The high oxygen peak is only observed in the active region of the QD samples, suggesting that it is related to droplet epitaxy QD growth. This is problematic because a high oxygen impurity could reduce the internal quantum efficiency of the laser device significantly. The oxygen impurities create non-radiative recombination centre, [171]and thus would be another reason for the no lasing of the QD samples shown in the LI measurements (Fig 4. 44). Usually, the origin of high oxygen content link to the Al-containing layers in the active regions. However, for the current DE of InAs QD on InGaAs interlayers, there is no Al-containing layer in the active-region structure. By closely examining the SIMS results of both QD samples, the high oxygen peak always sat at the beginning of the DE growth of the first InAs QD layer. This implies that either the precursor of trimethyl aluminium (TMAl) or the Indium sources had high oxygen concentrations. Therefore, to further investigate the origin of such high O impurities, the Al concentration of the 7xQW and 7xQD samples were compared, as shown in Fig 4. 45. In Fig 4. 45, the Al concentration at the beginning of the InAs QD layer

is ~10 times higher than that in the QW sample. The ratio is close to the oxygen concentration in Sample 7xQD compared with the background oxygen level.

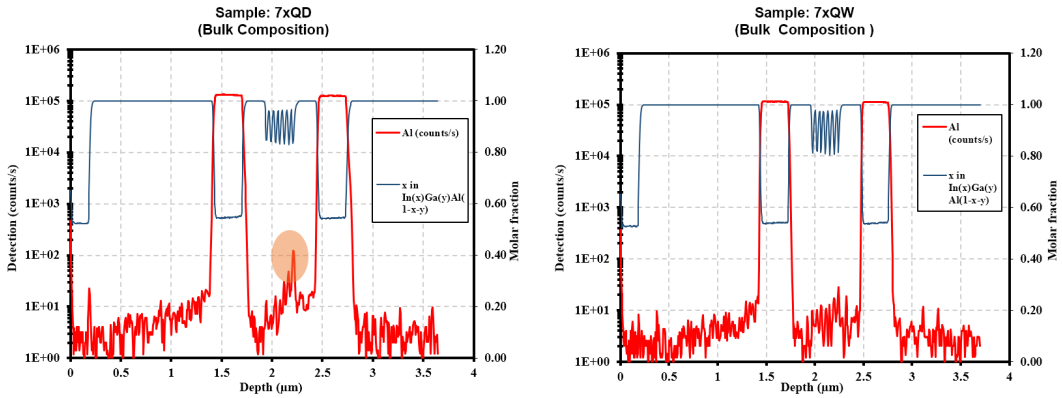

Fig 4. 45 SIMS analysis of Al counts and bulk composition of Indium of Sample F (7xQD) & E(7xQW). The In fraction are used for reference on the growth layer. The circle shows high Al presents in the QD active region

This implies that aluminium could be the reason for the high oxygen content presents in the QD samples. Since no oxygen impurity and Al concentration in the InP waveguide layer, the high aluminium counts observed in the 7xQD sample is not likely due to the diffusion of aluminium from the doped AlInAs lower cladding to the active region. One possibility could be the excess aluminium was remained in the chamber after the growth of AlInAs, which was then absorbed by the during the deposition of indium droplet.

Finally, to reduce the oxygen level in future growth of QD laser, optimise the growth temperature of the DE InAs QD could be considered. Also, by reducing the incorporation of Al atoms or by replacing AlInAs to InGaAsP material system, which completely eliminates any Al-containing layer in the chamber can be helpful as well. For the existing droplet epitaxy of InAs QD on 5 nm InGaAs QW, a quantum dot density of ~1.5 x 10^{10}/cm^2 has been achieved, which may not be sufficient for lasing. Thus, droplet epitaxy of InAs quantum dots grown on different materials to increase the QD density is another important topic for future investigation.

4.6 Conclusion

In conclusion, the possibility of droplet epitaxy of InAs quantum dots on an InP substrate for 1.55μm laser applications in MOCVD were investigated. The results show that the optimised QD and QW samples had higher quantum efficiencies than the initially grown samples with InGaAs as waveguide material. The room-temperature EL spectrum suggests the successful tuning of the QDs' wavelength to 1530 nm for the InP waveguide material, which is much closer to the target 1.55 μm range. However, room-temperature lasing was not achieved for these QD & QW samples.

For the non-lasing of reference QW samples, one possible reason is likely due to the high As diffusion presents in the sample, which reduces the internal quantum efficiency significantly. In addition, the 7xQW sample's low temperature LI at 77 K shows a SLED-like LI spectrum, which implies that there is a low carrier density in the InGaAs quantum well. This can be improved by increasing optical confinement of the active region. Therefore, increasing the InGaAs QW thickness and replacing the InP waveguide layer with a higher refractive index material, such as $In_{0.528}Al_{0.238}Ga_{0.234}As$, is worth considering in the future QW laser structure. The simulation result of QW laser structure with incorporation of InAlGaAs material suggests a better confinement of the optical mode has been achieved, thereby increasing the gain of the laser.

From the SIMS analysis, in addition to the similar high As tail, a high concentration of oxygen impurities was also observed in these QD samples. This could be the main reason for the low quantum efficiency of the QD samples, even when compared with the reference QW sample. Different material system, such as InGaAsP could be considered to eliminate the Oxygen contamination brings by the excess aluminium in the chamber. Another growth-related issue that prevents lasing of these QD samples is the round defects observed in the Nomarski image of QD samples, which could also reduce the quantum efficiency significantly. Moreover, the low quantum dot density ($\sim 1.5 \times 10^{10}/cm^2$) of the current droplet epitaxy of InAs QD may not be sufficient to achieve room-temperature lasing. Therefore, optimisation of capping layer growth parameters to achieve high-density dots, such as the incorporation of high-temperature

annealing, reduction of the V/III ratio, and droplet epitaxy of InAs QD on different capping layer materials, is worth investigating in the future. Because it would be challenging to incorporate AlInGaAs in the active region of the laser device for MOCVD, continuing to optimise the quantum dot density based on current DE process and only changing the waveguide layer material to AlInGaAs would be the most feasible plan for the future growth of the DE InAs QD structure.

Finally, although most of the growth-related issues that are likely to impede the performance of the QD lasers have been discussed, the root causes of these growth issues are complicated and thus require further investigation via additional measurements such as XRD, TEM and SIMS measurements on the droplet epitaxy growth of InAs QD.

4.7 Reference

[147] C. Frigeri, S. Bietti, G. Isella, and S. Sanguinetti, 'Structural characterization of GaAs self-assembled quantum dots grown by Droplet Epitaxy on Ge virtual substrates on Si', *Appl Surf Sci*, 2013, doi: 10.1016/j.apsusc.2012.07.154.

[148] J. S. Kim, I. S. Han, S. J. Lee, and J. D. Song, 'Droplet Epitaxy for III-V Compound Semiconductor Quantum Nanostructures on Lattice Matched Systems', *Journal of the Korean Physical Society*, 2018, doi: 10.3938/jkps.73.190.

[149] A. Kors, J. P. Reithmaier, and M. Benyoucef, 'Telecom wavelength single quantum dots with very small excitonic fine-structure splitting', *Appl Phys Lett*, vol. 112, no. 17, p. 172102, Apr. 2018, doi: 10.1063/1.5023184.

[150] M. Shahzadeh and M. Sabaeian, 'The effects of wetting layer on electronic and optical properties of intersubband P-to-S transitions in strained dome-shaped InAs/GaAs quantum dots', *AIP Adv*, vol. 4, no. 6, p. 067113, Jun. 2014, doi: 10.1063/1.4881980.

[151] J. Wu *et al.*, 'Strain-free ring-shaped nanostructures by droplet epitaxy for photovoltaic application', *Appl Phys Lett*, vol. 101, no. 4, p. 043904, Jul. 2012, doi: 10.1063/1.4738996.

[152] P. Yu, J. Wu, L. Gao, H. Liu, and Z. Wang, 'InGaAs and GaAs quantum dot solar cells grown by droplet epitaxy', *Solar Energy Materials and Solar Cells*, vol. 161, pp. 377–381, Mar. 2017, doi: 10.1016/J.SOLMAT.2016.12.024.

[153] M. Gurioli, Z. Wang, A. Rastelli, T. Kuroda, and S. Sanguinetti, 'Droplet epitaxy of semiconductor nanostructures for quantum photonic devices', *Nature Materials*, vol. 18, no. 8. Nature Publishing Group, pp. 799–810, Aug. 01, 2019. doi: 10.1038/s41563-019-0355-y.

[154] A. Kors, K. Fuchs, M. Yacob, J. P. Reithmaier, and M. Benyoucef, 'Telecom wavelength emitting single quantum dots coupled to InP-based photonic crystal microcavities', *Appl Phys Lett*, 2017, doi: 10.1063/1.4974207.

[155] E. M. Sala, Y. I. Na, M. Godsland, A. Trapalis, and J. Heffernan, 'InAs/InP Quantum Dots in Etched Pits by Droplet Epitaxy in Metalorganic Vapor Phase Epitaxy', *Physica*

Status Solidi - Rapid Research Letters, vol. 14, no. 8, Aug. 2020, doi: 10.1002/PSSR.202000173.

[156] T. Mano, T. Kuroda, K. Mitsuishi, Y. Nakayama, T. Noda, and K. Sakoda, 'GaAs⁄AlGaAs quantum dot laser fabricated on GaAs (311)A substrate by droplet epitaxy', *Appl Phys Lett*, vol. 93, no. 20, p. 203110, Nov. 2008, doi: 10.1063/1.3026174.

[157] T. Mano *et al.*, 'Annealing-induced structural evolution of InAs quantum dots on InP (111)A formed by droplet epitaxy', *Cryst Growth Des*, vol. 21, no. 7, pp. 3947–3953, Jul. 2021, doi: 10.1021/acs.cgd.1c00276.

[158] H. Wang, J. Yuan, R. P. J. van Veldhoven, and R. Nötzel, 'Effect of low-temperature InP cap layer thickness on InAs quantum dot photoluminescence', *J Cryst Growth*, vol. 318, no. 1, pp. 570–571, Mar. 2011, doi: 10.1016/J.JCRYSGRO.2010.08.048.

[159] M. A. Stevens, S. Tomasulo, S. Maximenko, T. E. Vandervelde, and M. K. Yakes, 'Surface diffusion measurements of in on InGaAs enabled by droplet epitaxy', *J Appl Phys*, vol. 121, no. 19, May 2017, doi: 10.1063/1.4983257.

[160] J. Wu and Z. M. Wang, 'Droplet epitaxy for advanced optoelectronic materials and devices', *Journal of Physics D: Applied Physics*, vol. 47, no. 17. Institute of Physics Publishing, Apr. 30, 2014. doi: 10.1088/0022-3727/47/17/173001.

[161] H. Sugiura, Y. Noguchi, R. Iga, T. Yamada, and H. Yasaka, 'In0.53ga0.47as/inp multiquantum well lasers grown by metalorganic molecular beam epitaxy (mombe)', *Jpn J Appl Phys*, vol. 30, no. 2B, pp. L286–L288, 1991, doi: 10.1143/JJAP.30.L286.

[162] S. Bauer *et al.*, 'On the differences in dynamical properties of quantum-dot lasers with and without p-doping in the active region and tunneling injection quantum wells', *https://doi.org/10.1117/12.2548498*, vol. 11301, pp. 18–24, Feb. 2020, doi: 10.1117/12.2548498.

[163] D. Garbuzov, 'Broadened waveguide design for separate confinement quantum well lasers', *Conference Proceedings - Lasers and Electro-Optics Society Annual Meeting-LEOS*, vol. 1, pp. 344–345, 1996, doi: 10.1109/LEOS.1996.565274.

[164] W. X. Zou, J. L. Merz, and L. A. Coldren, 'Analysis and optimization of quantum-well thickness for GaAs/AlGaAs and InGaAs/GaAs/AlGaAs quantum-well lasers', *J Appl Phys*, vol. 72, no. 11, p. 5047, Jun. 1998, doi: 10.1063/1.352033.

[165] W. Rudno-Rudziński *et al.*, 'Control of Dynamic Properties of InAs/InAlGaAs/InP Hybrid Quantum Well-Quantum Dot Structures Designed as Active Parts of 1.55 μm Emitting Lasers', *Physica Status Solidi (A) Applications and Materials Science*, 2018, doi: 10.1002/pssa.201700455.

[166] N. Chand, E. E. Becker, J. P. van der Ziel, S. N. G. Chu, and N. K. Dutta, 'Excellent uniformity and very low (50 A/cm^2) threshold current density strained InGaAs quantum well diode lasers on GaAs substrate', *Appl Phys Lett*, vol. 58, no. 16, pp. 1704–1706, Apr. 1991, doi: 10.1063/1.105114.

[167] M. Buda *et al.*, 'Effects of Zn Doping on Intermixing in InGaAs/AlGaAs Laser Diode Structures', *J Electrochem Soc*, vol. 150, no. 8, p. G481, 2003, doi: 10.1149/1.1588304.

[168] H. Sugiura, Y. Noguchi, R. Iga, T. Yamada, and H. Yasaka, 'In0.53ga0.47as/inp multiquantum well lasers grown by metalorganic molecular beam epitaxy (mombe)', *Jpn J Appl Phys*, vol. 30, no. 2B, pp. L286–L288, 1991, doi: 10.1143/JJAP.30.L286.

[169] K. Vanhollebeke, M. D'Hondt, I. Moerman, P. van Daele, and P. Demeester, 'Zn doping of InP, InAsP/InP, and InAsP/InGaAs heterostructures through metalorganic vapor phase diffusion (MOVPD)', *Journal of Electronic Materials 2001 30:8*, vol. 30, no. 8, pp. 951–959, 2001, doi: 10.1007/BF02657716.

[170] S. Chichibu, M. Kushibe, K. Eguchi, M. Funemizu, and Y. Ohba, 'High concentration Zn doping in InP grown by low-pressure metalorganic chemical vapor deposition', *J Appl Phys*, vol. 68, no. 2, pp. 859–861, 1990, doi: 10.1063/1.346769.

[171] A. Knauer, H. Wenzel, G. Erbert, B. Sumpf, and M. Weyers, 'Influence of oxygen in AlGaAs-based laser structures with Al-Free active region on device properties', *Journal of Electronic Materials 2001 30:11*, vol. 30, no. 11, pp. 1421–1424, 2001, doi: 10.1007/S11664-001-0195-8.

[172] W. Rudno-Rudziński *et al.*, 'Carrier delocalization in InAs/InGaAlAs/InP quantum-dash-based tunnel injection system for 1.55 μm emission', *AIP Adv*, 2017, doi: 10.1063/1.4975634.

[173] Y. Yang *et al.*, 'Design optimization of silicon-based 1.55 μm InAs/InGaAs quantum dot square microcavity lasers with output waveguides', *Laser Phys*, vol. 31, no. 6, Jun. 2021, doi: 10.1088/1555-6611/abf732.

[174] A. Chelny *et al.*, 'The influence of quantum well geometry on wavelength of AlInGaAs/InP laser diodes', *J Phys Conf Ser*, vol. 1695, no. 1, Dec. 2020, doi: 10.1088/1742-6596/1695/1/012079.

[175] W. T. Tsang, 'Ga0.47In0.53As/InP multiquantum well heterostructure lasers grown by molecular beam epitaxy operating at 1.53 μm', *Appl Phys Lett*, vol. 44, no. 3, p. 288, Jun. 1998, doi: 10.1063/1.94727.

[176] P. Rees, P. Blood, M. J. H. Vanhommerig, G. J. Davies, and P. J. Skevington, 'The temperature dependence of threshold current of chemical beam epitaxy grown InGaAs-InP lasers', *J Appl Phys*, vol. 78, no. 3, pp. 1804–1807, 1995, doi: 10.1063/1.360212.

[177] J. O'Carroll *et al.*, 'Dynamic characteristics of InGaAs/InP multiple quantum well discrete mode laser diodes emitting at 2 μm', *Electron Lett*, vol. 50, no. 13, pp. 948–950, Jun. 2014, doi: 10.1049/EL.2013.3257.

[178] A. Al-Muhanna and A. Salhi, 'Numerical analysis of InGaAs-InP multiple-quantum well laser emitting at 2 μ m', *Opt Quantum Electron*, vol. 46, no. 7, pp. 851–861, 2014, doi: 10.1007/S11082-013-9796-8.

[179] W. T. Tsang *et al.*, '1.3 μ InGaAsP/InP multiquantum well buried heterostructure lasers grown by chemical-beam epitaxy', *Appl Phys Lett*, vol. 59, no. 24, pp. 3084–3086, 1991, doi: 10.1063/1.105796.

[180] H. Temkin, N. K. Dutta, T. Tanbun-Ek, R. A. Logan, and A. M. Sergent, 'InGaAs/InP quantum well lasers with sub-mA threshold current', *Appl Phys Lett*, vol. 57, no. 16, p. 1610, Jun. 1998, doi: 10.1063/1.104085.

[181] H. Temkin, T. Tanbun-Ek, and R. A. Logan, 'Strained InGaAs/InP quantum well lasers', *Appl Phys Lett*, vol. 56, no. 13, p. 1210, Jun. 1998, doi: 10.1063/1.102562.

Chapter 5: Conclusion and Further Work

The objective of this dissertation is to develop quantum dot lasers around the important telecom wavelengths of 1300nm and 1550nm for optical fibre communication using both a conventional Stranski-Krastanov (S.K) growth process and a novel droplet epitaxy (DE) process. This chapter will provide a brief summary of Chapters 3 and 4 and discuss future work related to the development of quantum dot lasers.

In the first experimental chapter (Chapter 3), 1.1 μm InAs/GaAs QD lasers grown on on-axis GaAs(100) and also substrates offcut by 3° towards (110) was compared. The optical gain and lasing thresholds of broad area lasers containing 3x and 5x layers of InAs/GaAs QDs were measured. The impact of on-axis and off-axis growth on the gain of 3 & 5-layer QD lasers has been demonstrated by multisection gain measurements. The results have demonstrated that the QD laser grown on the 3-degree off-axis substrate has lower threshold current density and higher gain than on the on-axis substrate. The obtained EL measurement result shows a ~20% increase in the QD density for the 3-degree off-axis sample compared to the on-axis sample, which is correlated with the transmission electron microscopy (TEM) images. As determined by transmission electron microscopy, the higher QD density of the off-axis sample can be attributed to the sample's GaAs spacer layer morphology changing, with more steps forming on the surface of GaAs, which provides a favourable growth site for QDs. It would be interesting to investigate the quantum dot density of these lasers on a GaAs substrate with an off-axis angle of 6, 9, or 12 degrees. After the incorporation of strain relaxing layer (SRL), the GaAs spacer thickness can be reduced further, which should increase quantum dot density and decrease the laser's threshold current density. An InGaAs stain relaxing layer (SRL) layer would also increase the QD laser's emission wavelength to the desired 1300 nm. Hence, further

investigation into the density of dots of new lasers with strain balancing layers on higher degree off-axis substrates is a clear direction for further research based on the results of this thesis.

In the second experimental chapter (Chapter 4), the design, growth, and characterization of InAs quantum dots (QD) by Droplet epitaxy (DE) on 5nm InGaAs interlayer was investigated for the development of 1550nm lasers. Based on RT-PL and AFM analysis, we have achieved greater uniformity and higher dot density using DE of InAs QD on 5nm InGaAs than on InP directly. The LaserMod simulation demonstrated the lasing capability of the 5nm InGaAs QW and 35nm InP spacer reference QW laser structure which should translate into lasing of the corresponding structures that include QDs. The initial 3x and 5x QD and QW pulsed LI results exhibit a spectrum similar to SLED for all samples but no lasing, probably because of the low quantum efficiency of these samples. With decreased Zn doping and varying InP waveguide layer thicknesses, improved laser structures containing 5x&7x layers of QDs or QW were grown. By decreasing the Zn doping and increasing the QD layer stacking, the improved QD samples exhibit a 5-fold increase in intensity relative to the initial growth samples, as measured by pulsed LI. The change from InGaAs to InP in the waveguide layer material significantly improves the carrier injection into the QD and blue-shifts the QDs' wavelength to 1530nm, which is close to the target wavelength of 1550nm. Unfortunately, none of the samples exhibit lasing. Incorporating stacked DE QDs results in the formation of round defects, which is thought to be one of the reasons why the lasing operation of these QD samples is inhibited. From SIMS analysis, a high arsenic diffusion tail is observed in all QW and QD samples and also high oxygen impurities is observed in some of the QD samples which is a clear potential reason for such low quantum efficiency of these samples. These growth-related issues are likely to impede the performance of the lasers and result in no lasing operation. The causes of these issues are unclear and thus require further investigation via additional measurements such as XRD, TEM and SIMS measurements on the bulk material growth. Future growth would benefit from replacing the InP waveguide layer with $In_{0.528}Al_{0.238}Ga_{0.234}As$ in order to achieve lasing at room temperature. The simulation results indicate that $In_{0.528}Al_{0.238}Ga_{0.234}As$ has superior optical confinement to InP due to its higher reflectivity. Since incorporating AlInGaAs in the

active region would be challenging, continuing to optimise InGaAs QW thickness, increasing quantum dot density based on the 20nm InP capping layer would be the next plan for the optimisation of DE InAs QD structure.

Overall, this project demonstrates a significant progress towards the first 1.5μm quantum dot lasers grown using droplet epitaxy by MOCVD. With successful tuning the emission wavelength of these QD laser. The potential advantages of these DE QD lasers, such as the reducing the influence of wetting layers compared to S.K growth, may be demonstrated for future high performance telecoms wavelength laser applications.